NSF/CEE-83023

PB83-211037

STRUCTURAL RESEARCH SERIES NO. 8302

83-SS-0084

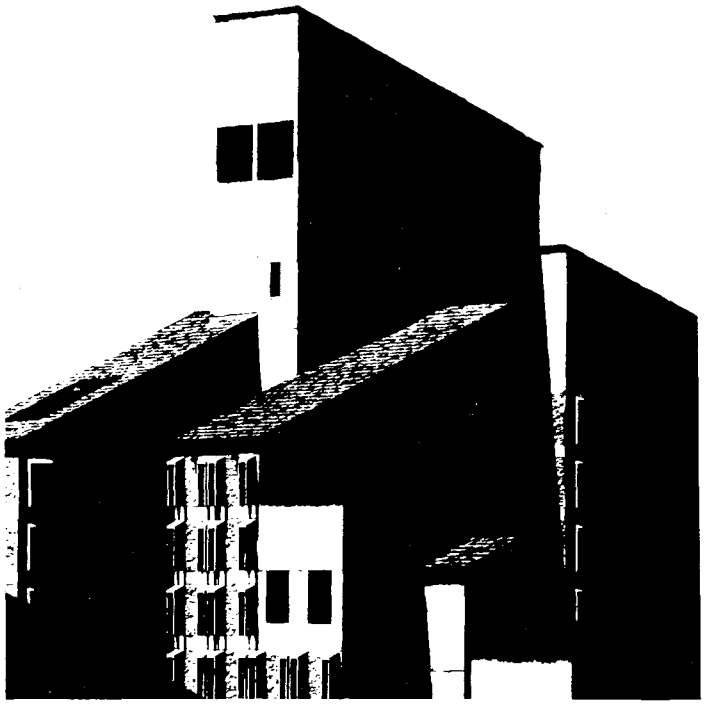

SCALE RELATIONSHIPS OF CONCRETE COLUMNS

by Richard J. Bedell and Daniel P. Abrams

A Report to the National Science Foundation
Research Grants CEE-8119385 and PFR-8007094

Department of Civil, Environmental,
and Architectural Engineering

College of Engineering
and Applied Science

University of Colorado, Boulder

INFORMATION RESOURCES
NATIONAL SCIENCE FOUNDATION

Structural Research Series No. 8302:

SCALE RELATIONSHIPS OF CONCRETE COLUMNS

by

Richard J. Bedell

and

Daniel P. Abrams

A report to the

NATIONAL SCIENCE FOUNDATION

Research Grant CEE-8119385
and PFR-8007094

Department of Civil, Environmental, and
Architectural Engineering

College of Engineering and Applied Science

University of Colorado
Boulder

January 1983

ABSTRACT

The objective of the experimental study was to examine the behavior of reinforced concrete columns subjected to shear and axial force reversals, and to compare the behavior with that of small-scale models. Two large-scale columns were tested with a ratio of shear to axial force equal to 0.25 to simulate the loading on an exterior base-story column in a slender multistory building subjected to lateral loads. Loads were applied slowly according to a pattern of reversals representative of what would occur during a strong earthquake motion. In addition, a sustained axial force was applied to each specimen which represented gravity loading. This axial force was varied for the two specimens to examine differences in behavior attributable to inconsistent modeling of gravitational accelerations. With the use of a numerical model, response of the large-scale specimens was compared with measured response of small-scale (approximately one-twelfth scale) models which were tested as part of a previous investigation.

ACKNOWLEDGEMENTS

The investigation described in this report was part of a continuing study of reinforced concrete structures subjected to earthquake motions. The work was funded by the National Science Foundation under grants PFR-8007094 and CEE-8119385. Experimental work was done at the Structural Research Laboratory at the University of Colorado.

The writers wish to express their appreciation to Professors Tulin and Gross for their critical review of the manuscript, and to numerous graduate students, particularly John Stewart and Nevis Cook, for their unselfish assistance. Acknowledgement is also due to Dave Jones and his staff for their skillful fabrication of the test apparatus. A special note of thanks is extended to Deborah Borin for typing the report.

This report was prepared as a thesis for the degree of Master of Science in Civil Engineering by Richard J. Bedell under the direction of Professor Daniel P. Abrams. Any opinions, findings, and conclusions or recommendations expressed in this publication are those of the authors and do not necessarily reflect the views of the National Science Foundation.

TABLE OF CONTENTS

	Page
ACKNOWLEDGEMENTS	i
LIST OF TABLES	iv
LIST OF FIGURES	v
CHAPTER	
I. INTRODUCTION	1
1.1 Object and Scope	1
1.2 Previous and Related Research	3
II. OUTLINE OF EXPERIMENTAL WORK	7
2.1 Introduction	7
2.2 Description of Test Specimens	7
2.3 Description of Test Apparatus	9
2.4 Materials	10
2.5 Fabrication	11
2.6 Instrumentation	12
2.7 Data Acquisition System	13
2.8 Testing Procedure	14
III. OBSERVED BEHAVIOR	31
3.1 General	31
3.2 Column Specimen L4D2	31
3.3 Column Specimen L4D3	34
IV. INTERPRETATION OF OBSERVED RESPONSE	63
4.1 Introduction	63

CHAPTER		Page
	4.2 The Numerical Model	63
	4.3 Column Specimen L4D2	66
	4.4 Column Specimen L4D3	70
V.	INVESTIGATION OF SCALING	79
	5.1 Introduction	79
	5.2 Comparison of Behavior for Small and Large Specimens with Equal Gravity Load Stress	80
	5.3 Differences in Response Due to Inconsistent Gravity-Load Scaling	84
VI.	SUMMARY AND CONCLUSIONS	109
	6.1 Summary	109
	6.2 Conclusions	110
	6.3 Recommendations for Future Research	112
REFERENCES		113
APPENDIX A		117
APPENDIX B		129

LIST OF TABLES

TABLE		Page
4.1	Percentage of Overall Deflection Due to Base Rotation	72
4.2	Effective Stiffnesses for the Column Above the Base (Specimen L4D2)	74
5.1	Comparison of EI/EIg for Small-Scale Specimens	97
5.2	Comparison of Measured Properties: Specimens L4D2 and L4D3	101

INTENTIONALLY BLANK

LIST OF FIGURES

FIGURE		Page
2.1	Representative Multistory Structure . . .	16
2.2	Specimen Description	17
2.3	Cross-Section Details	18
2.4	Column Connection Detail	20
2.5	Top of Column Detail	21
2.6	Test Apparatus	22
2.7	Concrete Stress-Strain Properties	24
2.8	Steel Stress-Strain Properties	26
2.9	Reinforcing Cage and Formwork	27
2.10	Instrumentation	28
2.11	Location of Strain Measurements	29
2.12	Displacement History	30
3.1	Measured Response of Specimen L4D2	37
3.2	Photographs of Base Region, Specimen L4D2	49
3.3	Measured Crack Width and Crack Patterns, L4D2	50
3.4	Load Configuration	53
3.5	Measured Response of Specimen L4D3	54
3.6	Photographs of Base Region, Specimen L4D3	58
3.7	Crack Widths	59
3.8	Crack Patterns	60
4.1	Identification of Points for Table 4.1 . .	73
4.2	Identification of Points for Table 4.2 . .	74

FIGURE		Page
4.3	Stress-Strain Laws Used in the Numerical Model	75
4.4	Comparison of Measured and Calculated Results, Specimen L4D2	76
4.5	Load-Moment Interaction Diagram	77
4.6	Comparison of Measured and Calculated Results, Specimen L4D3	78
5.1	Moment-Curvature Comparison of Small and Large-Scale Beams (Evans and Clarke)	91
5.2	Load-Rotation Comparison for Small and Large-Scale Beam-Column Elements (Stewart and Abrams)	92
5.3	Comparison of Large and Small-Scale Material Properties	94
5.4	Comparison of Large and Small-Scale Measured Results, Phase I	96
5.5	Identification of Points for Table 5.1	97
5.6	Comparison of Large and Small-Scale Measured Results, Phase II	98
5.7	Comparison of Large and Small-Scale Measured Results, Phase III	99
5.8	Comparison of Initial Cycles for Specimens L4D2 and L4D3	100
5.9	Dynamic Model	102
5.10	Dynamic Response with Light Gravity Stress	103
5.11	Load-Moment Interaction Diagram (Small-Scale)	104
5.12	Dynamic Response with Full-Scale Gravity Stress	105
5.13	Photographs of Failure for Large-Scale Specimens	106

FIGURE Page

5.14 Dynamic Response with a Heavy Gravity Stress 107

5.15 Structural Model 108

CHAPTER 1

INTRODUCTION

1.1 Object and Scope

The overall objective of this experimental study was to examine the behavior of reinforced concrete base story columns in a slender multistory structure and to compare the behavior with small-scale models. The scope of the study was limited to exterior base story columns in which the applied vertical load could be expected to vary with the horizontal load when the structure was subjected to strong base motions. The test variables were the size of specimen and the amount of sustained load representing gravity loads in a multistory structure.

Two reinforced concrete columns were constructed and subjected to slowly applied load reversals. Although the specimens were approximately one-half scale, they were felt to represent the behavior of components constructed at full-scale since a standard concrete mix and Grade 60-No. 6 reinforcing bars were used. Response of these large-scale specimens was compared with that of specimens constructed at approximately one-twelfth scale. The steel and concrete properties as well as the reinforcing ratios were similar so that a comparison of

load-deflection characteristics for the large- and small-scale specimens could be evaluated. The small-scale models were tested by Gilbertson and Moehle (Ref. 9) at the University of Illinois.

To investigate the differences in response attributable to scaling of the section properties, a sustained load was applied so that the resulting normal stress would be similar for both large- and small-scale specimens. The ratio of axial to shear force was constant (4:1) to provide a comparison of the behavior of large and small specimens.

Actual gravity stresses in a small-scale model are difficult to apply because of the need for massive weights. Often this constraint is not met and stresses in the model are lighter. For this reason, a larger sustained load was applied to a second large-scale specimen to produce a gravity stress equal to that in a full-scale multistory structure.

To predict the response for other loading patterns and gravity stress levels, a nonlinear dynamic analysis was developed to simulate the response of a base story column to strong ground motions. This analysis was a filter to observe differences in hysteretic response of each specimen.

1.2 Previous and Related Research

In the past, many small-scale models of reinforced concrete elements have been studied by several investigators (Refs. 12, 10, 13, 23). Principal areas of research have included columns, beam-columns, structural walls and frame-wall interaction. Base story columns were investigated by Gilbertson and Moehle (Ref. 9) in which one-twelfth scale columns were subjected to slowly applied load reversals. A number of columns were loaded with a changing axial load to model behavior of an exterior column.

Small-scale beam-column assemblages were tested by Abrams and Kreger (Ref. 2). Stiffness characteristics of interior- and exterior-joint specimens were found to vary significantly in load reversal regions. The response was also found to be highly dependent on loading history.

Frame-wall interaction was researched by Abrams and Sozen (Ref. 1). Ten story frame-wall structures with different wall strengths were excited by motion at the base. Arbitrary softening of the walls resulted in a more economical structure with no loss of serviceability. It was also determined that the response of the combined frame-wall system contained characteristics of structures behaving linearly.

Numerous tests of large-scale reinforced concrete elements has also been completed with regard to columns,

beam-columns and structural walls. Park, Priestly and Gill (Ref. 14) subjected a series of large-scale (approximately full-scale) reinforced concrete columns to load reversals. A constant sustained load was used as one of the test variables. Test results showed a high degree of ductility and significantly larger flexural strengths than calculated using current provisions of the American Concrete Institute (ACI 318-77).

Large-scale beam-column subassemblages under monotonic and cyclic loads were investigated by Viwathanatepa, Popov and Bertero (Ref. 22). The study examined strength, stiffness, ductility and energy-dissipation characteristics of the subassemblages as well as repair techniques.

Vallenas, Bertero and Popov (Ref. 21) examined reinforced concrete structural walls subjected to high shear earthquake loading conditions. Good agreement was obtained between measured results and analytic predictions for flexural behavior and crack patterns.

A relatively small data base has existed for the comparison of small- and large-scale reinforced concrete behavior under cyclic loading conditions. As part of this investigation, Stewart and Abrams (Ref. 20) investigated one-twelfth and three-quarter scale models of beam-column assemblages. Good agreement was found for most aspects of behavior with the greatest difference attributed to slip of the

reinforcement. The difference in response due to slip was found to have a greater effect on the interior-joint than on the exterior-joint specimens.

The scaling characteristics of small-scale models and reinforced concrete prototypes have been studied by many investigators (Refs. 7, 8, 16, 19, 24). Principal areas of research have included microconcrete mix designs, small-scale reinforcement and bond similitude.

Currently, the most significant work being done elsewhere is the U.S.-Japan cooperative effort at the Building Research Institute, Tsukuba, Japan (Ref. 15). A full-scale seven-story structure at the BRI has been subjected to lateral loads and tested to failure. As part of this effort many subprojects have sprouted in the United States. A one-tenth scale shaking table model is currently being tested at the University of Illinois (Ref. 18). A one-fifth scale shaking table model is being studied at the University of California, Berkeley (Ref. 6). Large-scale components of the BRI structure are being tested at the University of Texas, Austin. These projects form a comprehensive study of testing reinforced concrete buildings for earthquake resistance. Results from this study should also be of assistance in this area.

Another multi-investigator research program in progress is a study of the Imperial County Services Building in El Centro, California which was damaged severely by an earthquake in 1979. Large-scale components of this building are being tested in California. A one-tenth scale model is being tested on an earthquake simulator in Illinois to test the usefulness of small-scale models in estimating response of full-scale structures. Results of this study should also be of use in the project.

CHAPTER II

OUTLINE OF EXPERIMENTAL WORK

2.1 Introduction

Two large-scale specimens were fabricated and tested to represent columns at the base story of a multistory frame structure (Fig. 2.1). A specific ratio of lateral load to axial load (1:4) remained constant for each specimen. The test variable was the amount of dead load applied to each specimen. The first specimen, L4D2, represented a large-scale version of a small-scale column tested by Gilbertson and Moehle (Ref. 9). The second specimen, L4D3, was identical except that the dead load was three times larger than the first specimen.

2.2 Description of the Test Specimens

The test specimens were large-scale models of first story external columns. The large-scale specimens were constructed to approximately one half of full scale, and six times larger than their small-scale counterparts. A detailed description of each specimen is presented in Fig. 2.2.

Loads were applied at the top of each column specimen which represented a hypothetical point of contraflexure in the multistory frame. The base was fixed against translation and rotation by anchoring the base girder to the structural test floor with steel rods.

Design of the specimens was controlled so that flexural behavior would dominate the response. The longitudinal reinforcing ratio, as defined by the area of steel divided by the gross area of concrete, remained constant for both the large- and small-scale specimens.

Each specimen was reinforced longitudinally with four #6 deformed bars (area of steel = 1.64% of the gross area). Development length was determined according to ACI Code (Ref. 4) requirements. Shear reinforcement was provided by #3 closed hoops and overdesigned by a minimum factor of safety of three so that a failure in shear would not result. The base girder was designed so that cracking would not occur. This was accomplished by providing #6 longitudinal bars and #3 closed hoops. In addition, the base girder was post-tensioned with two steel bars just below the top of the girder. For nominal dimensions, reinforcing details and column cross-sections, see Fig. 2.3.

A load transfer bracket in the form of a steel double tee section (Fig. 2.4), with built-in bearings, was bolted to

the top of the column to provide the connection of the specimen to the testing apparatus. The bracket was bolted to two 3 x 3 x 3/8 inch angles welded to the longitudinal reinforcement and cast in place as shown in Fig. 2.5.

2.3 Description of the Test Apparatus

The function of the test apparatus (Fig. 2.6) was to transfer the lateral force from the actuator to the top of the column specimen. Because of the difference in elevation between these points, a force couple was produced which was reacted by the couple provided by the pin-ended steel member and the axial force in the column. Dimensions of the apparatus were chosen so that the ratio of vertical to lateral force applied to the top of the column specimen would be four. Roller bearings were used at the top and bottom of the simulated roller support as well as at the connection to the specimen to produce connections with essentially no resistance to rotation. The apparatus used perpendicular stay cables at four locations to prevent out-of-plane motion.

The simulated dead load due to gravity was applied independently using hydraulic actuators which were mounted within a steel harness around the specimen. The desired load was applied by increasing the pressure in the actuators which in turn created tension in the harness and axial compression in the

specimen. The load was measured using a load cell and a pressure gauge mounted on the pump.

The lateral force was applied using a 160 KN servo-controlled actuator. It was operated in force control rather than displacement control so that nonlinear geometric effects would not influence the loading. A swivel assembly built into both ends of the actuator allowed the system to rotate with negligible friction. The actuator reacted against a steel frame anchored to the test floor with steel rods.

2.4 Materials

The concrete used to construct the specimens was mixed and delivered by a local pre-mix concrete firm. The maximum aggregate size was 20mm and the mix used Type 1 Portland Cement. The mix proportions were 1:2.3:3.6 @ w/c = 0.6 by weight. Physical properties of each batch were determined from test cylinders (152mm x 305mm and 76mm x 153mm) and prisms (51mm x 51mm x 305mm) taken at the time of casting. Each cylinder and prism was tested the day after each column specimen was tested. A summary of concrete properties is presented in Fig. 2.7. Compressive and splitting strengths of the concrete were determined using a 1300 KN capacity Baldwin testing machine. Strains were measured using a mechanical dial gauge accurate to .025mm over a gauge length of 127mm. A 45 KN capacity Instron

machine was used for the modulus-of-rupture tests on the prisms.

The reinforcing bars and hoops were purchased from a local manufacturer. The longitudinal reinforcing steel consisted of deformed bars conforming to ASTM A-615 Specification for grade 60 steel. The stress-strain characteristics are presented in Fig. 2.8. The tests were conducted using a 520 KN Tinius Olsen testing machine. Stress-strain data was recorded using a LVDT over a two inch gauge length.

2.5 Fabrication

The casting procedure was conducted in such a way as to parallel actual construction techniques. Strain gauges were placed on longitudinal reinforcing bars in the positions shown in Fig. 2.11. Each specimen was cast in an upright position (Fig. 2.9) and was compacted with a conventional high-frequency vibrator. A slump test was performed prior to casting and concrete samples were taken throughout the casting process to determine material properties at a later date. Forms were removed one week after casting. All samples as well as each specimen were air-cured until the test date.

2.6 Instrumentation

Four parameters of response were measured for each specimen: applied load, displacement at the top of the column, rotation at the base of the column and strains in the reinforcement. The applied load was measured using a 160 KN capacity load cell built into the servo-controlled actuator. The calibration of the load cell and the sensitivity of 0.1% was verified by the National Bureau of Standards. Displacement was measured with a linear variable differential transformer (LVDT). The LVDT was mounted, independent of the system, at the same elevation as the lateral load. A wire was attached to the specimen and to the core of the LVDT. In order to keep the wire taut during measurement, a free hanging weight was attached to a fishing line strung over a pulley and connected to the opposite end of the LVDT core.

Since considerable damage was expected at the bottom of the column, the base rotation was measured at a distance equal to the effective depth of the column (254mm) above the base. At this point, an aluminum bar was attached to each side of the specimen spanning 1524mm to the outside edges of the base (Fig. 2.10). LVDTs were mounted with swivel connections on the outside edge of each side of the base and a wire was attached from the aluminum bar to the LVDT core. Here again weights were employed to keep the wires taut during operation. An average

value for the base rotation could be calculated by adding the displacements and dividing by the distance between them. Mechanical dial gauges were mounted alongside the LVDTs to check the electronic measurements.

All three of the LVDTs used had a sensitivity of less than 0.5% within the range of each particular transducer. Before implementation, each LVDT was calibrated on a Bridgeport vertical milling machine which was accurate to .003mm.

Strains on the reinforcing bars were measured at twelve locations as shown in Fig. 2.11. A groove 3mm deep and 2.4mm wide was milled in the reinforcing bar for a length of 762mm to carry the wires attached to the strain gauges. The reduction of steel area due to the groove was 1.2%.

2.7 Data Acquisition System

The voltage outputs from the load cell, LVDTs and eight of the twelve strain gauges were input into an analog-to-digital convertor. The binary coded number from the convertor was fed into a Hewlett-Packard 9830 A computer. Software written for the test converted the number to the appropriate measurement and stored the data on permanent tape. From this tape, the data was reduced and plotted using a Hewlett-Packard 9862 A calculator-plotter. The remaining four strain gauges were recorded by hand using a strain measurement device.

2.8 Testing Procedure

Each specimen was loaded in accordance with the displacement measured at the top of the column. This parameter was chosen since it could easily be non-dimensionalized as a percent of the height. This non-dimensional characteristic allowed for the reproduction of the displacement history of the small-scale specimens. The displacement history (Fig. 2.12) consisted of three phases of which Phase I constituted three cycles at $\pm$18mm (1.2% of the height). Phases II and III consisted of three cycles each at $\pm$36mm and $\pm$54mm respectively. After Phases II and III, a small amplitude cycle of $\pm$18mm was executed. Upon completion of these cycles the column was taken to failure.

Throughout each test, the load-displacement relation and load-rotation relation were monitored continuously on x-y plotters. Data points for all test parameters were taken intermittently to produce a smooth curve when the data was reduced subsequently. Dial gauge readings were taken at every data point for the first few cycles to insure proper operation of the electronic instruments and less frequently throughout the remainder of the test. Crack patterns were monitored carefully throughout the test and photographed at the maximum positive and negative displacements for each cycle. Crack widths, for prominent cracks, were also measured at the maximum

displacements. The entire test, through to failure, covered a time span of approximately nine hours.

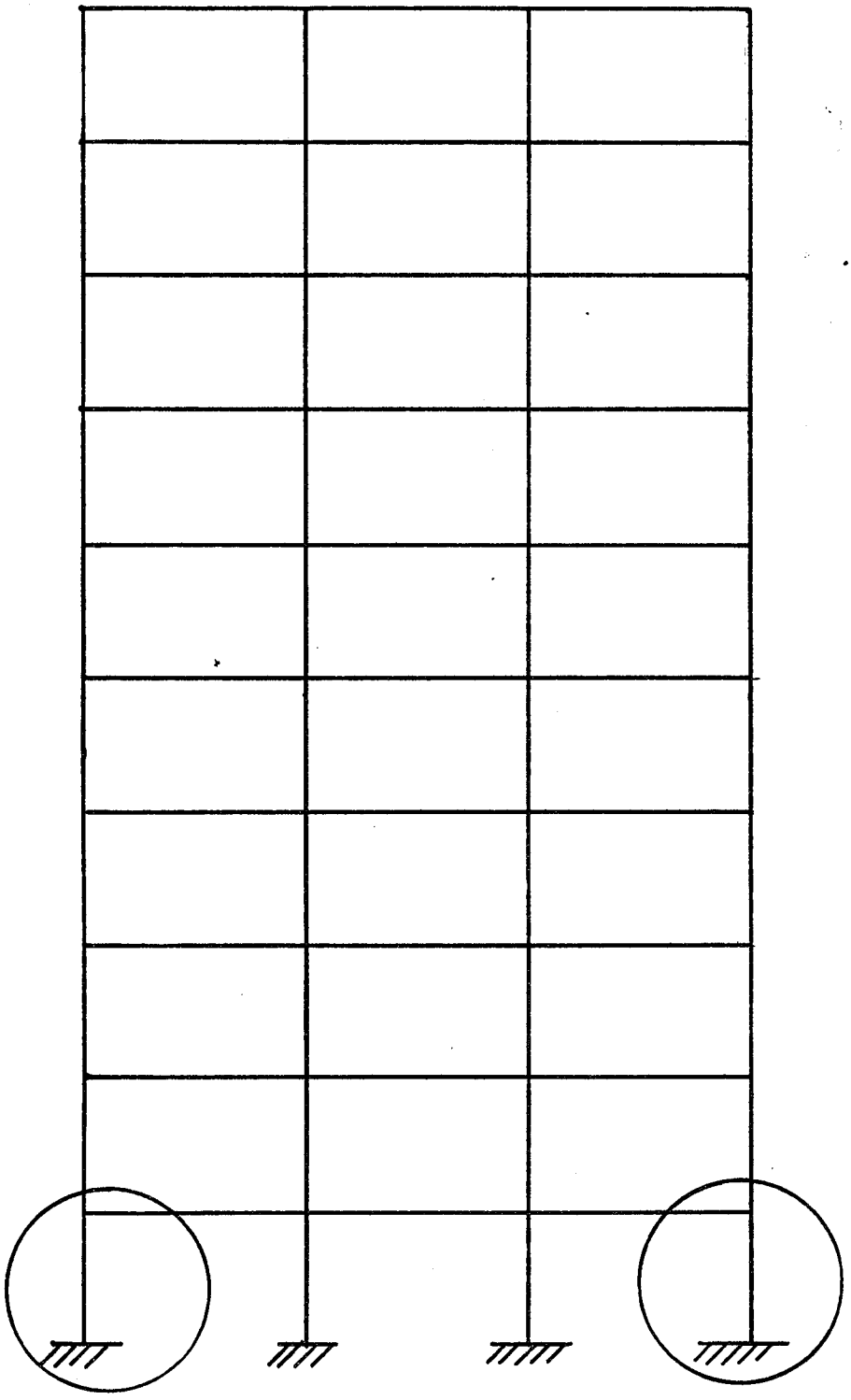

Fig. 2.1 Representative Multistory Structure

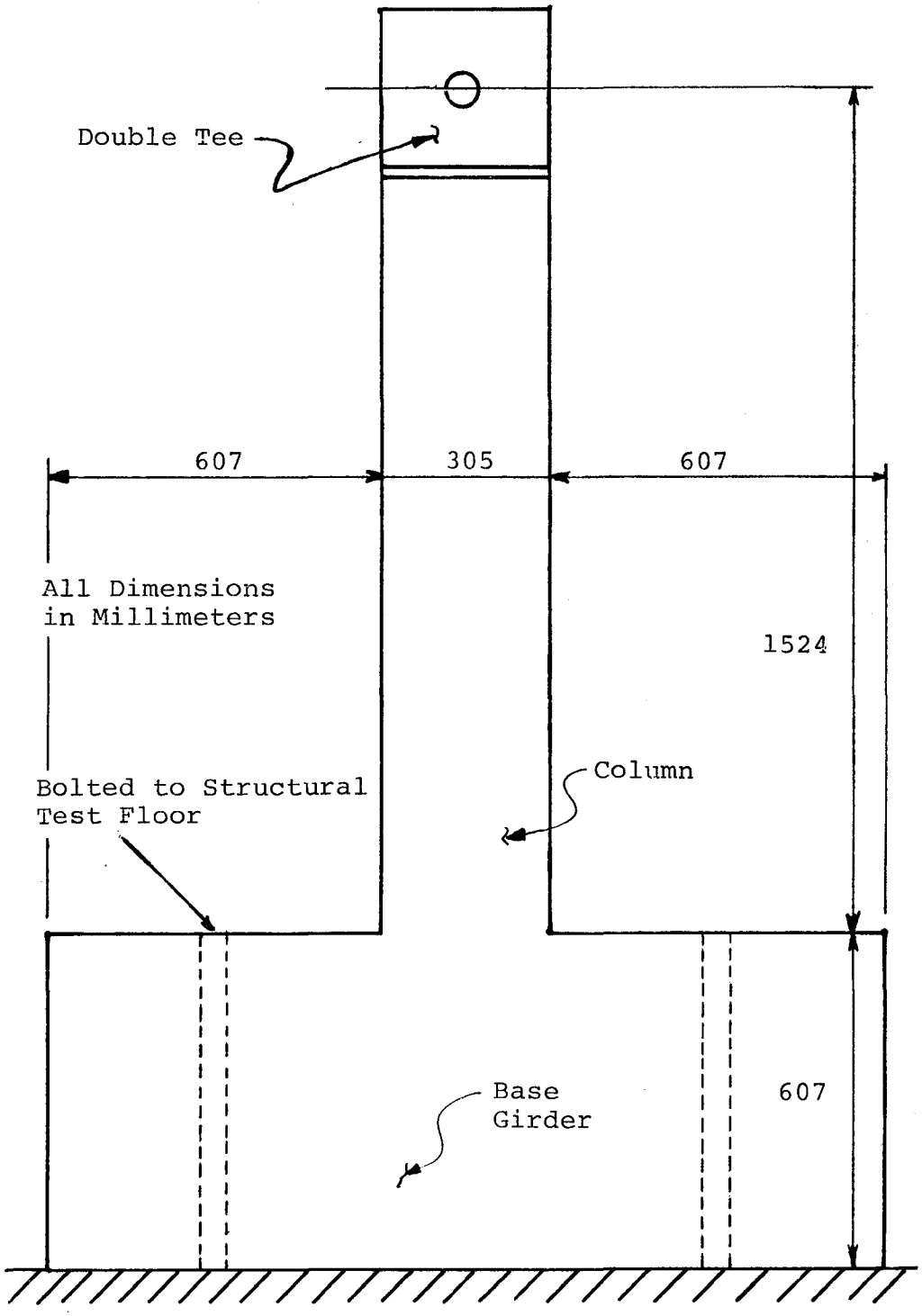

Fig. 2.2 Column Description, Specimens L4D2 and L4D3

Note: All dimensions
in millimeters

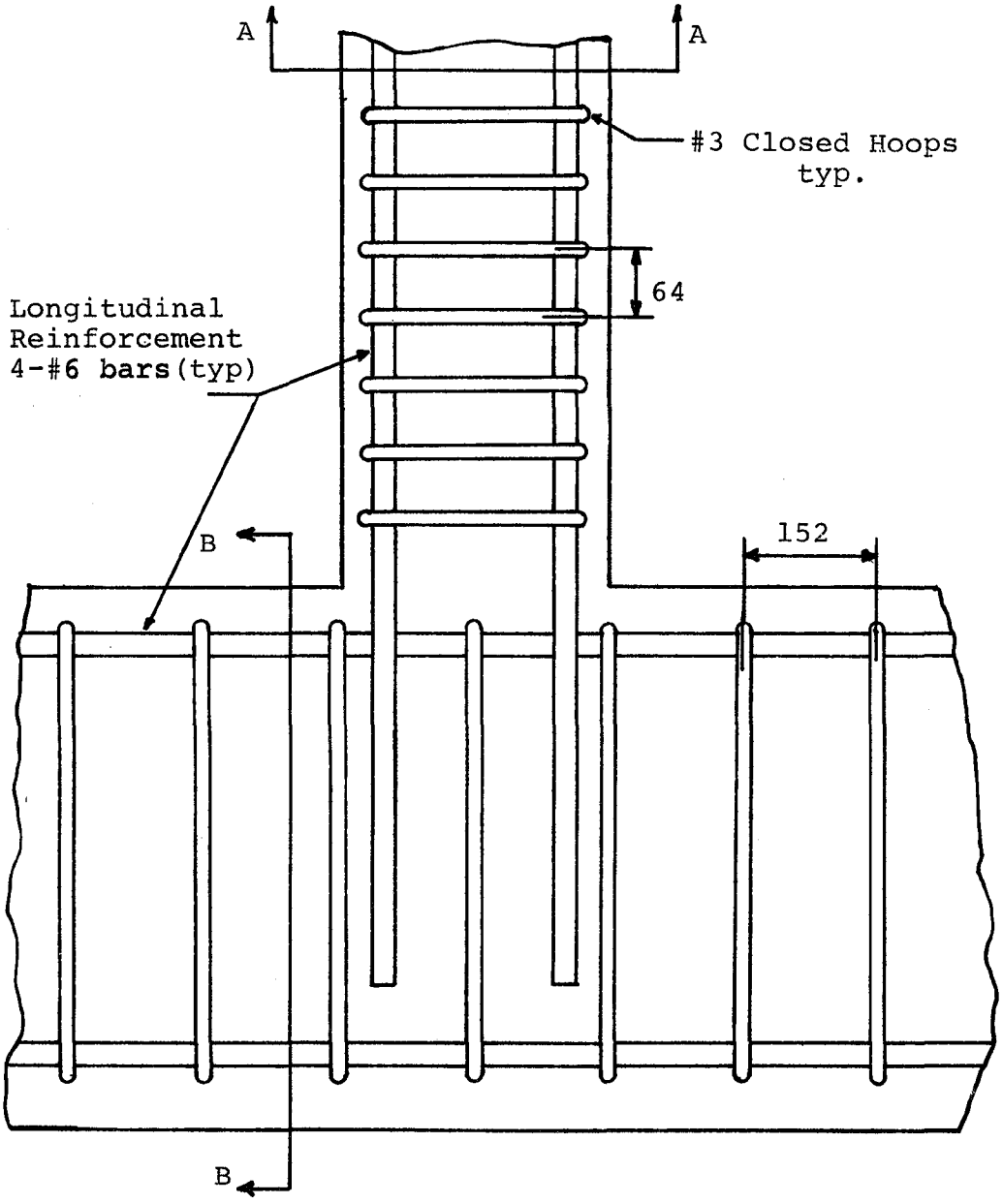

Fig. 2.3(a) Reinforcing Details

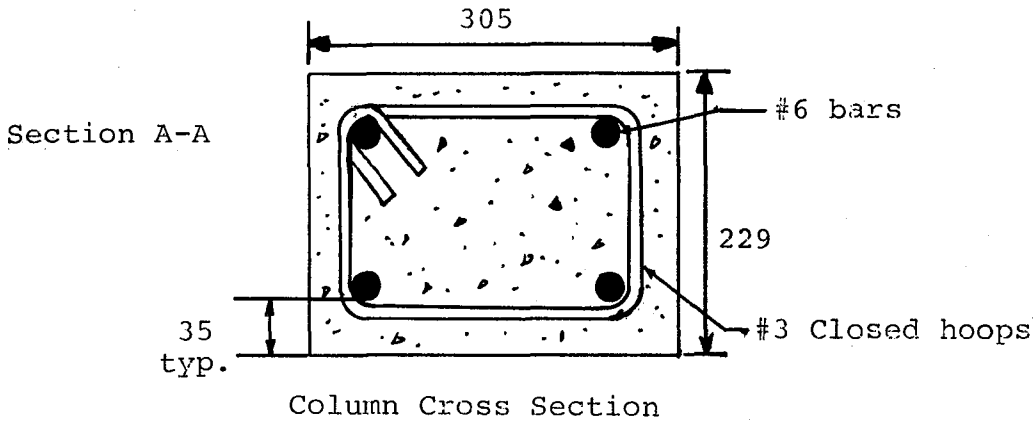

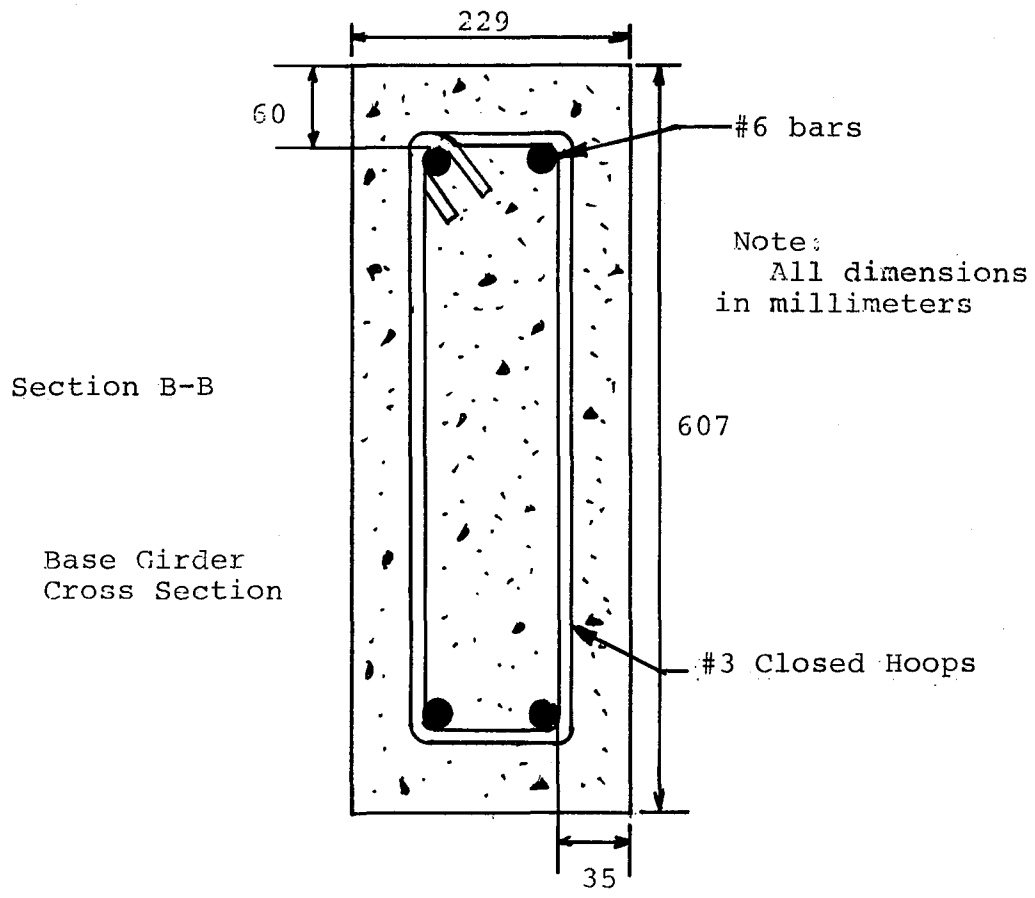

Fig. 2.3(b) Cross-section Details

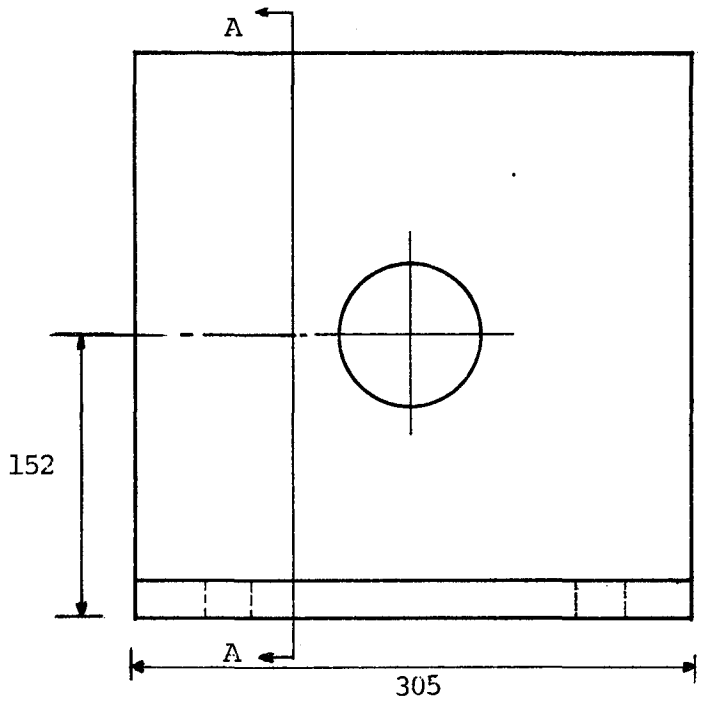

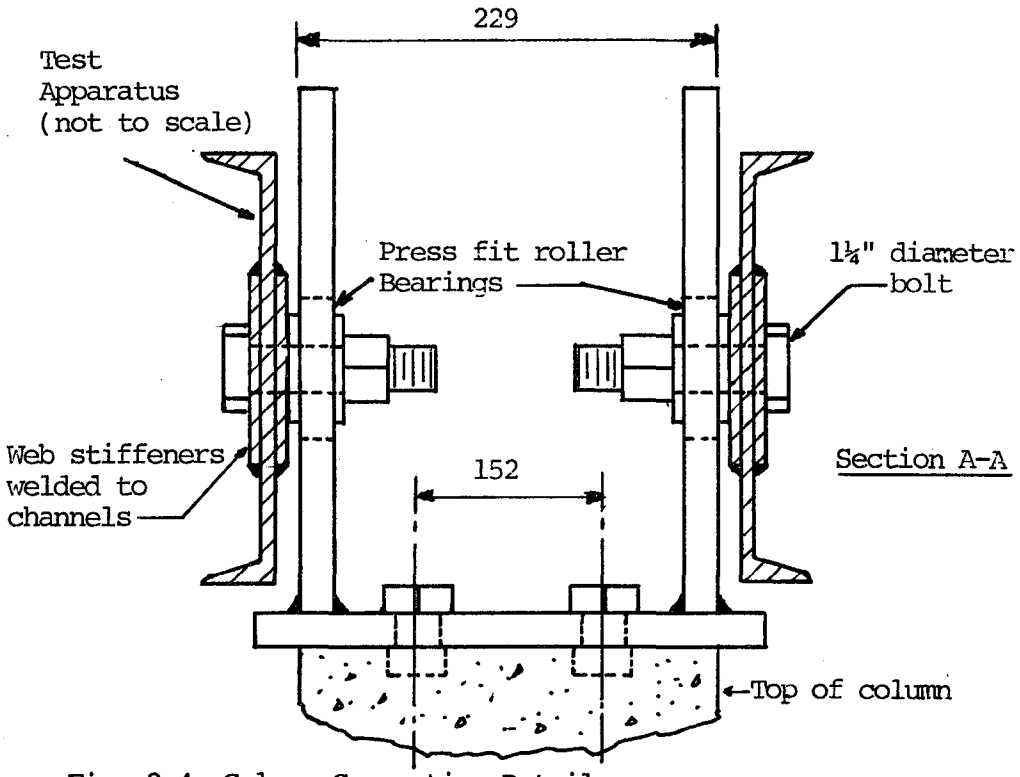

Fig. 2.4 Column Connection Detail

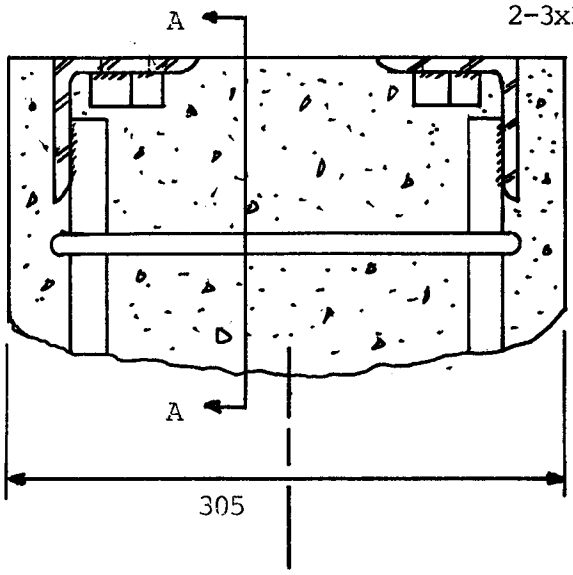

All dimensions
in Millimeters

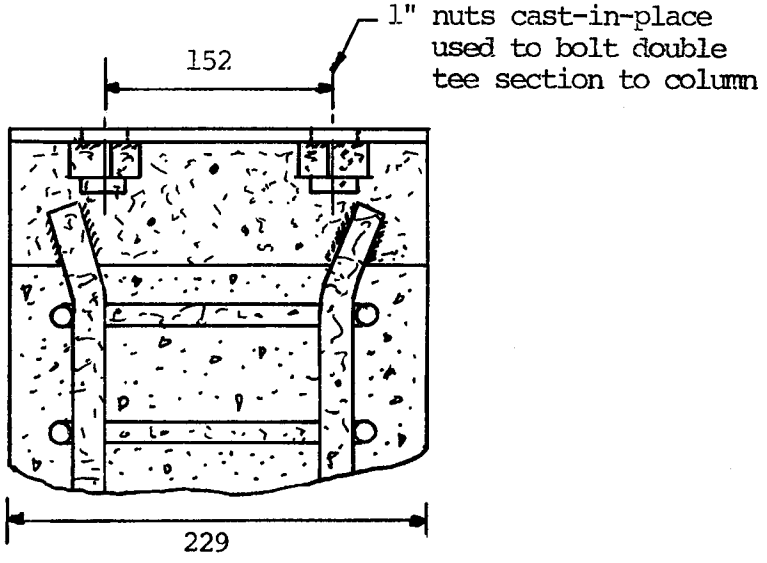

Fig. 2.5 Top of Column Detail

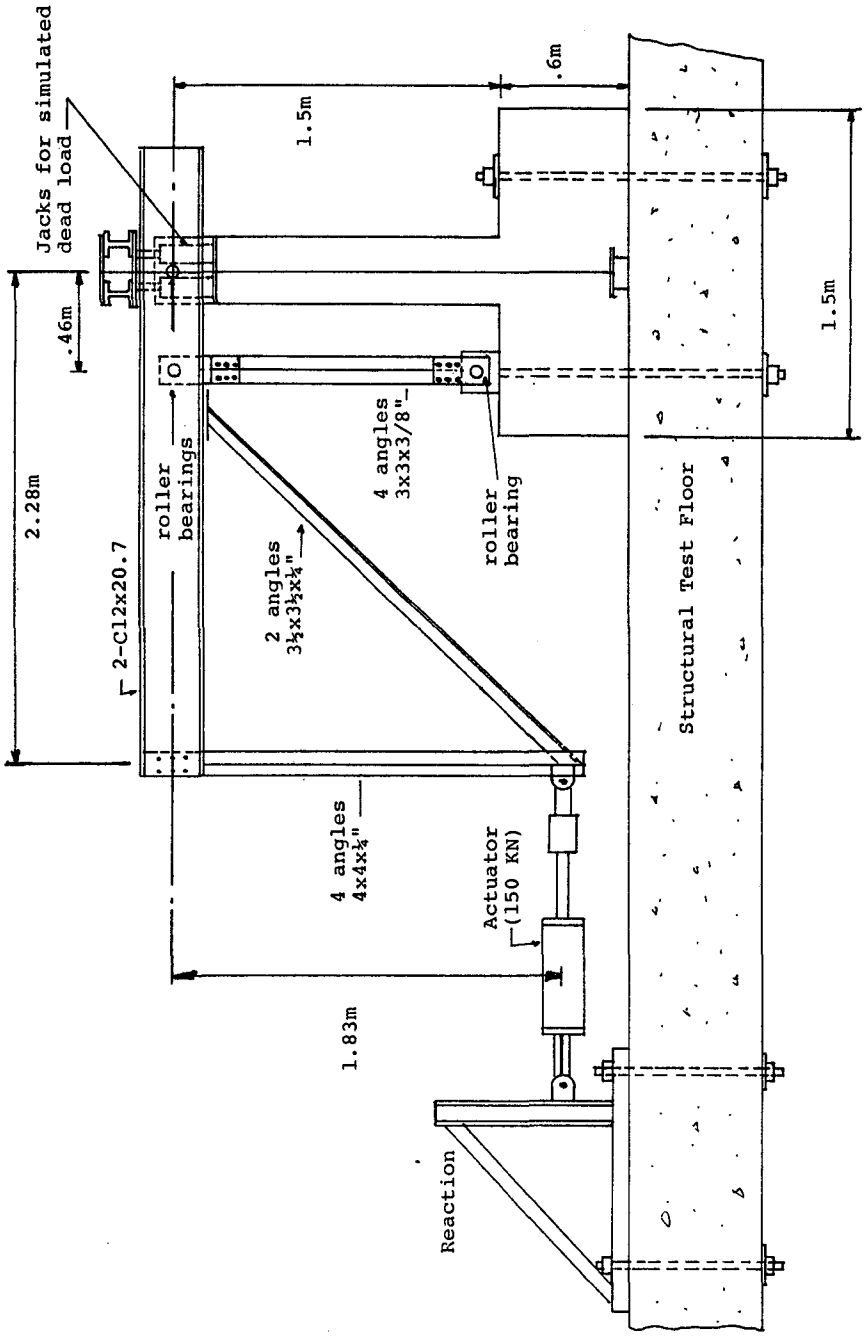

Fig. 2.6(a) Test Apparatus

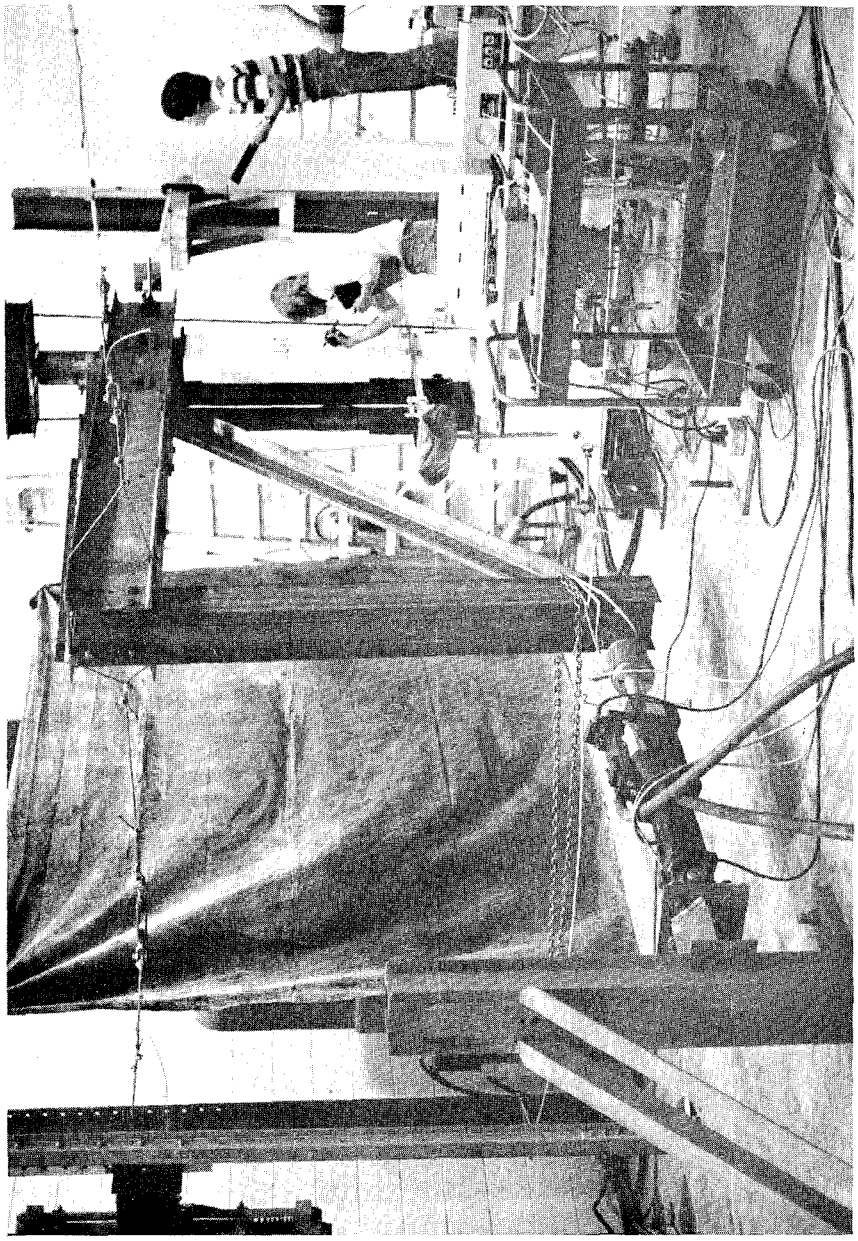

Fig. 2.6(b) Photograph of Test Apparatus

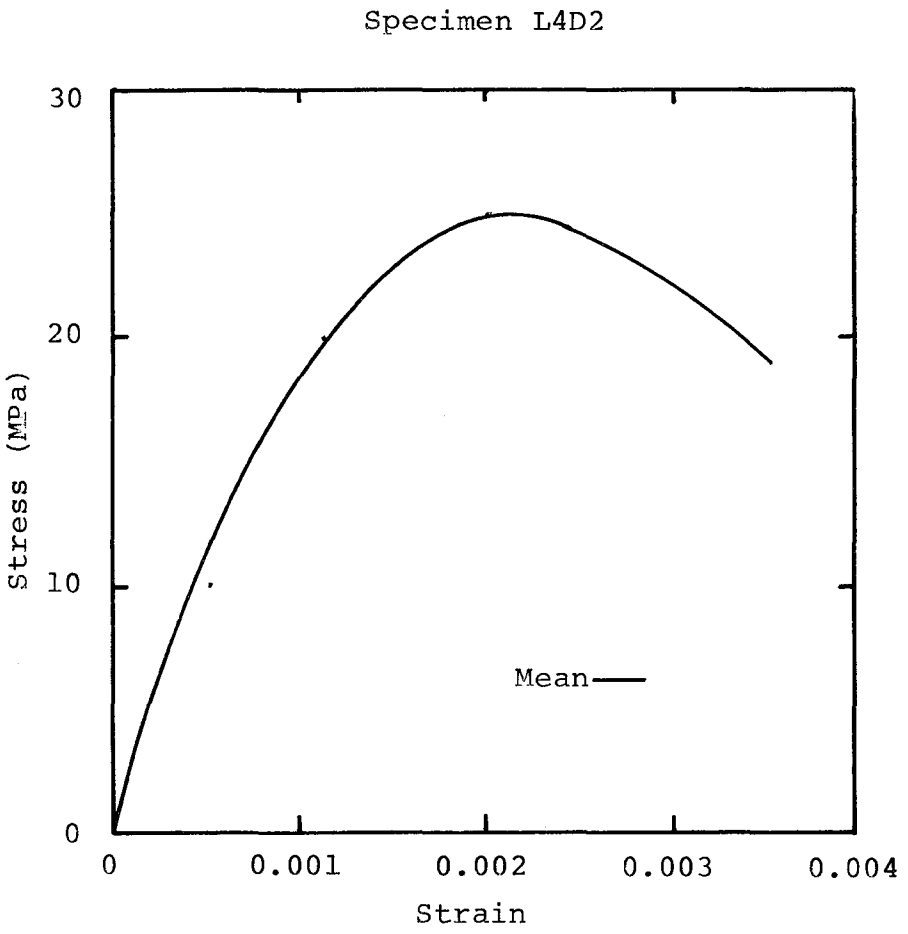

Property	Number of Samples	Mean (MPa)	Std. Dev. (MPa)
Compressive Strength	5	24.1	1.88
Modulus of Rupture	6	4.82	0.31
Splitting Strength	6	3.20	0.42

Fig. 2.7(a) Measured Concrete Properties, L4D2

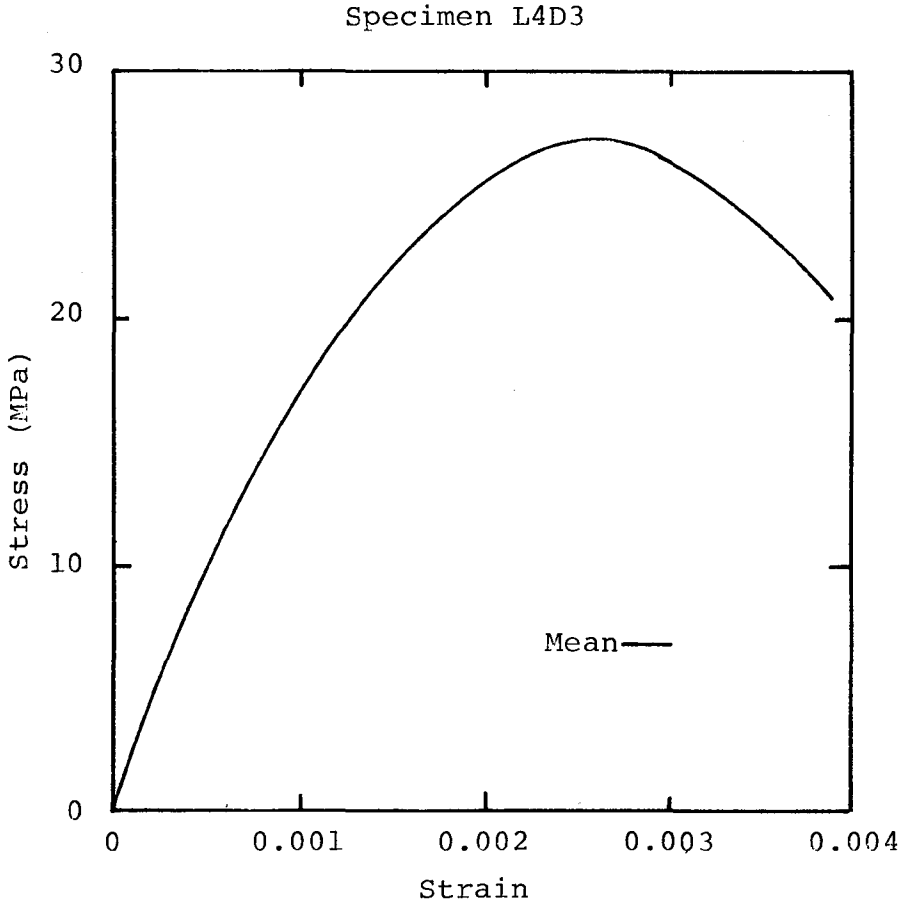

Property	Number of Samples	Mean (MPa)	Std. Dev. (MPa)
Compressive Strength	7	27.4	2.80
Modulus of Rupture	6	3.72	0.69
Splitting Strength	5	2.89	0.35

Fig. 2.7(b) Measured Concrete Properties, L4D3

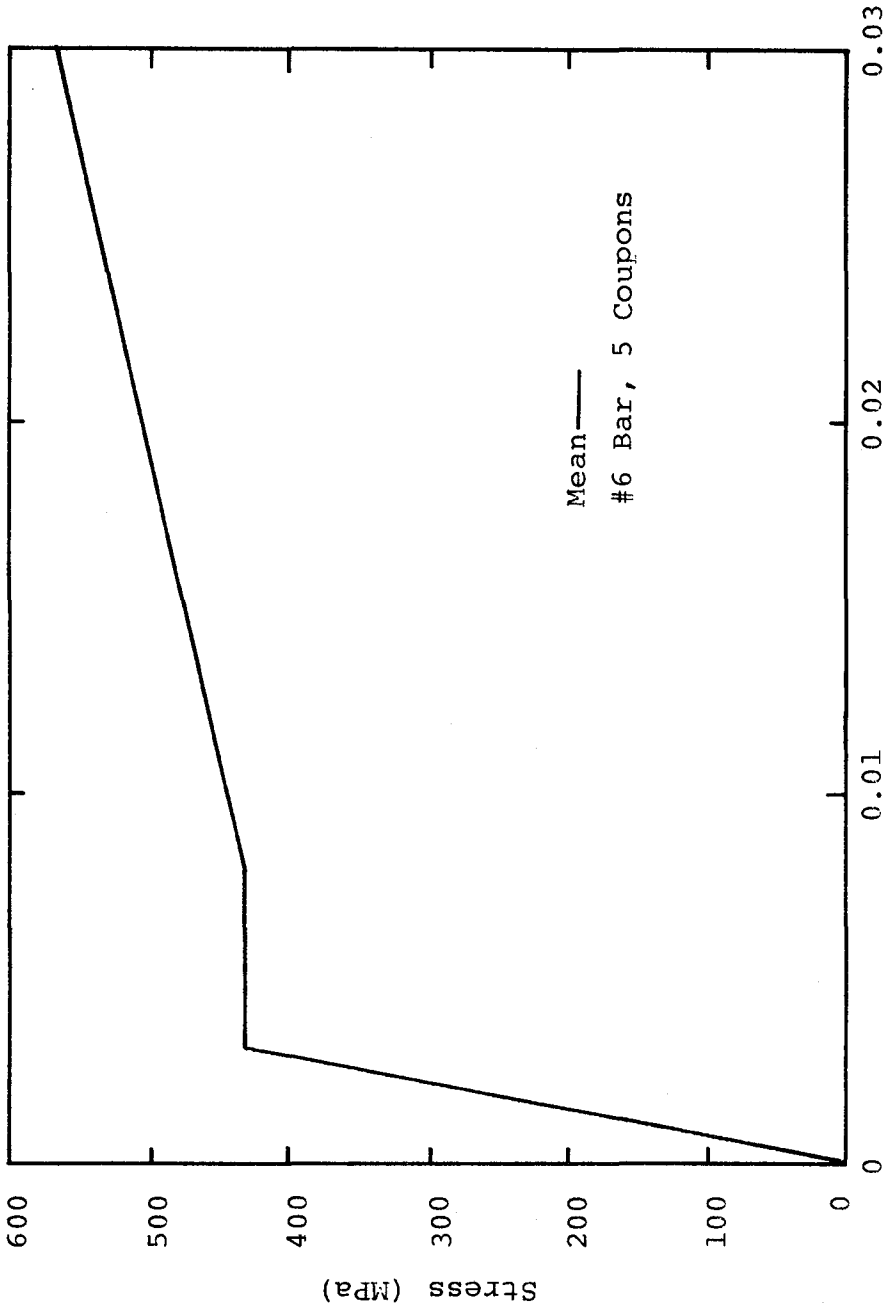

Fig. 2.8 Measured Stress-Strain for Longitudinal Reinforcement

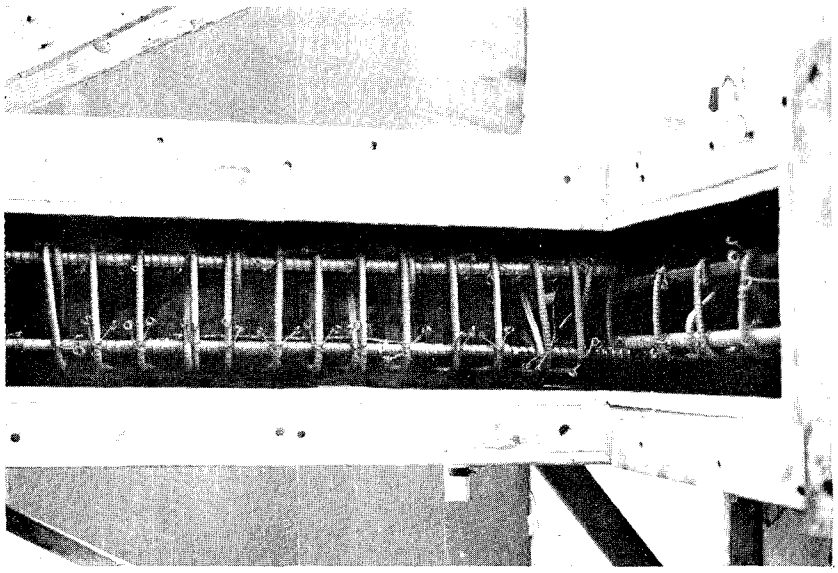

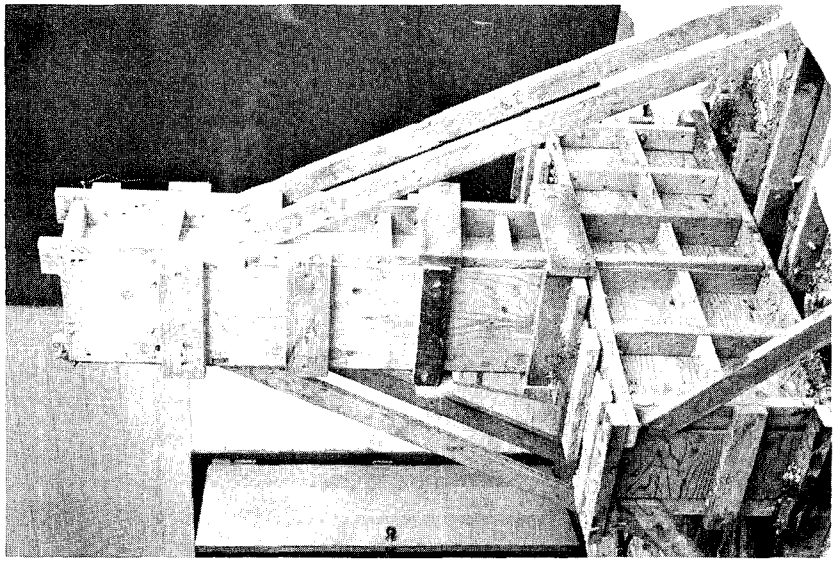

Fig. 2.9 Formwork and Reinforcing Cage

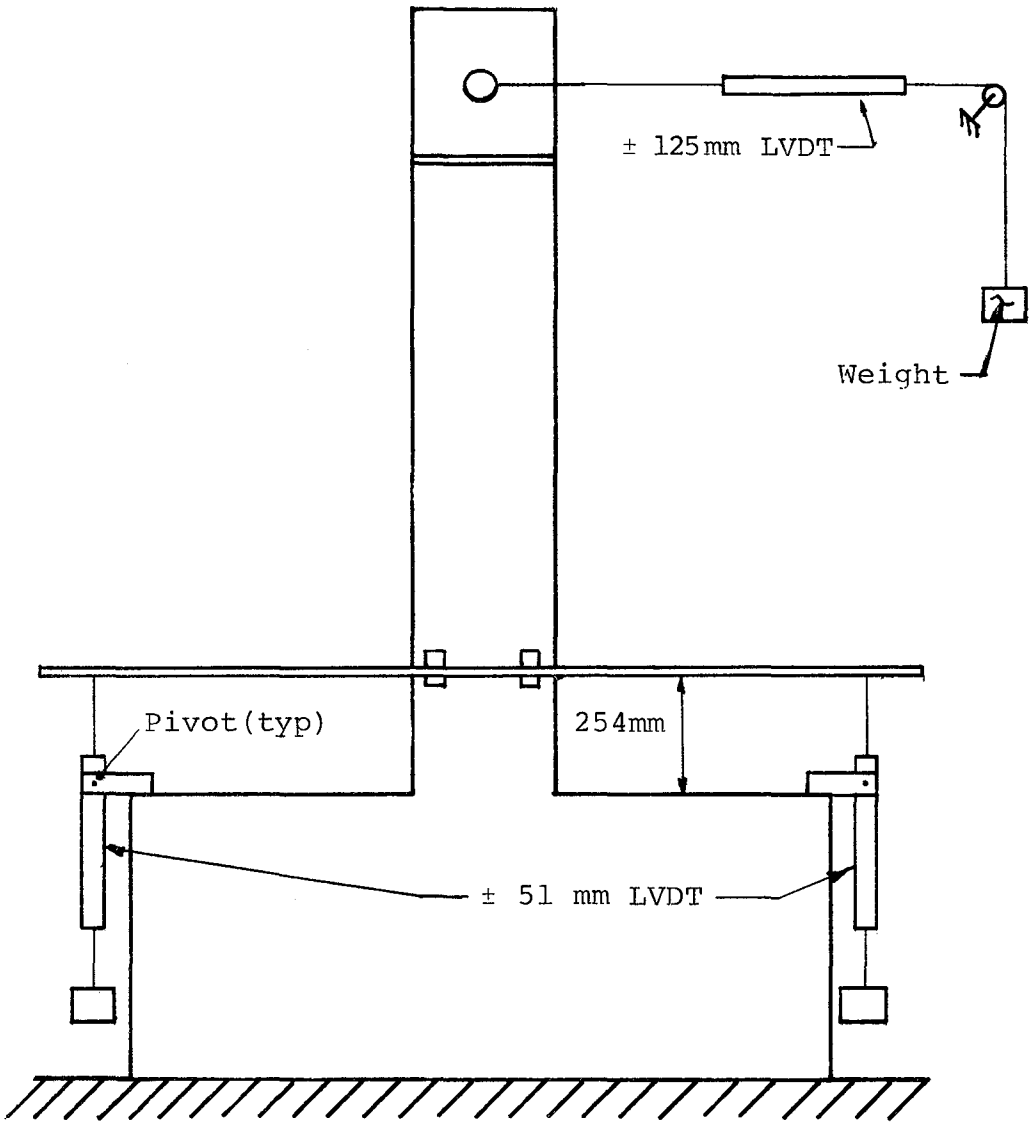

Fig. 2.10 Instrumentation

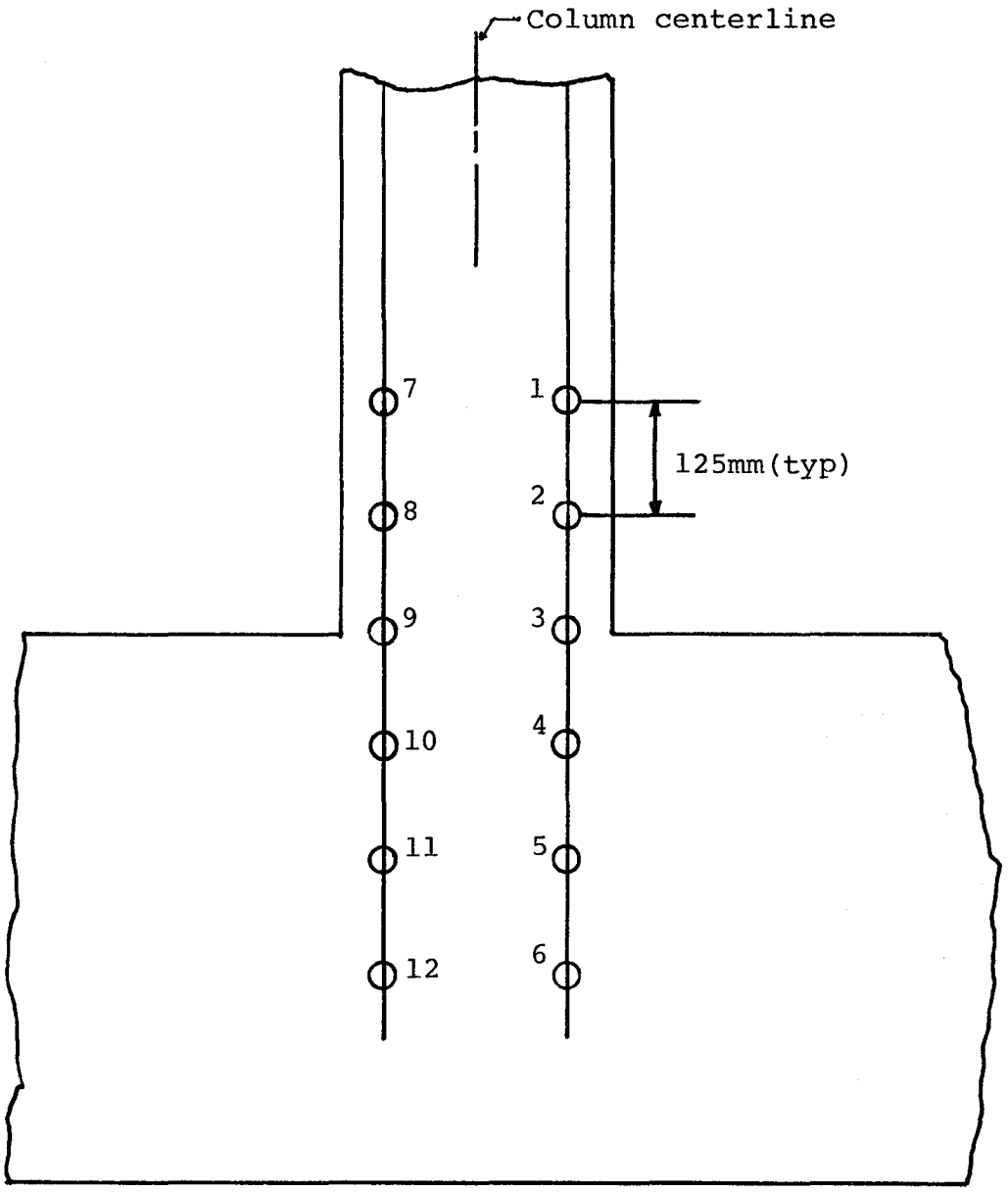

Fig. 2.11 Location of Strain Measurements

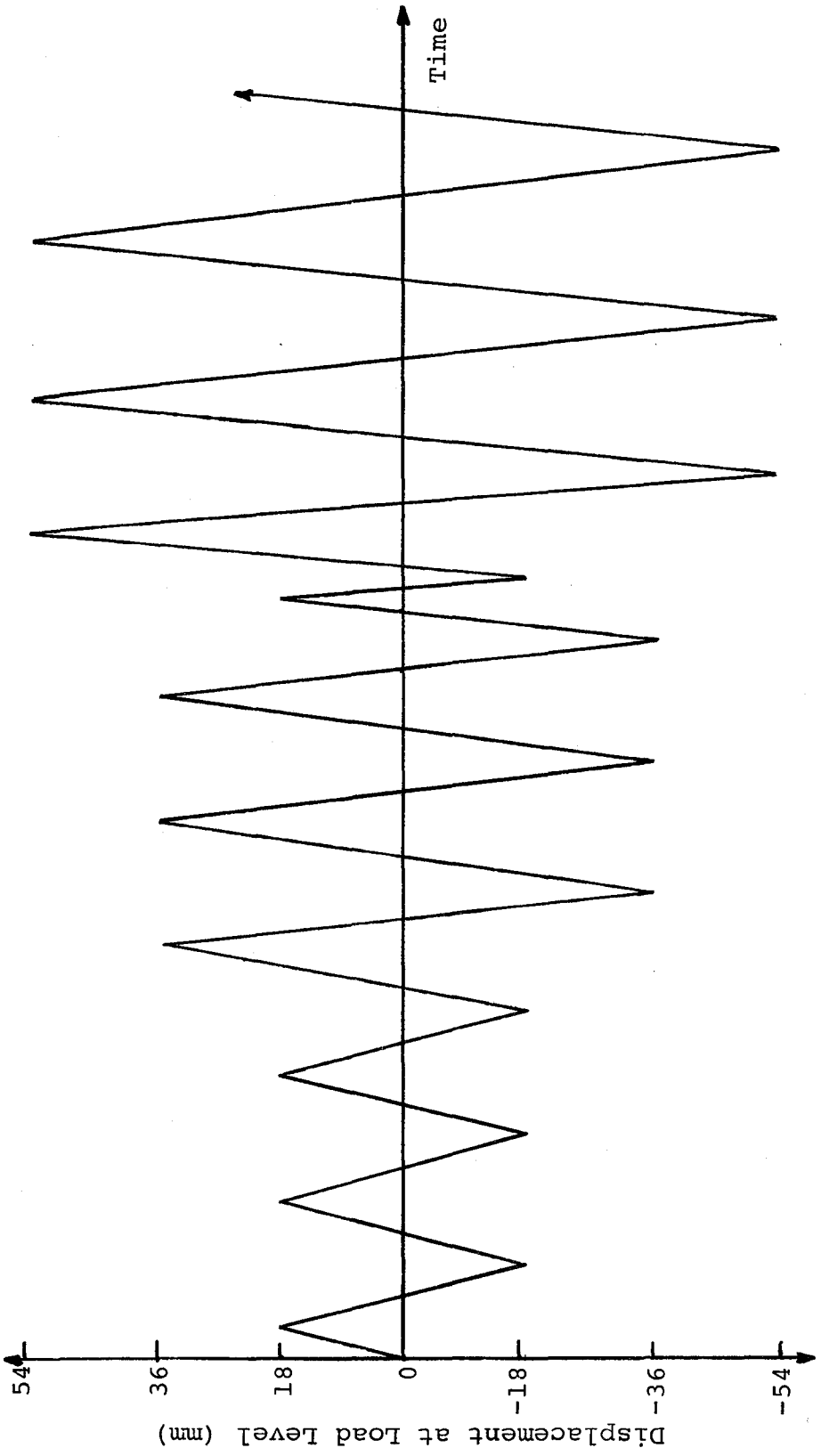

Fig. 2.12 Displacement History

CHAPTER III

OBSERVED BEHAVIOR

3.1 General

Two column specimens were tested: one with a light dead load, L4D2, and one with a heavy dead load, L4D3. The behavior of each specimen is presented in this chapter in terms of measured response, recorded observations and photographs.

3.2 Column Specimen L4D2

A vertical load equal to 117 KN, representing dead load in a multistory building, was applied to the specimen. This load was scaled so that the results could be compared directly with the small-scale test. This was accomplished by imposing the same state of normal stress on both large- and small-scale specimens (see Appendix B). By doing so, it was determined that the large-scale dead load should be the square of the length scale factor times the small-scale dead load. Measured relationships of the applied load with displacement, rotation and reinforcing strains are presented in Fig. 3.1 (a-l). Photographs of the base region are shown in Fig. 3.2, and measured widths of significant cracks are presented in Fig. 3.3.

Loading in the first half cycle (Fig. 3.4) consisted of a constantly decreasing axial compression combined with the lateral load. Eventually, at a lateral load of 29 KN, the net axial force applied to the specimen was tensile. The first crack was observed at the base at a load of 11 KN whereas the calculated cracking load (based on the uncracked section and measured material properties, Sec. 2.4) was found to be 9.2 KN. The uncracked stiffness (ratio of load to displacement) was calculated to be 20% larger than the measured stiffness up to this load point. With the development of flexural cracks the stiffness of the column decreased significantly. The observed stiffness was nearly half of the calculated stiffness for the first quarter cycle. Unloading in the first half cycle showed a stiffness identical to the cracked stiffness after an initial decrease in the load. Closure of the flexural cracks was observed during unloading.

As loading proceeded into the second half of cycle one (increasing axial compression) the first flexural crack was observed at a load of 18 KN. The calculated cracking load was 14.1 KN. The calculated stiffness was 25% larger than the observed stiffness. As seen in the first half cycle, unloading was accompanied by closing of the flexural cracks. A summary of crack widths and patterns is shown in Fig. 3.3.

Observations of the general hysteretic behavior for subsequent cycles are listed below.

1. The curves are not symmetric about the axis of zero load. The column was consistently stiffer in regions of increasing compressive axial load (lower half of figure) as compared to regions of decreasing compressive load.

2. The shapes of the load vs. rotation (Fig. 3.1e) and load displacement (Fig. 3.1a) curves were nearly identical, indicating that behavior of the base region dominated overall response of the specimen.

3. A significantly softer response was observed subsequent to the fourth cycle when the maximum displacements were doubled (Fig. 3.1c).

4. Also for the first cycle of Phase II (the fourth cycle), regions of nearly zero stiffness at maximum loads were observed for both increasing and decreasing compressive axial loads. This behavior was attributable to yielding of longitudinal reinforcement as seen by strain measurements (Fig. 3.1j).

5. Unloading slopes for Phases I and II were nearly identical and did not decrease when a new maximum displacement was reached.

6. In the region of increasing axial compression, Phase III (Fig. 3.1d), a decrease in stiffness was observed upon loading after a new maximum was reached.

7. A slight decrease in strength was observed only in the region of increasing axial compression.

3.3 Column Specimen L4D3

A vertical load equal to 330 KN, representing dead load in a multistory building, was applied to the specimen. This load was chosen to simulate the normal stress (5 MPa) in a representative full-scale structure. This was a divergence from that in the small-scale models in an attempt to illustrate differences in behavior due to inconsistent scaling of gravity loads. Measured relationships of the applied load versus the rotation, displacement and selected reinforcing strains are shown in Fig. 3.5. Photographs of the column and damage in the base region are presented in Fig. 3.6.

Although the displacement history was identical to that for column Specimen L4D2, the load-deflection relationship was markedly different. The axial force for the first half cycle of loading (Fig. 3.5a) was a constantly decreasing axial compression. Because of the large initial load, no net axial tensions resulted. Flexural cracks were observed first at a load of 22 KN. The cracking load, based on material properties

and the uncracked section was calculated to be 16.7 KN. Up to this load point, the measured stiffness was approximately 7% less than the calculated stiffness. With progressive flexural cracking, the stiffness of the column gradually reduced to a negligible quantity. This was a distinct departure from the behavior of Specimen L4D2 for the first quarter cycle of loading. The calculated stiffness, considering a cracked section, was 40% larger than measured nominal stiffness. Initial unloading resulted in the closing of flexural cracks as the load approached zero.

Loading in the third quarter of cycle one saw flexural cracks appear at a load of 27 KN. The calculated cracking load for this region was determined to be 22 KN. There was no distinct change in the slope of the load deflection curve (Fig. 3.5a) when initial cracking was observed. Unlike the region of decreasing axial compression, the stiffness remained constant up to the point of maximum displacement and was observed to be 3.6 KN/mm. This value was 20% less than the calculated stiffness of 4.5 KN/mm. When the specimen was unloaded, the flexural cracks that developed on the third leg of the cycle closed.

In subsequent cycles of Phase I, no new cracks were observed to form. A significant decrease in strength was observed in the region of decreasing axial compression, due to a sudden drop in pressure sustaining the simulated dead load on

the previous cycle. Once the initial cycle was completed, a constant stiffness was observed (associated with the cracked section of each region) for both loading and unloading. A summation of measured crack widths of significant cracks at maximum loads is shown in Fig. 3.7 and the overall crack pattern is presented in Fig. 3.8.

Due to the necessary load-control mode of the actuator (Sec. 2.3) only three complete cycles were executed prior to a compression failure.

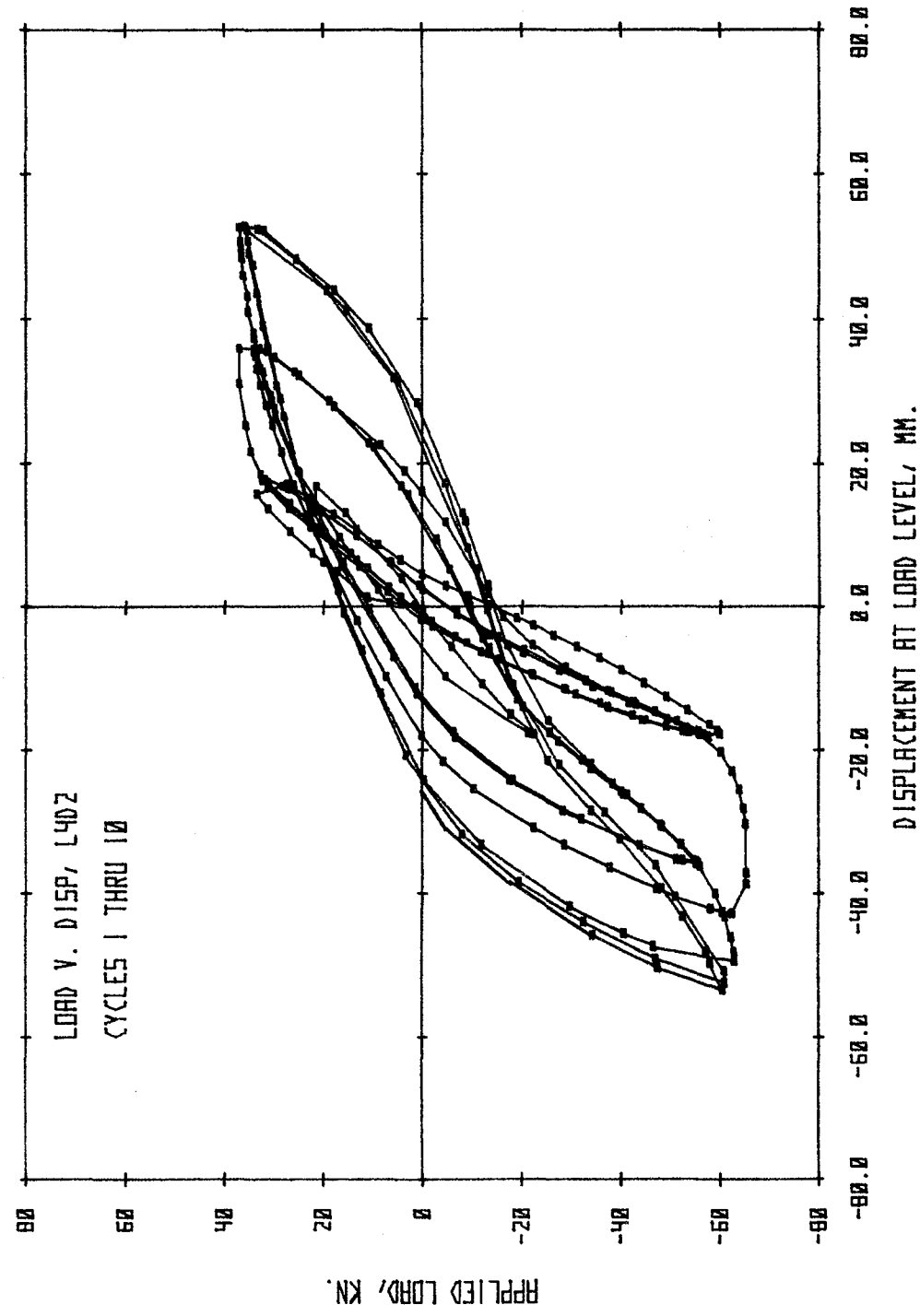

Fig. 3.1(a) Measured Response of Specimen L4D2

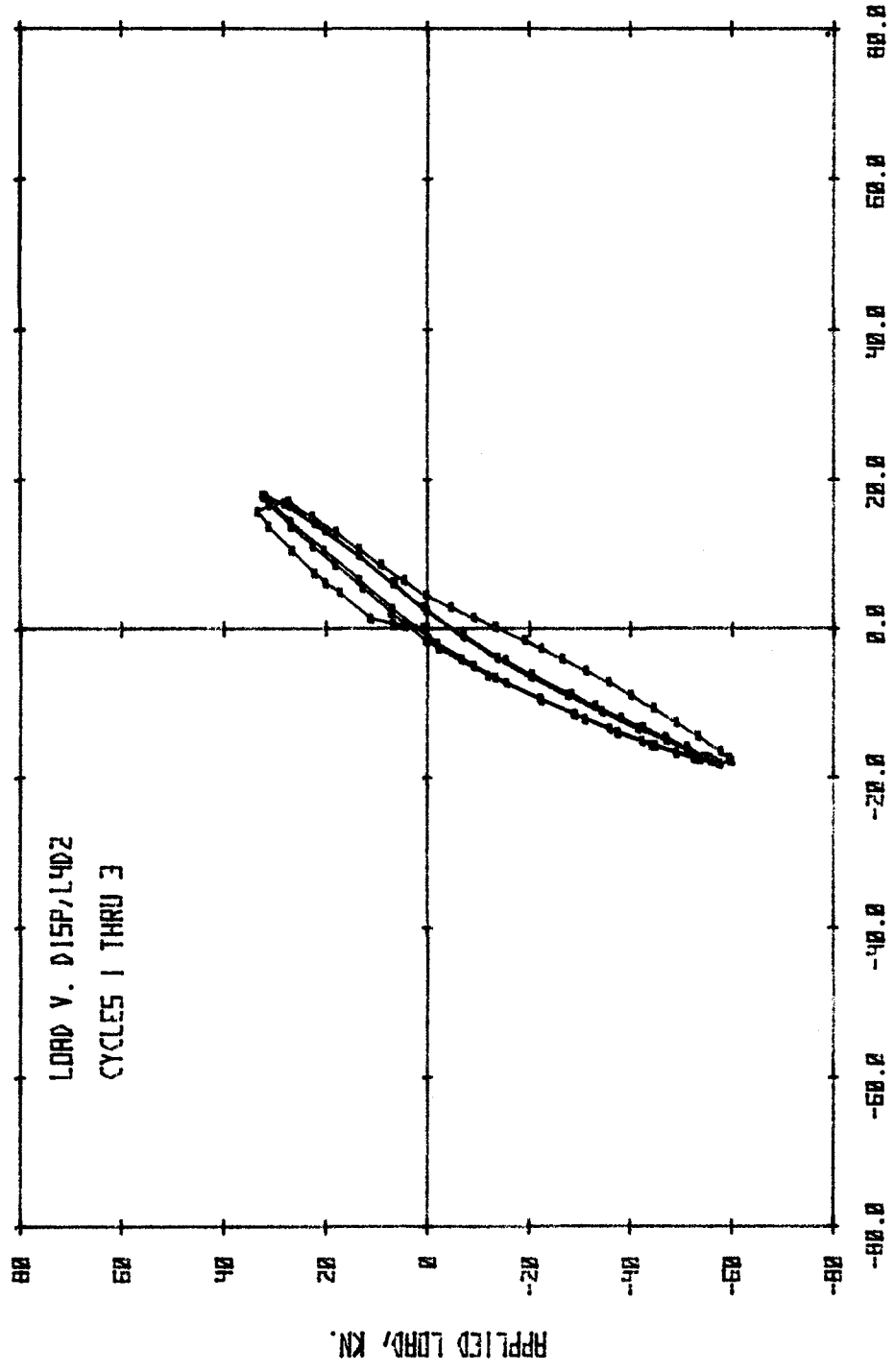

Fig. 3.1(b) Phase I, Measured Response of Specimen L4D2

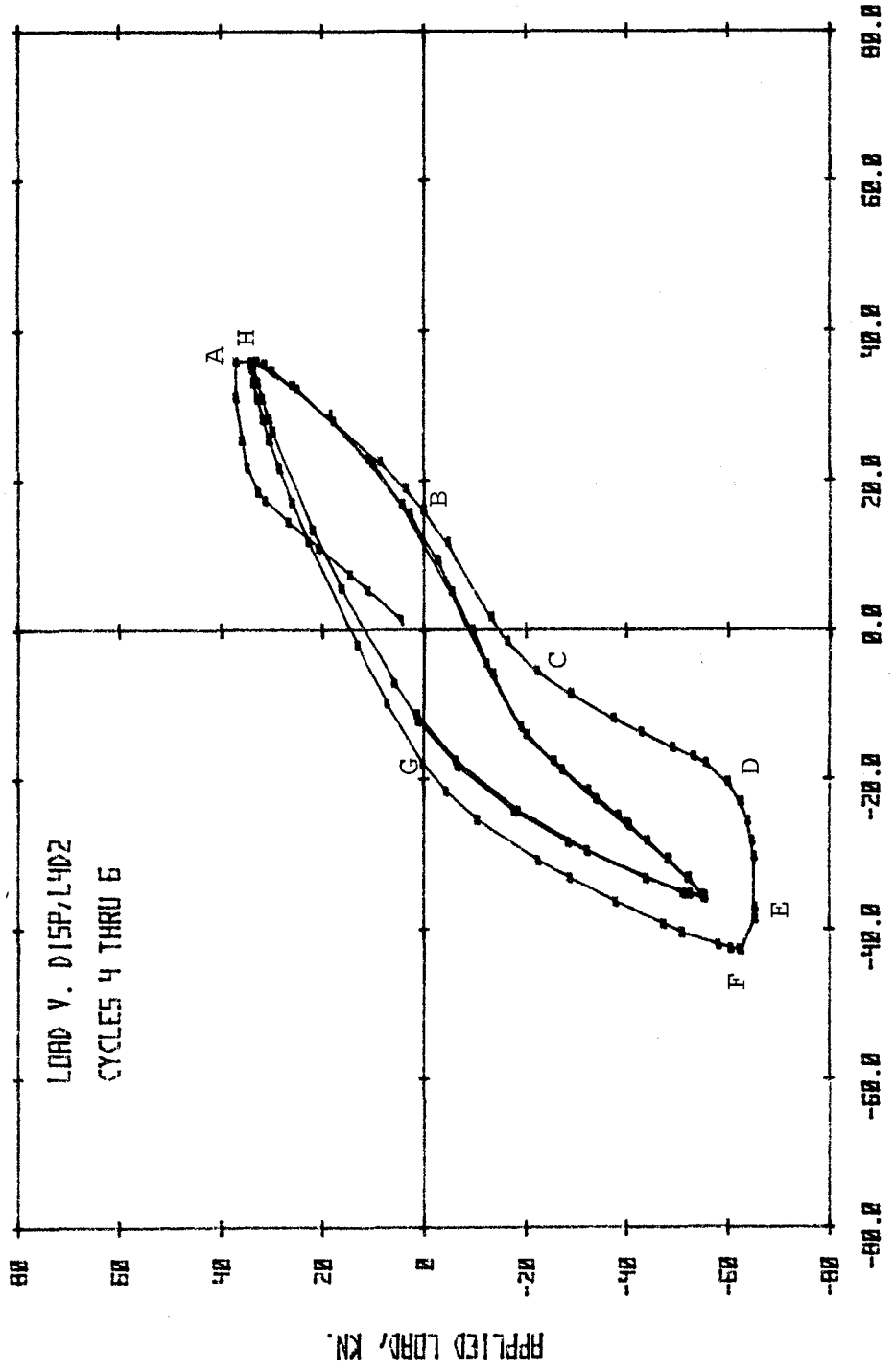

Fig. 3.1(c) Phase II, Measured Response of Specimen L4D2

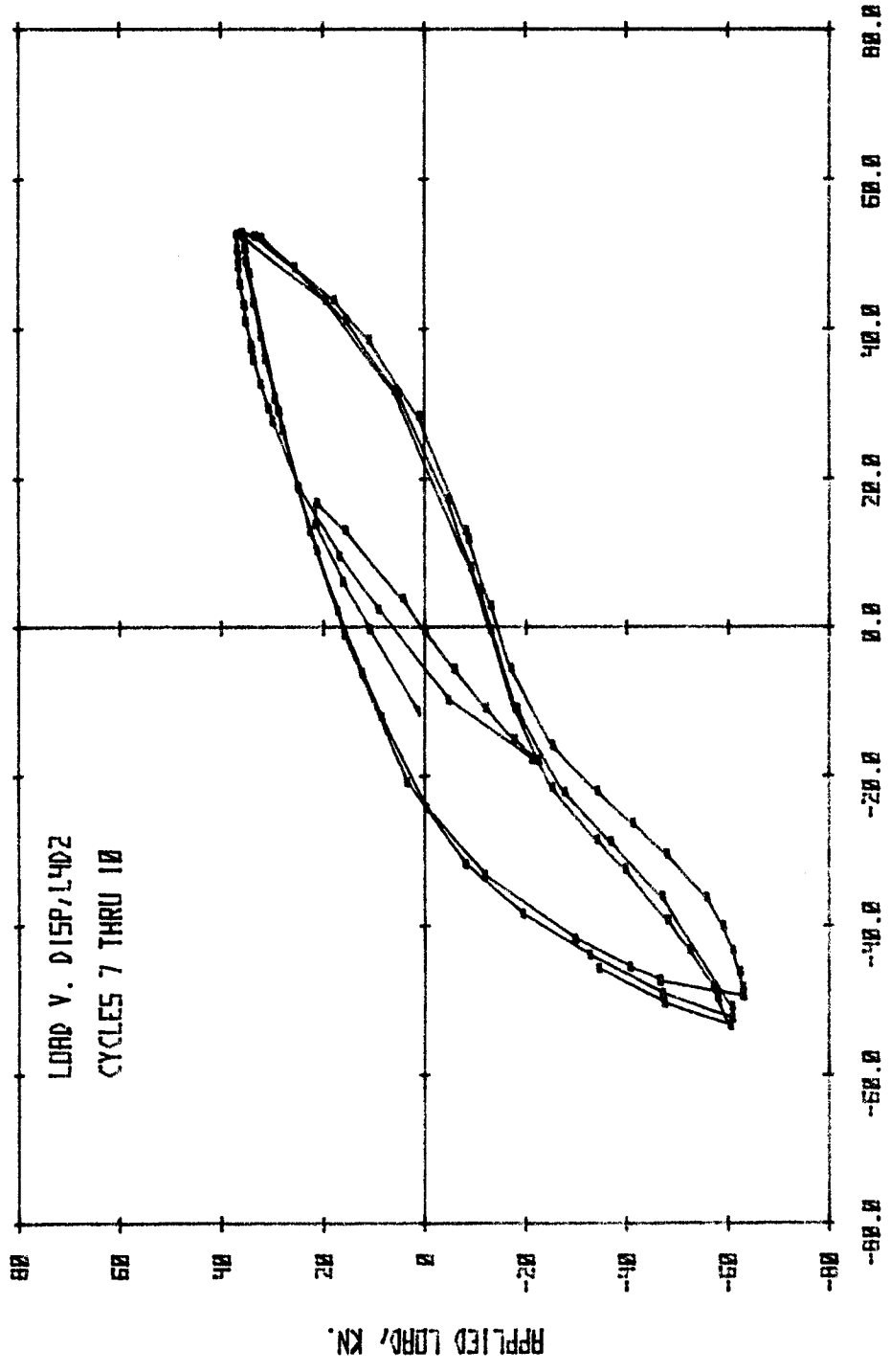

Fig. 3.1(d) Phase III, Measured Response of Specimen L4D2

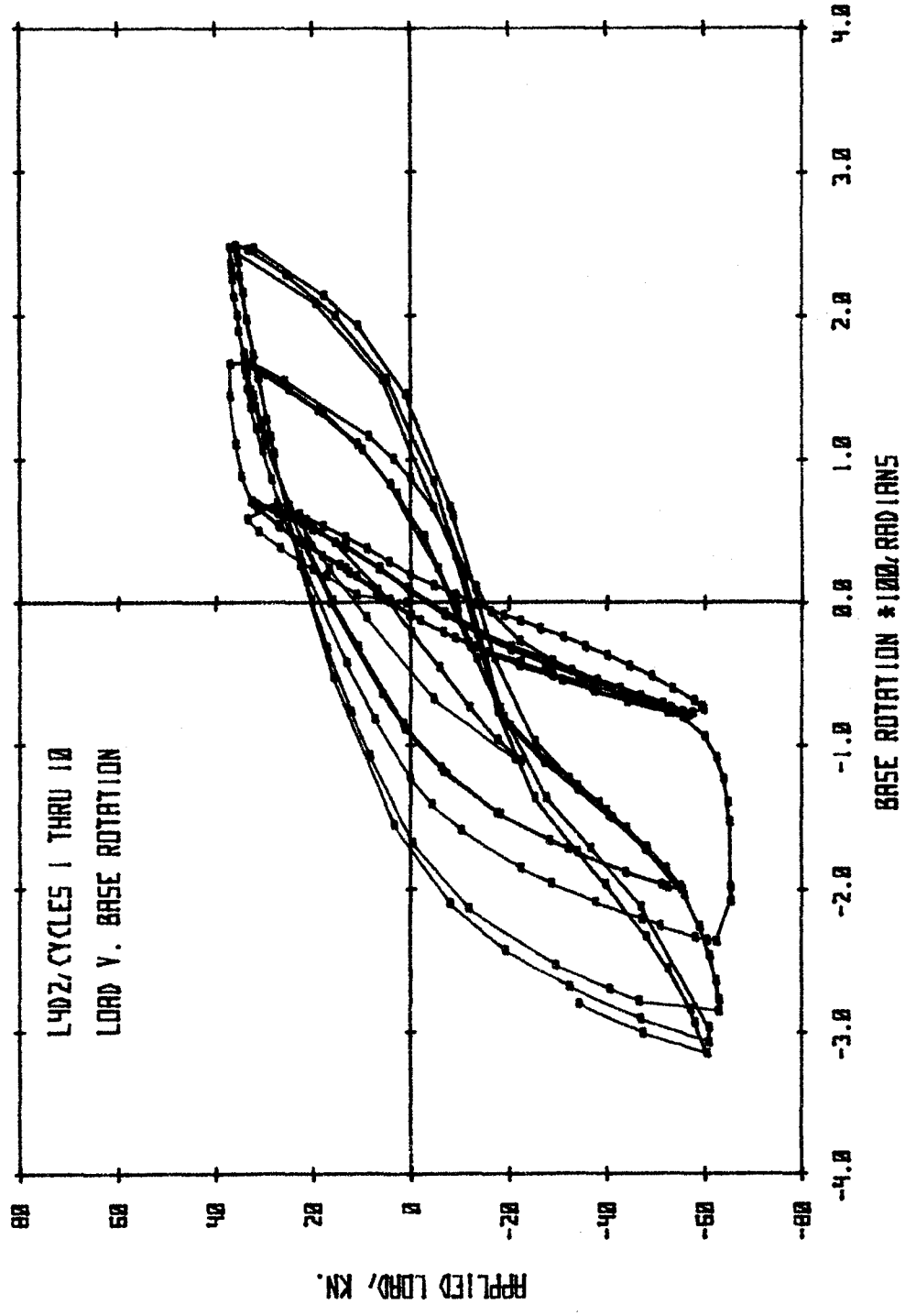

Fig. 3.1(e) Measured Response of Specimen L4D2

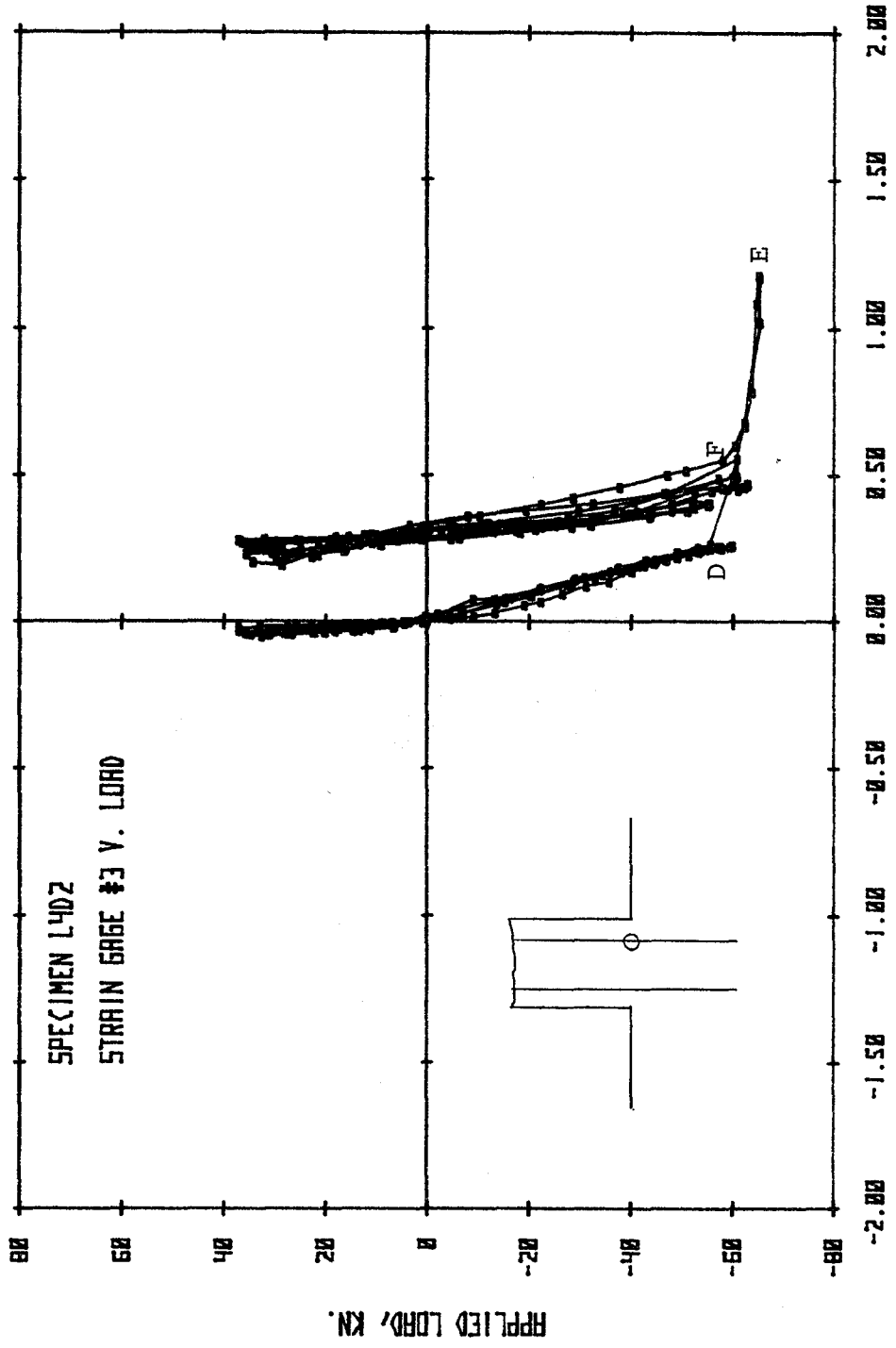

Fig. 3.1(f) Measured Response of Specimen L4D2

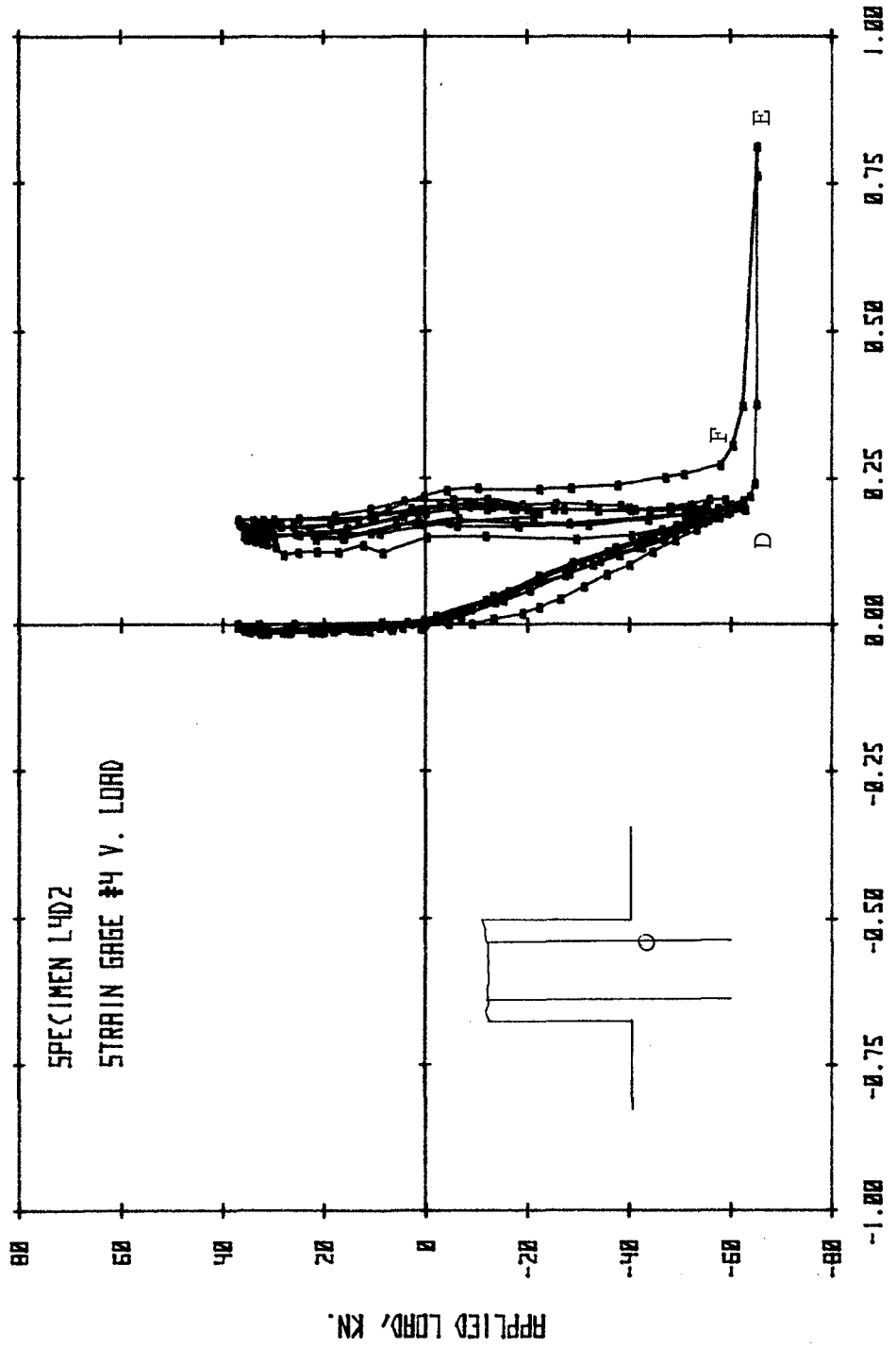

Fig. 3.1(g) Measured Response of Specimen L4D2

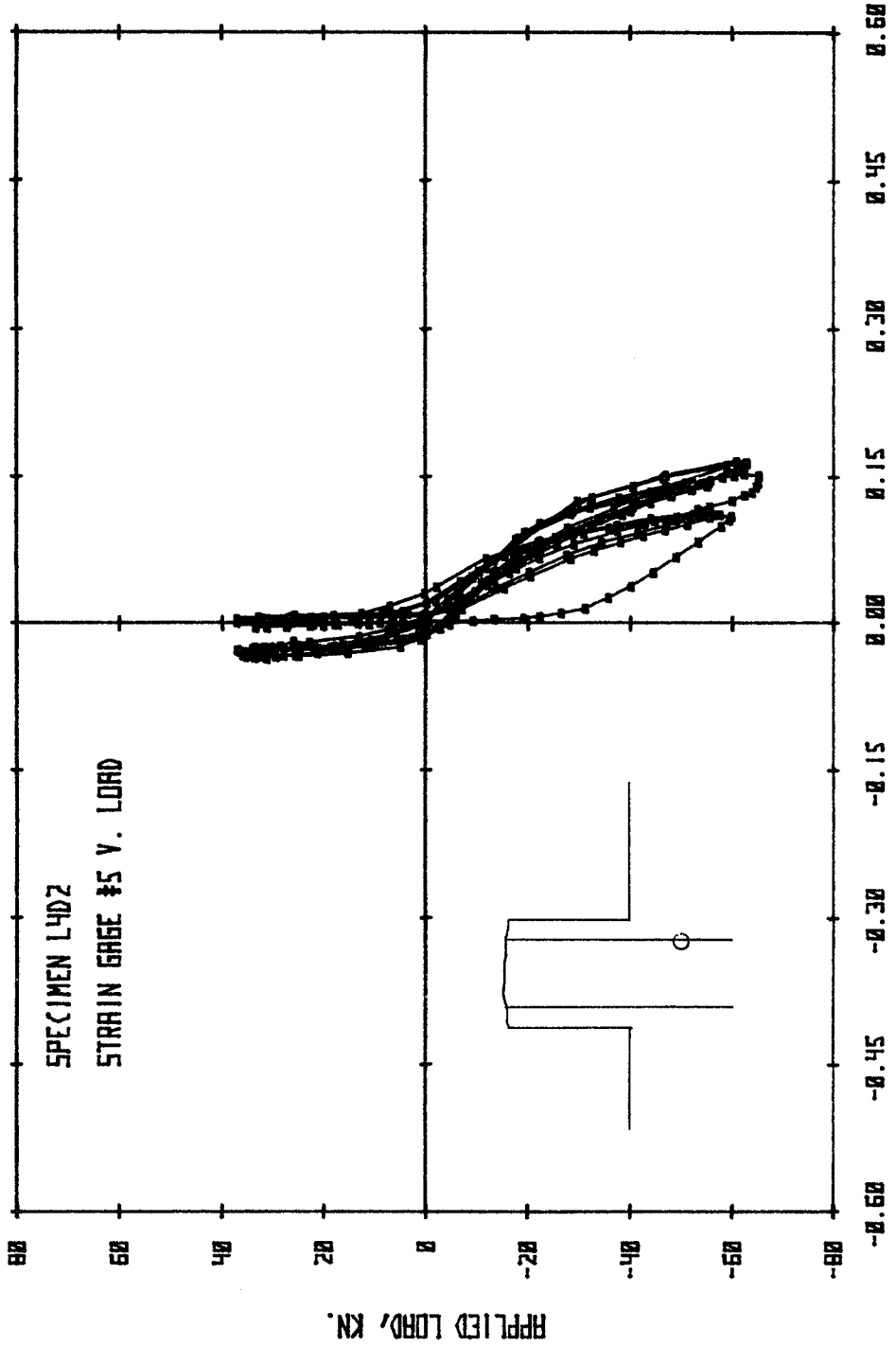

Fig. 3.1(h) Measured Response of Specimen L4D2

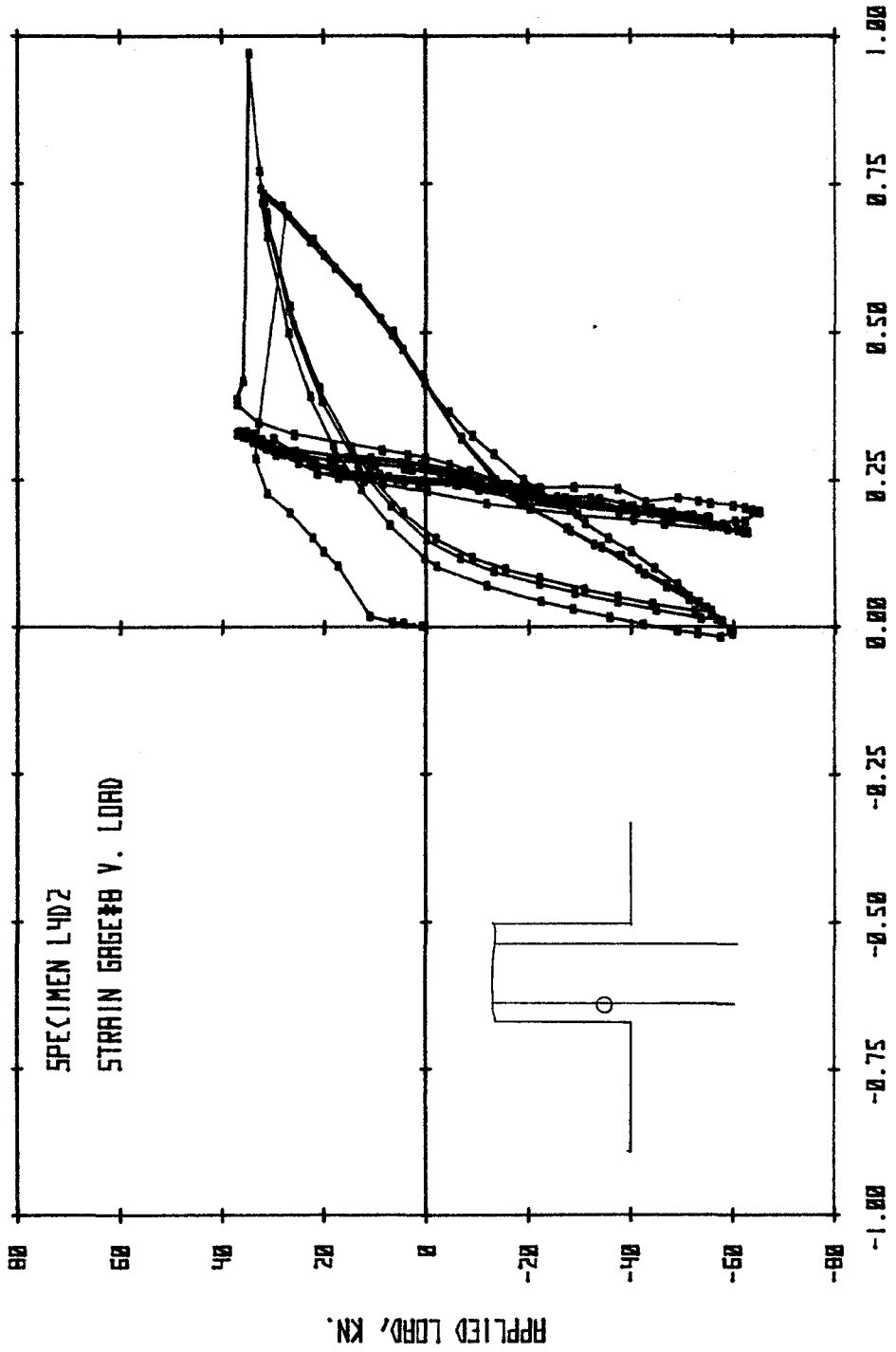

Fig. 3.1(i) Measured Response of Specimen L4D2

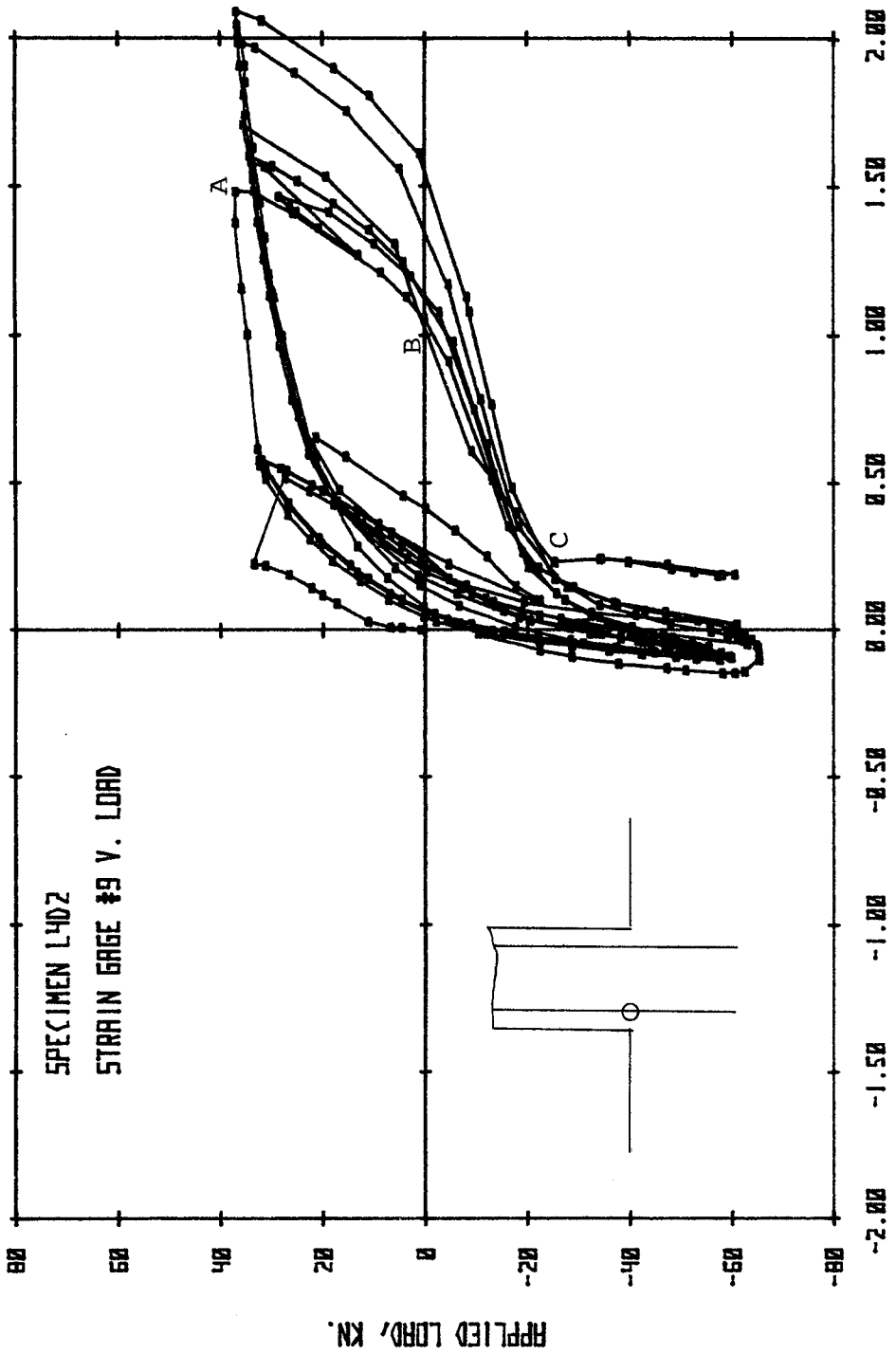

Fig. 3.1(j) Measured Response of Specimen L4D2

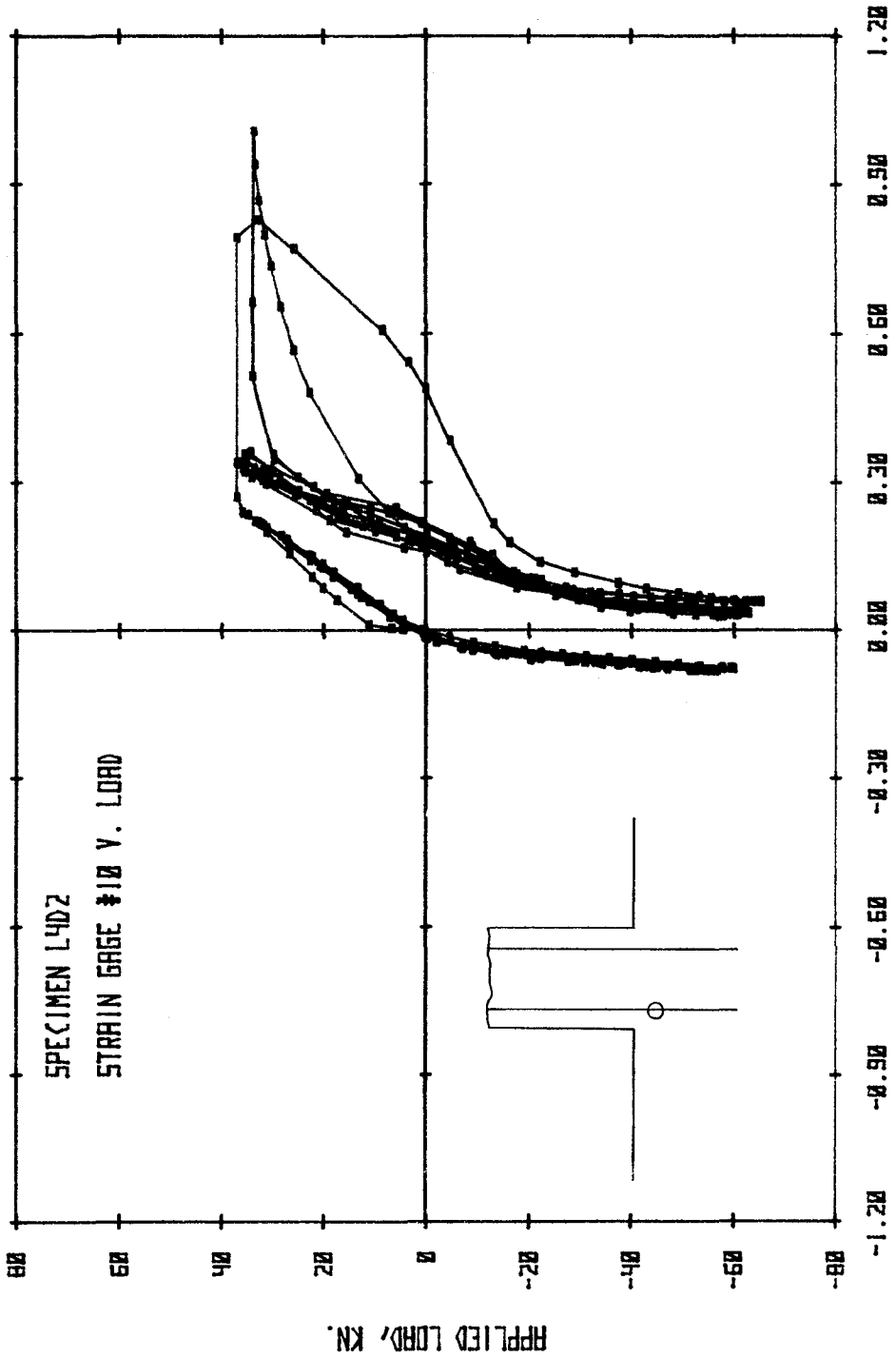

Fig. 3.1(k) Measured Response of Specimen L4D2

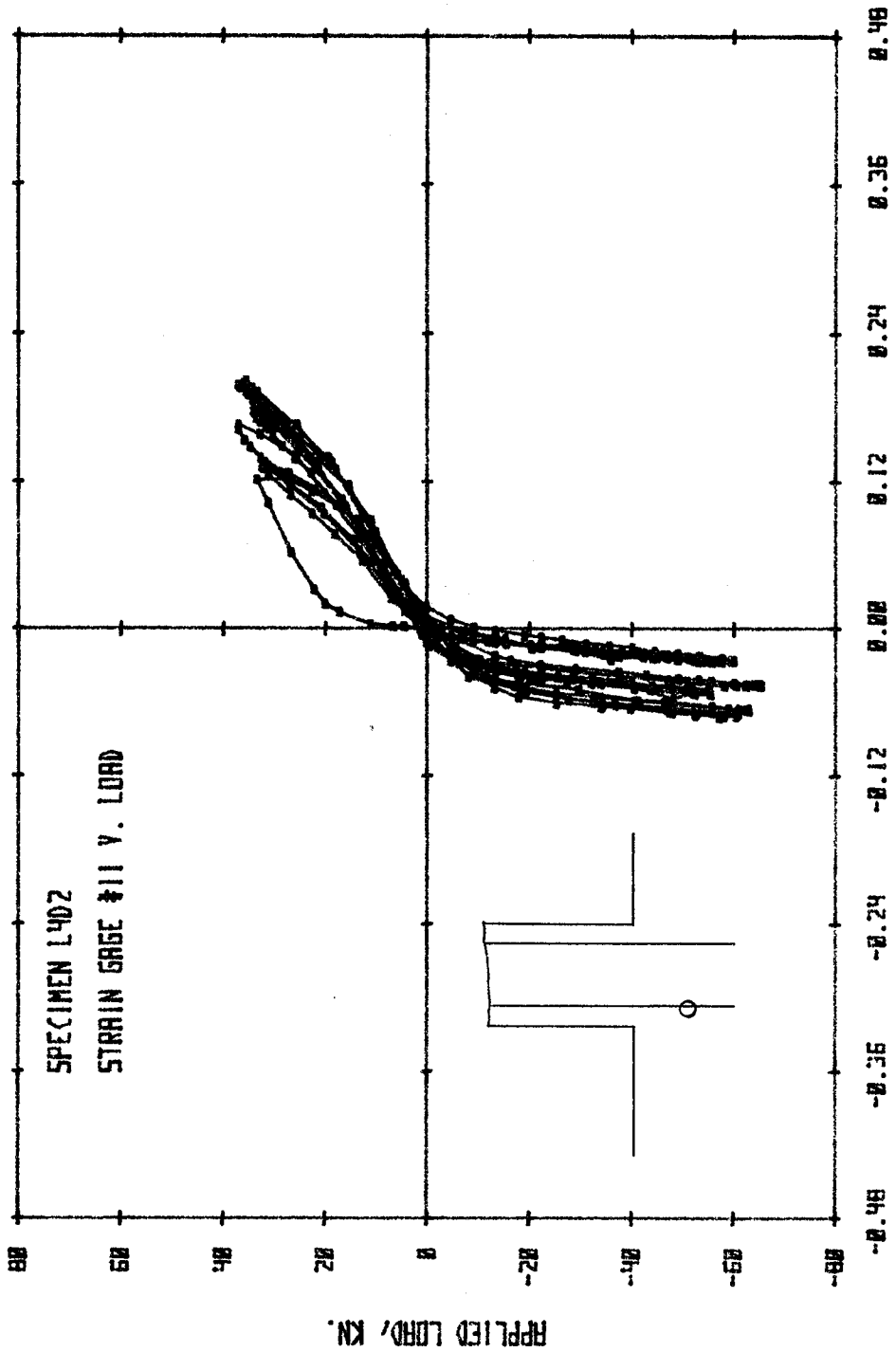

Fig. 3.1(1) Measured Response of Specimen L4D2

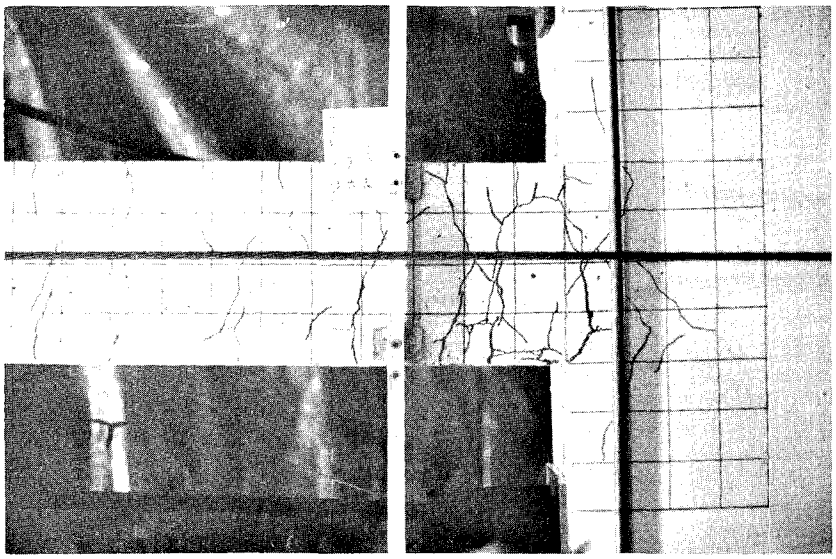

Cycle 8

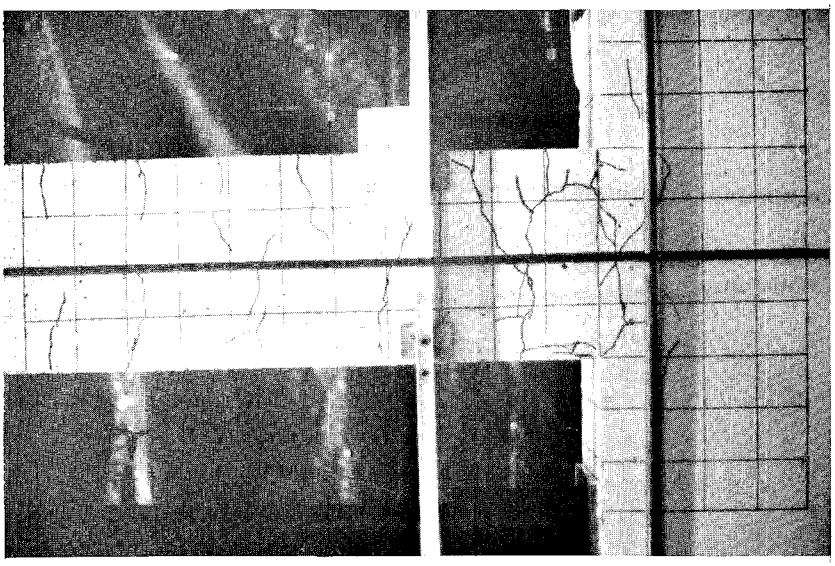

Cycle 4

Fig. 3.2 Photographs of Damage, Specimen L4D2

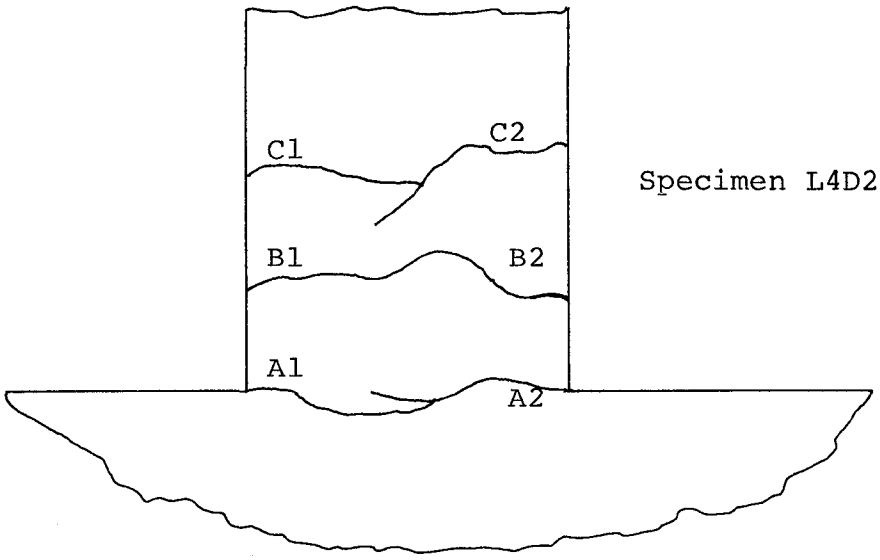

Measured Crack Widths at Maximum Loads (mm)						
Cycle #	A1	A2	B1	B2	C1	C2
1+	0.5	0	0.2	0	0.1	0
1-	0	0.8	0	0.3	0	0.1
4+	0.8	0	1.1	0	0.5	0
4-	0	2.3	0	1.1	0	1.6
8+	1.2	0*	1.8	0*	0.9	0*
8-	0**	3.4	0**	1.9	0**	2.4

* Only the portion of the crack from the steel to the outermost compression fiber, closed completely.

** Concrete crushed

Fig. 3.3(a) Measured Crack Widths, L4D2

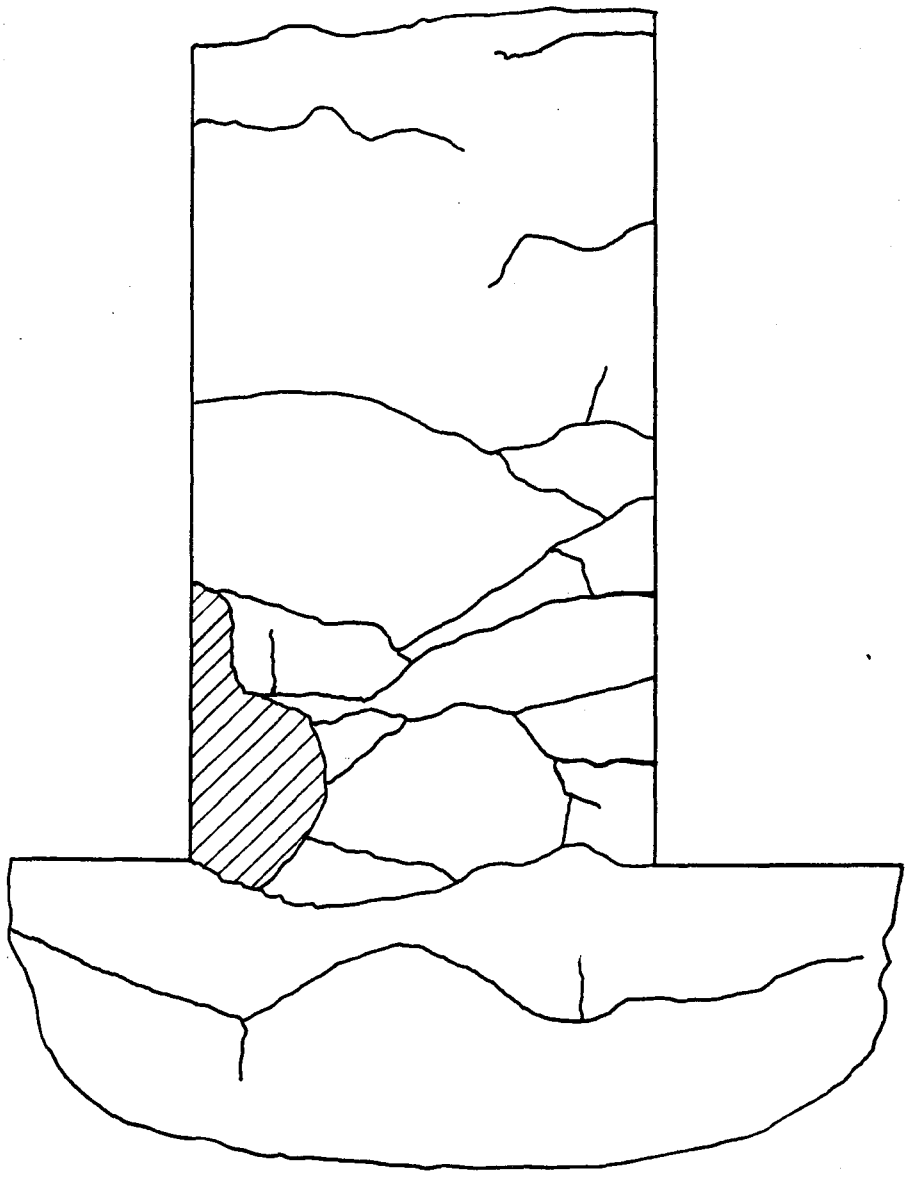

Fig. 3.3(b) Crack Pattern North Face, Specimen L4D2

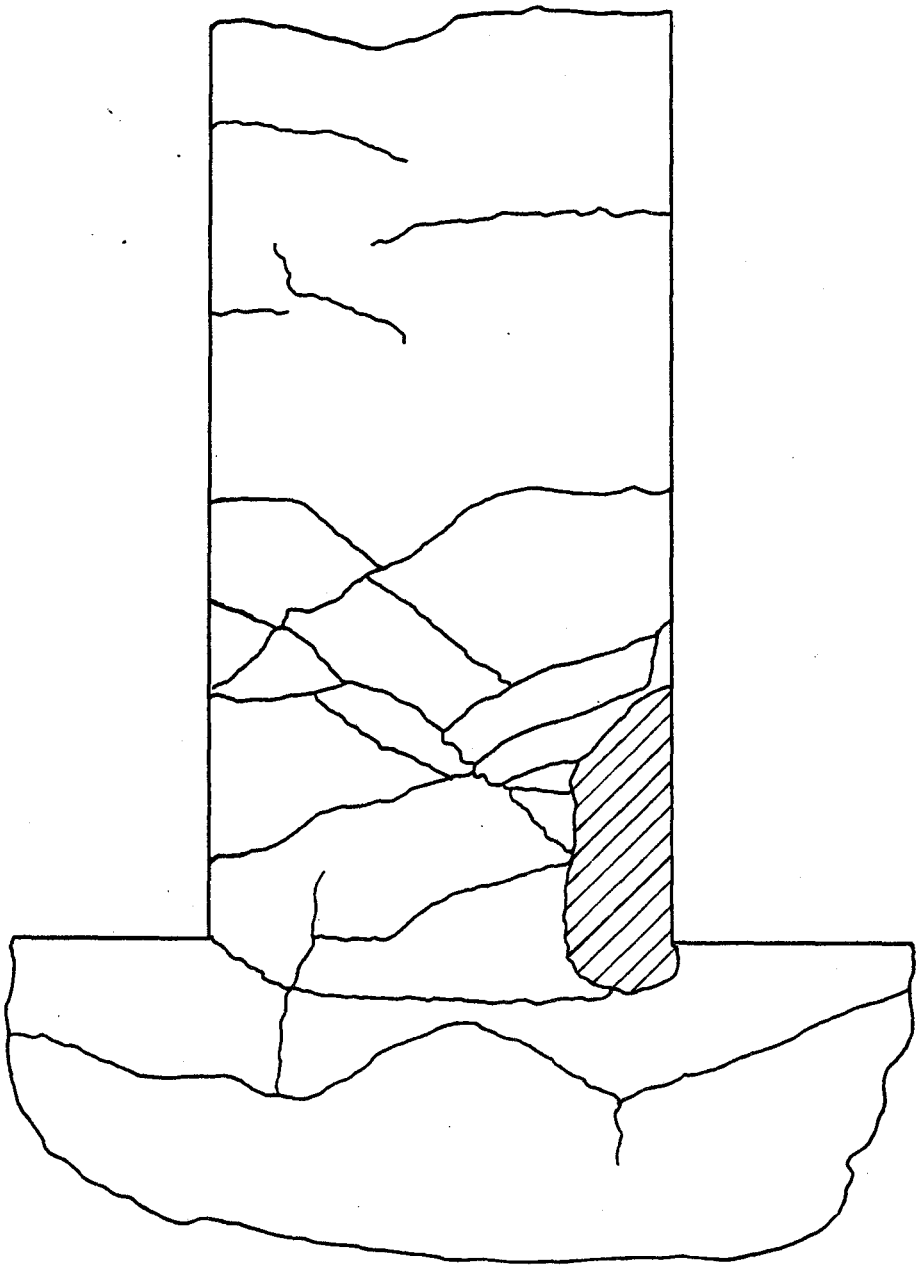

Fig. 3.3(c) Crack Pattern South Face, Specimen L4D2

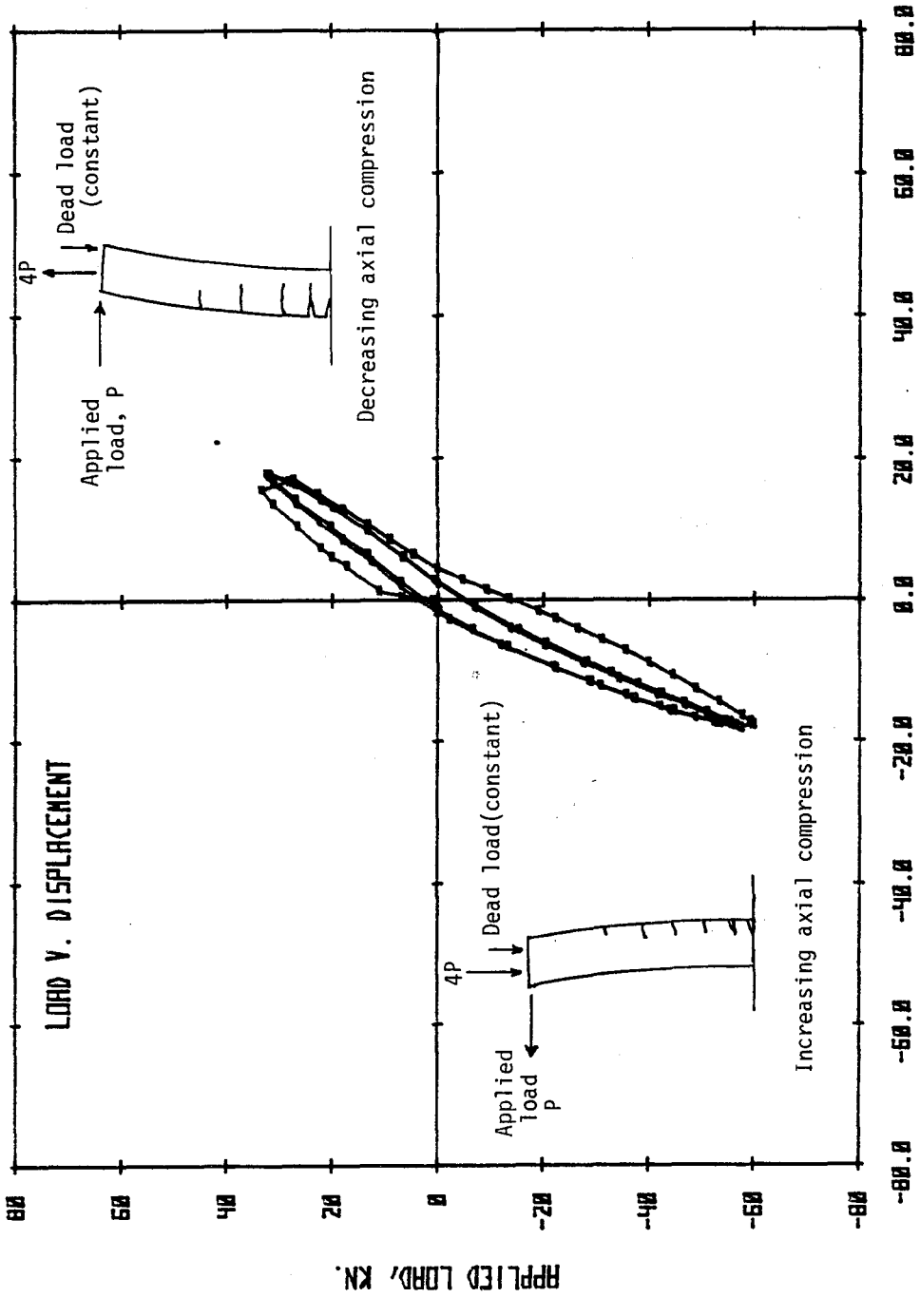

Fig. 3.4 Load Configuration

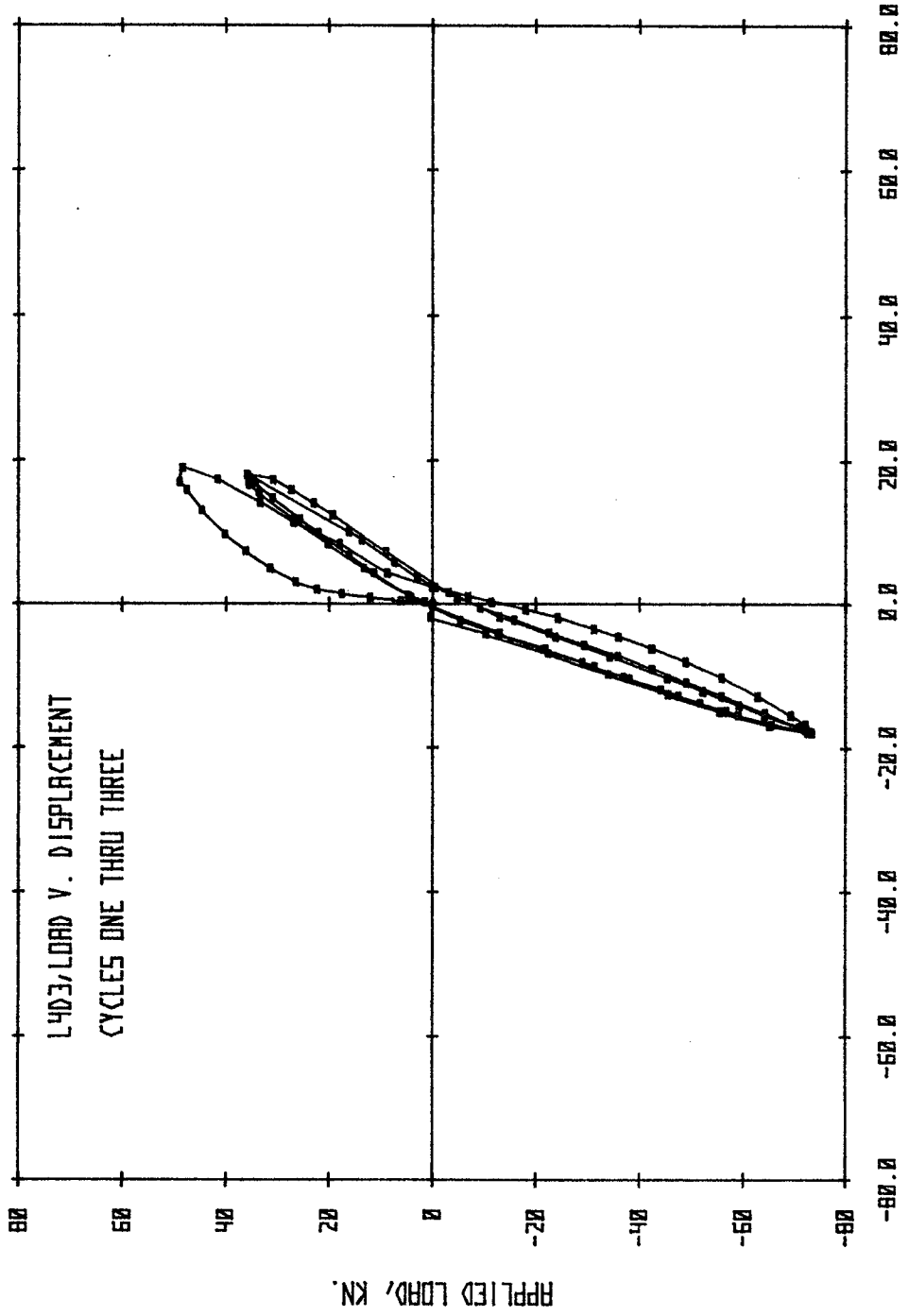

Fig. 3.5(a) Measured Response of Specimen L4D3

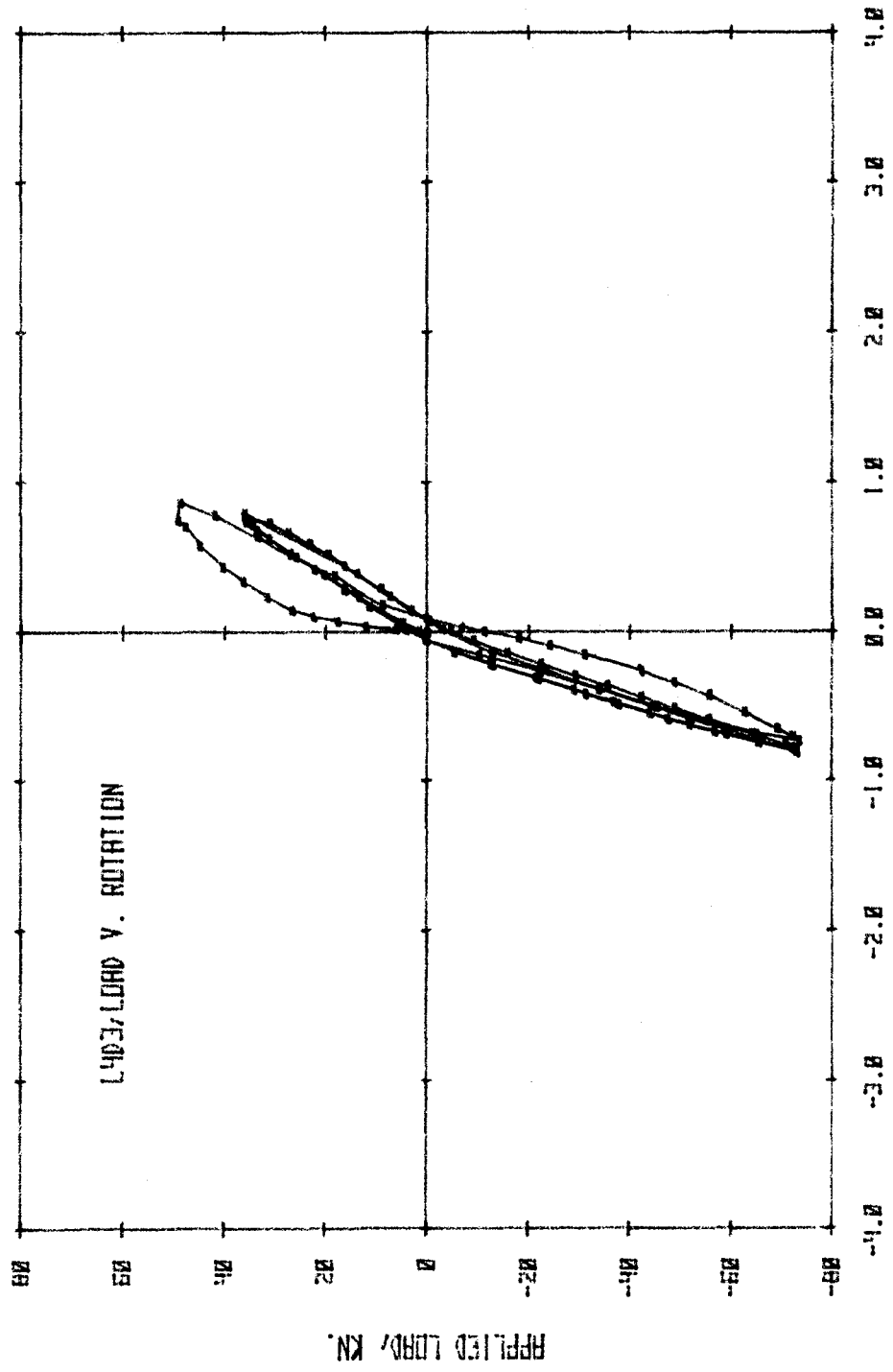

Fig. 3.5(b) Measured Response of Specimen L4D3

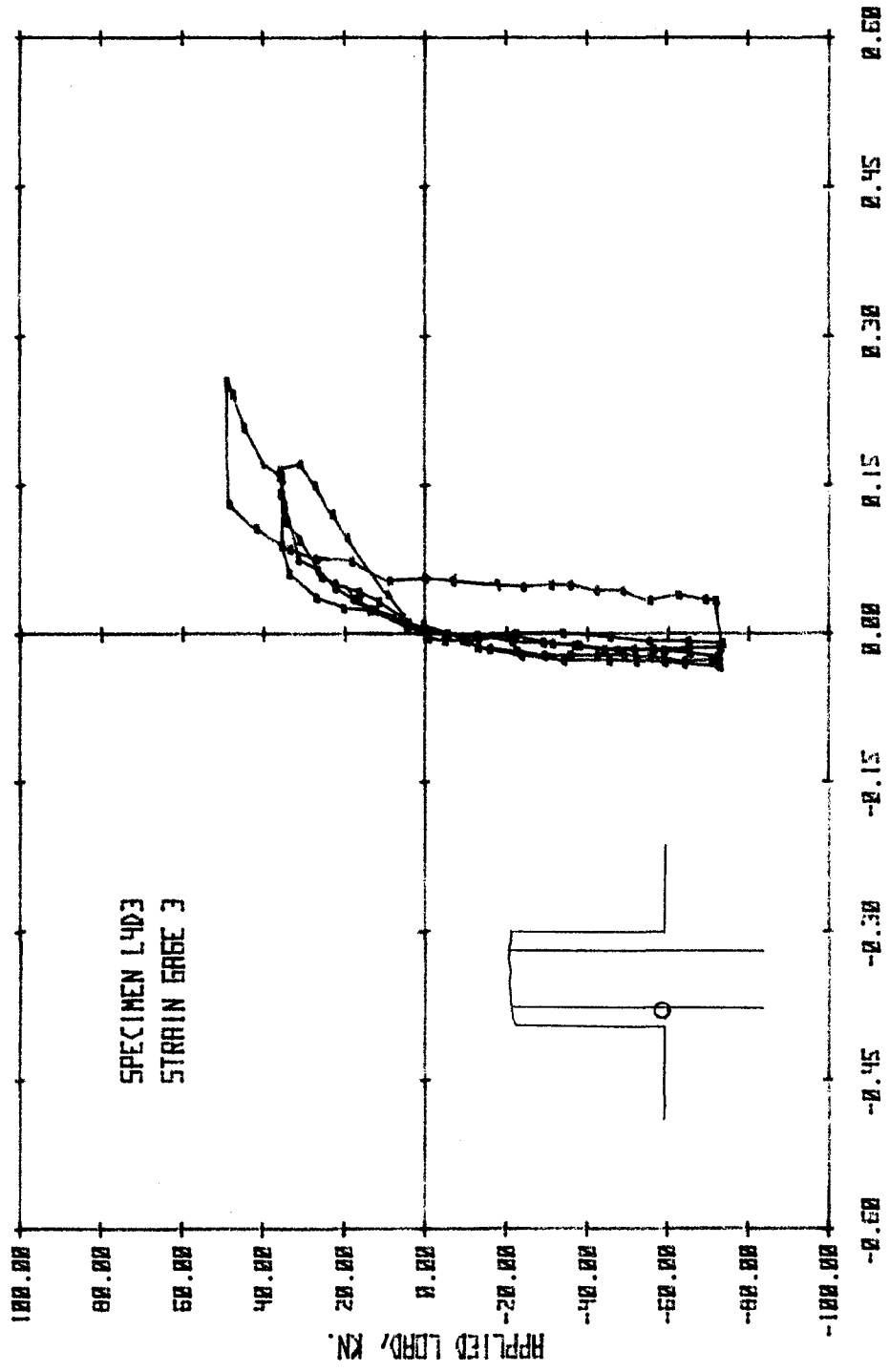

Fig. 3.5(c) Measured Response of Specimen L4D3

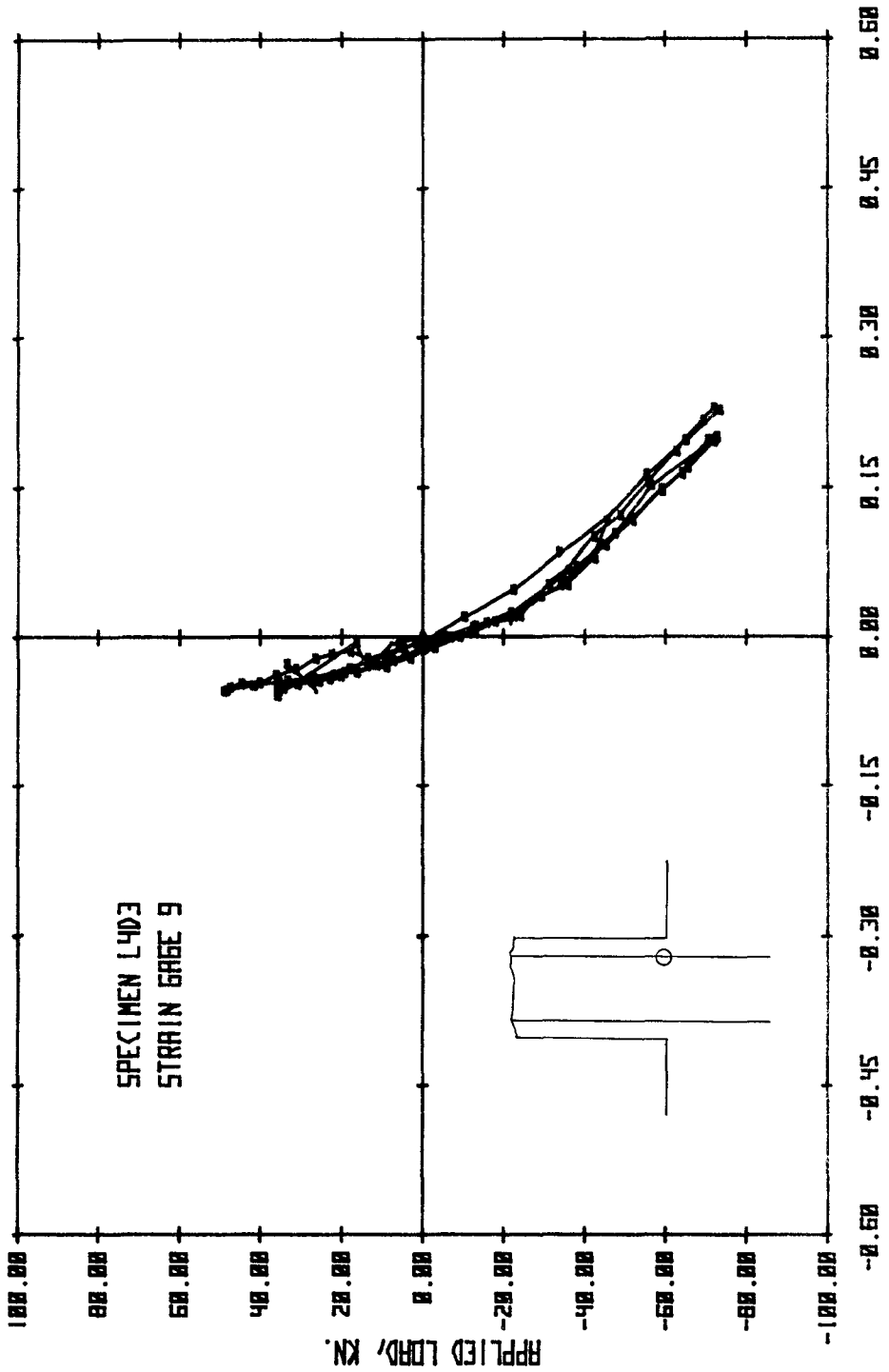

Fig. 3.5(d) Measured Response of Specimen L4D3

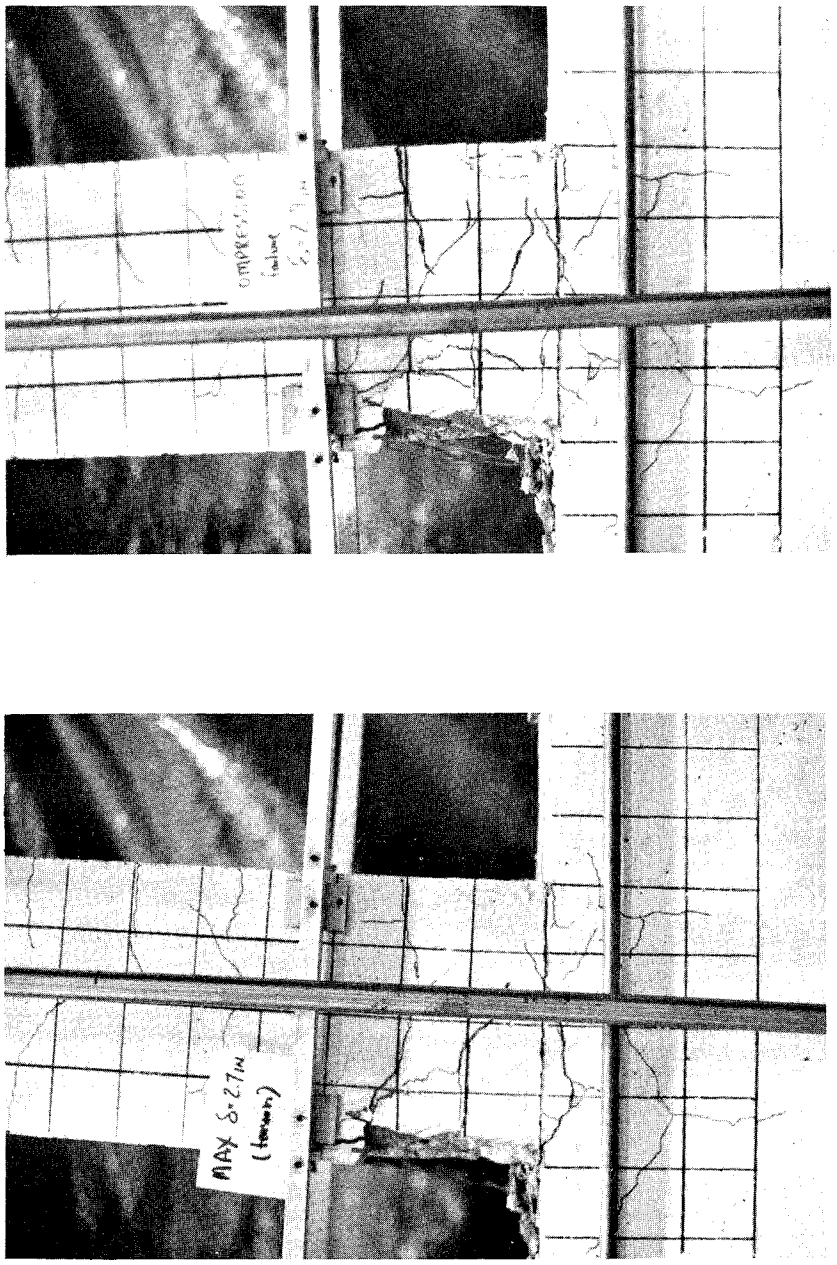

Max. + Disp.

Max. - Disp.

Fig. 3.6 Photographs of Damage, Specimen L4D3

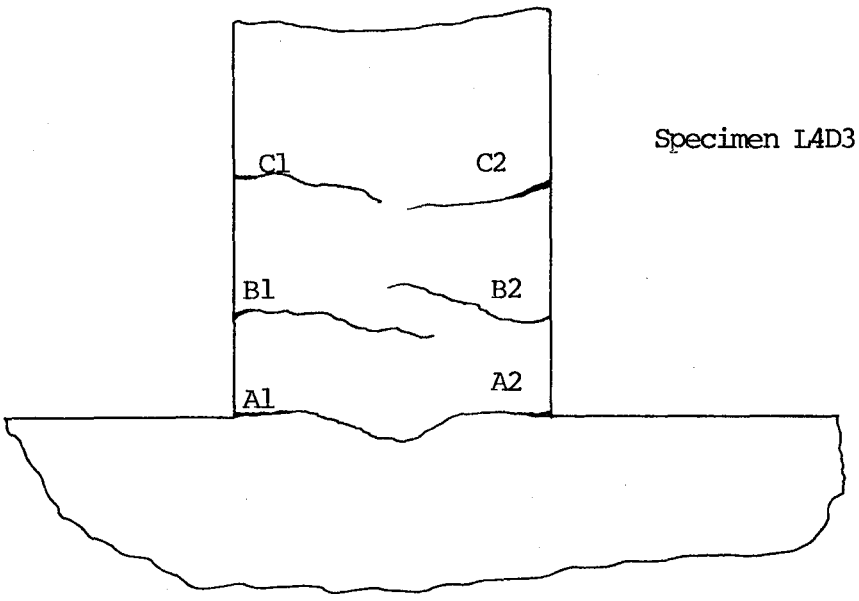

	Measured Crack Widths at Maximum Loads (mm)					
Cycle #	A1	A2	B1	B2	C1	C2
1+	0.5	0	0.3	0	0.2	0
1-	0	0.4	0	0.3	0	0.4
4+	2.0	0	1.6	0	1.2	0
*4-	0**	1.0	0**	1.1	0**	3.0

* Specimen failed in compression
** Concrete crushed

Fig. 3.7 Measured Crack Widths at Maximum Loads, L4D3

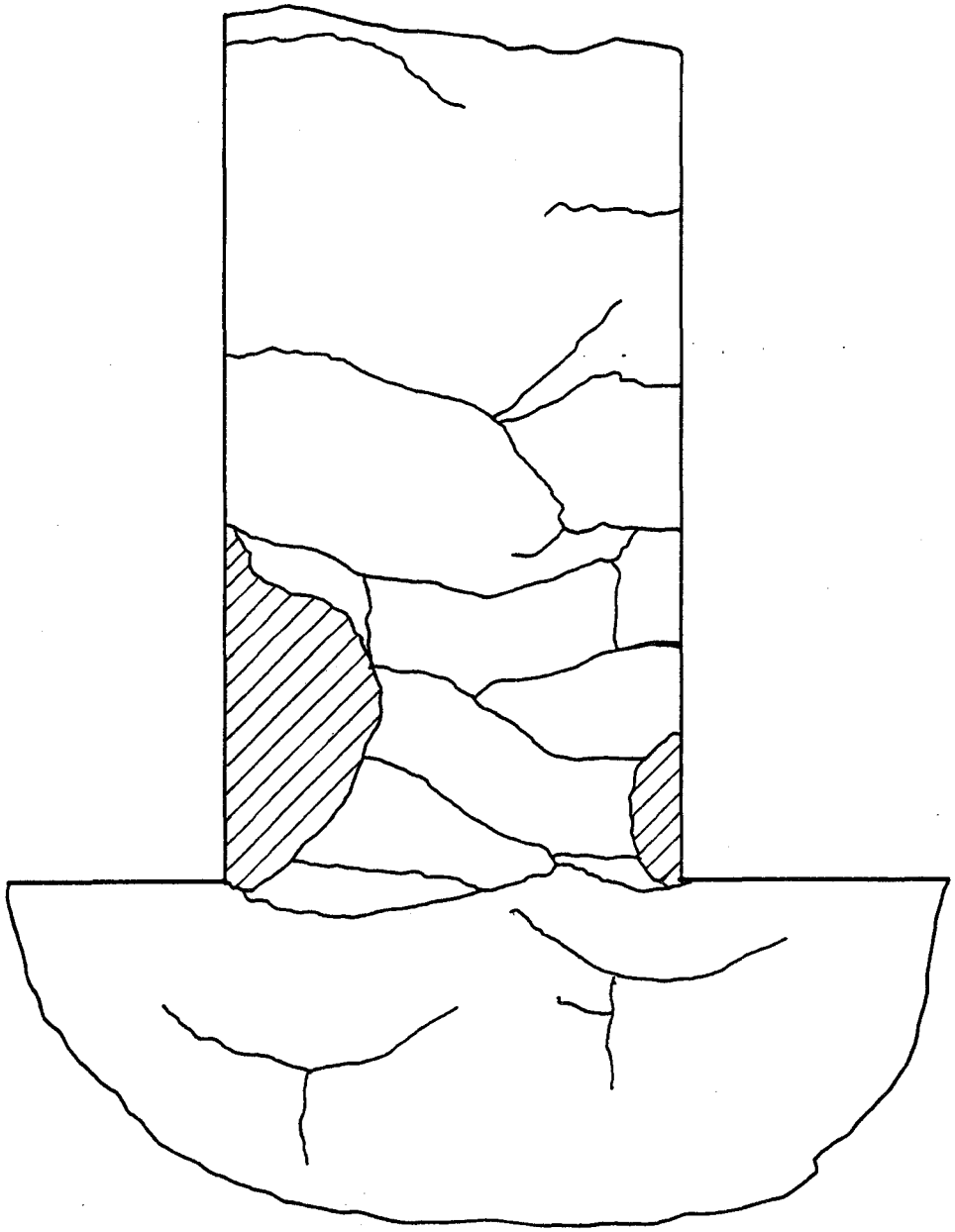

Fig. 3.8(a) Crack Pattern North Face, Specimen L4D3

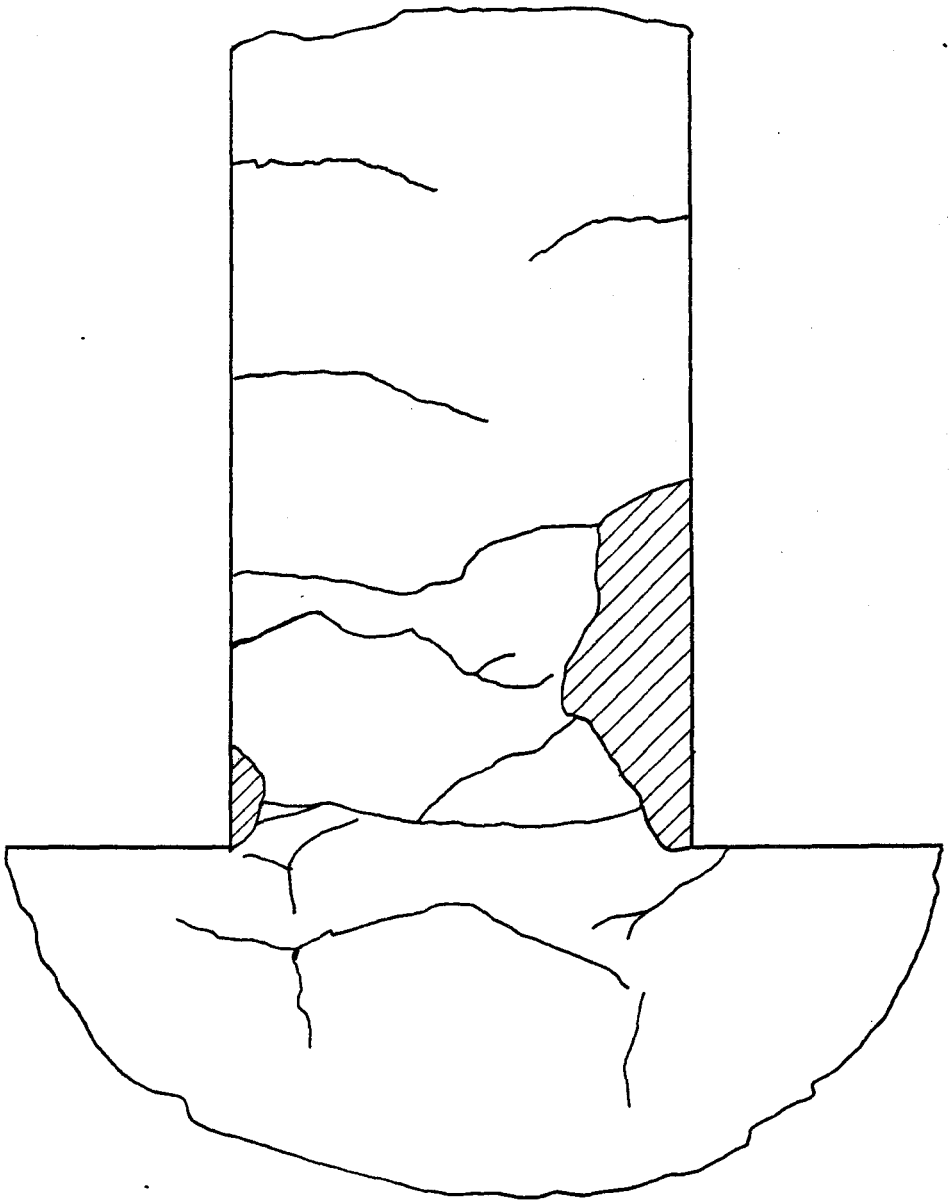

Fig. 3.8(b) Crack Pattern South Face, Specimen L4D3

INTENTIONALLY BLANK

CHAPTER IV

INTERPRETATION OF OBSERVED RESPONSE

4.1 Introduction

The objective of this chapter is to interpret the measured response in terms of the major load resisting mechanisms. A numerical model was developed to simulate behavior of the specimens (L4D2 & L4D3) and to aid in the identification of these resistance mechanisms. Before interpreting the measured response some general aspects behind the development of the numerical model are discussed.

4.2 The Numerical Model

The behavior of the column was investigated solely in terms of the moment-curvature relationship for the base of the column. Approximately 65 % of the deflection at the top of the column was attributed to rotation at the base. Furthermore, comparison of load-deflection and load-rotation curves (Fig. 3.1) suggested that all nonlinear behavior occurred within the base region. A detailed analysis of the importance of the base region is presented in Table 4.1. For specific loading points,

the total deflection, δ_t , is compared with that resulting from the base rotation, δ_r .

To show that the column is essentially linear above the base, an equivalent EI was calculated from tangential deviations determined from measured data. The data from Specimen L4D2 was used for the computation, as it represented a softer response due to the light dead load. The equivalent EI was calculated as follows:

$$\delta_t - \theta h = \frac{Ph^3}{3EI}$$

$$EI = \frac{Ph^3}{3(\delta_t - \theta h)}$$

where

δ_t = measured deflection at the top of the column

θ = measured rotation at the base of the column

P = applied horizontal load at the top of the column

h = height of the column

An arbitrary selection of points through the first three cycles is shown in Table 4.2. Each value of EI was normalized by the EI of the gross section. The elastic modulus of concrete was assumed to be 25 MPa on the basis of cylinder tests (Fig. 2.7). The values for the ratio of EI/EIg remained constant at

an average value of 0.3 for ranges of decreasing axial compression and roughly 0.5 for ranges of increasing axial compression.

The criteria for the computation of the moment-curvature relationship included the following considerations. The section was divided into slices with individual nonlinear stress-strain properties of steel or concrete. For a given displacement history, the moment and axial load were varied in small increments so that material properties could be updated according to the stress-strain law for each element. A more detailed presentation of the numerical model is presented in Appendix A.

Despite the usefulness of the numerical model, some limitations to its use should be mentioned. Two basic assumptions were used to develop the model. First, it was assumed that plane sections remain plane and therefore no shear deformations are present. Secondly, the strain in the concrete was assumed equal to the strain in the steel or that a perfect bond exists. In addition, values of moment and curvature generated by the model are only as accurate as the stress-versus-strain models used for the concrete and steel. The stress-strain characteristics for the steel and concrete are shown in Fig. 4.3. These models were based on more extensive work done by Aktan, Karlsson and Sozen (Ref. 3) and Sargin (Ref. 17).

4.3 Column Specimen L4D2

The first three cycles (Phase I) represented a nearly linear-elastic response of the cracked column as maximum displacements were approximately $\pm$1.0% of the column height (Fig. 3.16). The numerical model and measured strains indicated that the tension reinforcement had just begun to yield near the maximum displacement of Phase I. This did not have a significant impact on the response of the specimen as no decrease in stiffness was observed at maximum loads. Subsequent loading in Phase I followed slopes nearly identical to those defined in the first cycle.

Cycles 4 through 10 (Phases II and III, Figs. 3.1c and 3.1d) indicated a highly nonlinear response as maximum displacements approached 3% of the column height. Two very distinct characteristics of load resistance can be seen in the load-displacement relation. The load path from maximum positive displacement (Fig. 3.1c, point A) to maximum negative displacement (point F) had four significant changes in stiffness (points B, C, D, E). In contrast, loading from maximum negative displacement (point F) to maximum positive displacement (point A) resulted in a single change in stiffness which was very gradual.

The changes in stiffness observed for loading path ABCD may be attributed to closing of the flexural cracks which were

opened during the previous half cycle. Upon reversal of the load at point B, the compression reinforcement was the sole source of compression resistance. Closing of the crack was inhibited by permanent deformations in the steel which were a result of previous loading. After reversal of the displacement, point C, the crack closed and both the axial load and moment could be resisted by the concrete, in addition to the steel. The change in slope at point D may be attributed to yield of tensile reinforcement.

The behavior suggested in the foregoing discussion may be corroborated with strain readings and results of the numerical model. Strain measurements at the base of the column (Fig. 3.1j) indicated that yield of the reinforcement in tension had occurred at point A. Strain measurements were on the order of 1.5%. Upon reversal of the load, point B, a large decrease in tensile strain was measured for a small increase in load suggesting an open crack. During this range, three cracks were observed approximately 1 mm wide. The stiffening at point C can also be seen by the sudden change in slope of the load-strain curve. For a large increase in load, a small change in strain was observed suggesting an additional resistance in compression, or a closed crack. Yielding of the tensile steel at point D was measured with the gauge on the tension reinforcement (Fig. 3.1g).

The negative slope from points E to F (Fig. 3.1c) appeared to be due to crushing of the outermost compression fibers of the section. Points E and F of Fig. 3.1c coincide with points E and F in Fig. 3.1f. The abrupt change in strain with very little change in load indicates a redistribution of the stress at the section that may be attributed to crushing of the concrete.

The second major characteristic of the load-deflection curve was the gradual change in stiffness from maximum negative displacement (point F, Fig. 3.1c) to maximum positive displacement (point H). This change in stiffness appeared to be due to the flexural cracks, which opened during loading to point F, not closing. As the load approached zero (point G) a large permanent deformation was evident. The load reversal at this point resulted in a decreasing axial compression which eventually caused a net tensile axial load. This load configuration did not provide a compressive force large enough to overcome the permanent deformation in the reinforcement. Therefore the cracks did not close completely, even at the maximum load.

Strain measurements also suggested that the cracks did not close after reversal of the load (points FGH). Significant yielding can be seen in Figs. 3.1f and 3.1g in the range from D to E. Associated with the yielding of the reinforcement were

large cracks ranging from 1.1 to 2.25 mm wide. Unloading and reversal of the load resulted in a permanent strain which was constant for the remainder of the test. In addition, the slope of the load-deflection curve between points G and H coincided well with the stiffness of a cross-section composed of only the reinforcement. It should be noted that the stiffness of this section was influenced by the Bauschinger effect (a decrease in the elastic limit of the steel that accompanies loading and unloading through successive cycles in the opposite sense, Ref. 11). It can be seen in Fig. 3.1j that the tension reinforcement in the region of decreasing axial compression was strained sufficiently for the Bauschinger effect to have a significant impact on the response of the column.

These same tendencies addressed in the preceding discussion were observed for the remainder of the test (cycles 5 through 10). The remaining cycles in Phase II (Fig. 3.1c) were nearly identical, which indicated that the energy dissipation characteristics of the specimen were essentially constant. The stiffness for these cycles, in the region of increasing axial compression, were significantly less due to damage incurred during the fourth cycle. The stiffness in the region of decreasing axial compression, however, changed very little. Crushing of the concrete observed on cycle 4 seemed to cause a decrease in maximum load for subsequent cycles (see Phase III, Fig. 3.1d).

The numerical model was used to simulate column behavior and results for the first three cycles are shown in Fig. 4.4. A good correlation between calculated and measured results can be seen in the figure, indicating that the basic premises used to develop the model are valid. Initial yielding of the reinforcement at maximum positive and negative displacements correlated well with strain measurements. The two distinct stiffnesses associated with the ranges of increasing and decreasing axial compression also appeared to model well. Furthermore, identical energy dissipation characteristics (area enclosed by the load-deflection curve) for subsequent cycles at equal displacements were observed for the physical as well as the numerical model.

4.4 Column Specimen L4D3

Specimen L4D3 (simulated dead load three times larger than Specimen L4D2) exhibited many of the same load-resistance mechanisms as Specimen L4D2. The stiffness of the specimen was significantly larger below rather than above the axis of zero load due to the increasing axial compression. Maximum loads were associated with yielding of the tension reinforcement as seen in the load versus strain measurements in Fig. 3.5c. Once again, the cycles at equal displacement were very similar.

In general, the response of Specimen L4D3 was largely influenced by its position on the failure envelope of the load-moment interaction diagram (Fig. 4.5). Due to the large simulated gravity load and the given eccentricity, the intersection with the failure envelope (Fig. 4.5) was close to the balance point. By definition, the balance point is simultaneous yielding of the reinforcement and crushing of the concrete. This appears to have been the case with Specimen L4D3. A very unstable condition resulted from the balanced loading producing a compressive failure. The failure occurred while loading to maximum negative displacement during cycle 4. This was the same point at which crushing of the concrete was observed for Specimen L4D2. In the case of Specimen L4D3, however, crushing of the concrete was observed on a much larger scale due to the larger gravity load stress.

Calculated results of load versus rotation from the numerical model are shown with the measured response of Specimen L4D3 in Fig. 4.6. Maximum loads predicted by the model matched well with the measured maximum loads. The shallow slope at maximum loads was associated with yielding of the tension reinforcement which corresponded well with strain measurement (Fig. 3.5c). The load paths also modeled well as two distinct stiffnesses can be seen above and below the axis of zero load.

* Point	Load (KN)	δ_r (mm)	δ_t (mm)	δ_r/δ_t *100
1	2.39	0.09	0.20	45
2	17.3	2.87	4.94	58
3	22.2	4.27	7.52	57
4	33.4	8.96	15.7	57
5	27.3	10.6	17.2	62
6	22.6	9.50	15.1	63
7	13.3	7.01	11.0	64
8	9.03	5.76	8.66	66
9	4.58	4.37	6.55	67
10	0.18	3.00	4.54	66
11	-9.12	0.84	1.49	56
12	-19.0	-1.32	-1.52	87
13	-26.5	-2.76	-4.01	69
14	-35.7	-4.67	-7.11	66
15	-44.6	-6.76	-10.7	63
16	-57.8	-10.4	-16.4	63
17	-57.5	-11.7	-18.1	65
18	-42.2	-9.61	-15.1	64
19	-28.6	-7.42	-11.4	65
20	-11.7	-4.29	-6.30	68

* Points correspond to numbers in Fig. 4.1

Table 4.1 Percentage of Overall Deflection Due to Base Rotation

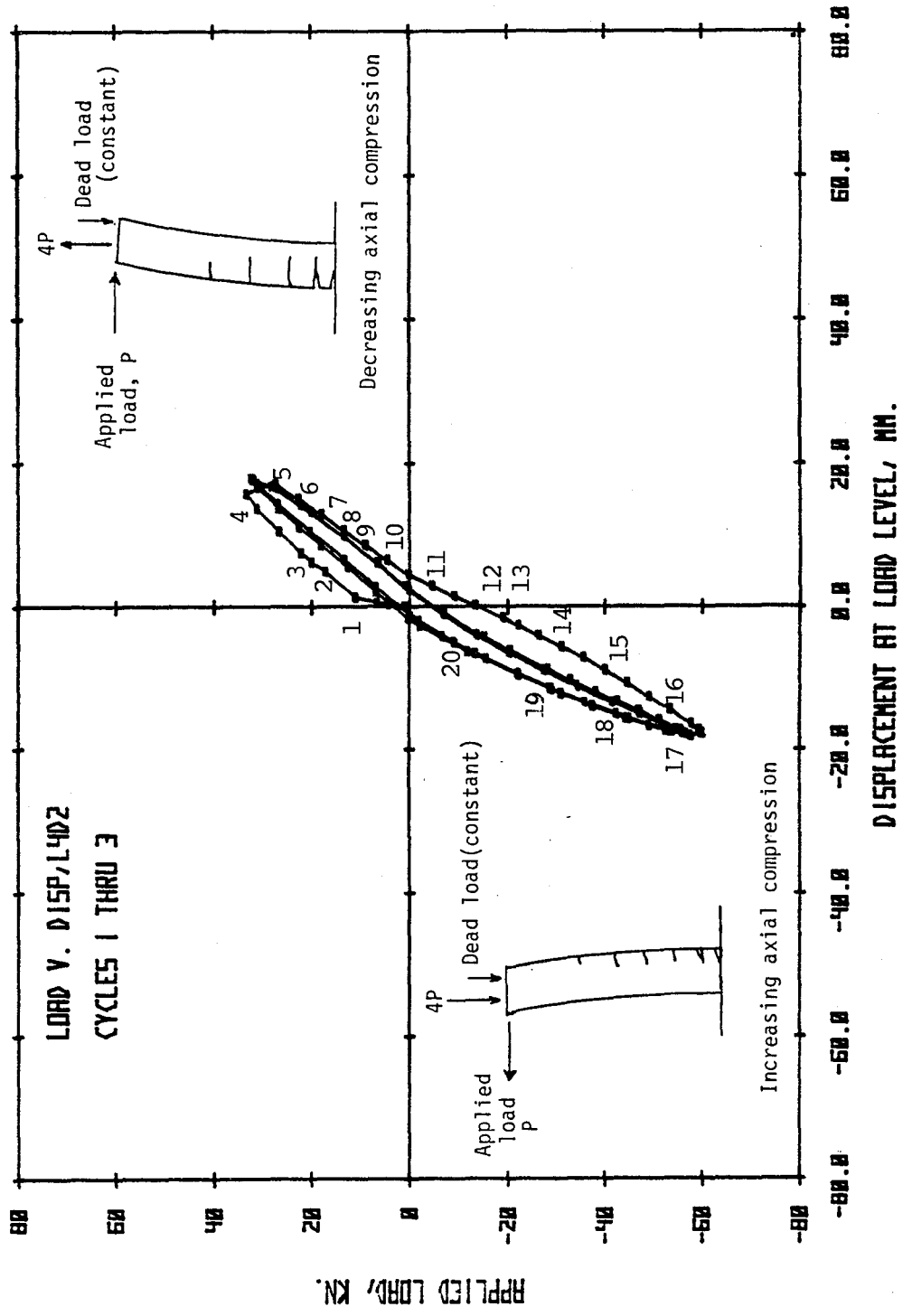

Fig. 4.1 Identification of Points for Table 4.1

Point	Load (KN)	EI/EI_g	Point	Load (KN)	EI/EI_g
1	20.1	.29	11	22.1	.33
2	33.4	.20	12	0.67	.32
3	13.3	.28	13	-15.1	.49
4	-22.3	.43	14	-46.7	.55
5	-35.6	.53	15	-56.7	.54
6	-53.3	.52	16	-22.1	.54
7	-35.8	.58	17	26.8	.26
8	-11.8	.50	18	20.0	.28
9	12.7	.26	19	6.54	.28
10	31.1	.26	20	-27.6	.51

Table 4.2 Effective Stiffnesses for the Column Above the Base (Specimen L4D2)

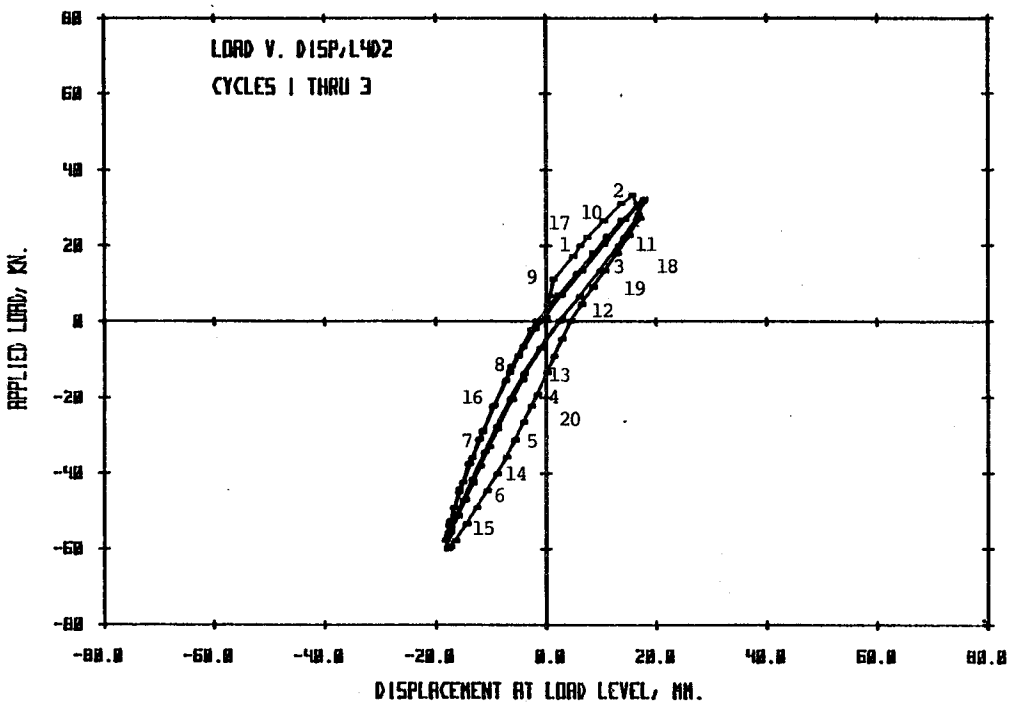

Fig. 4.2 Identification of Points for Table 4.2

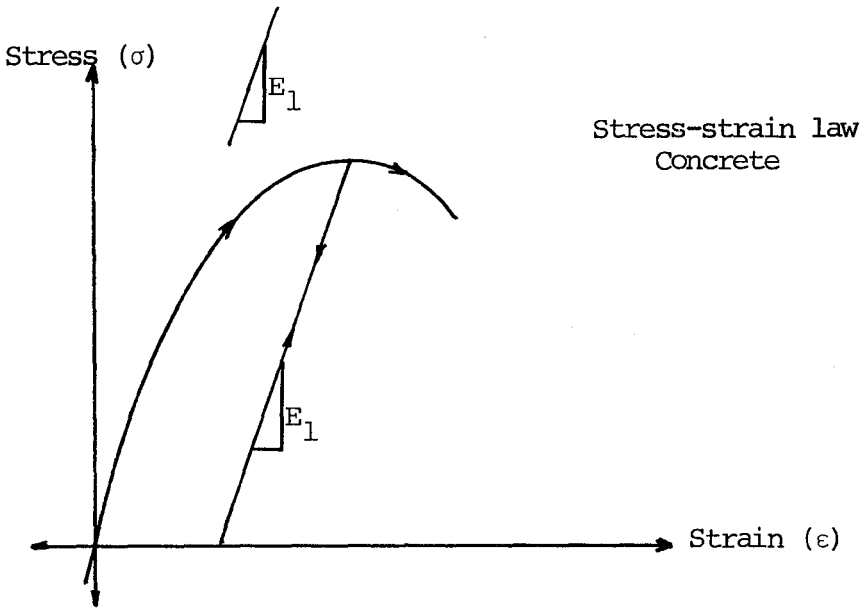

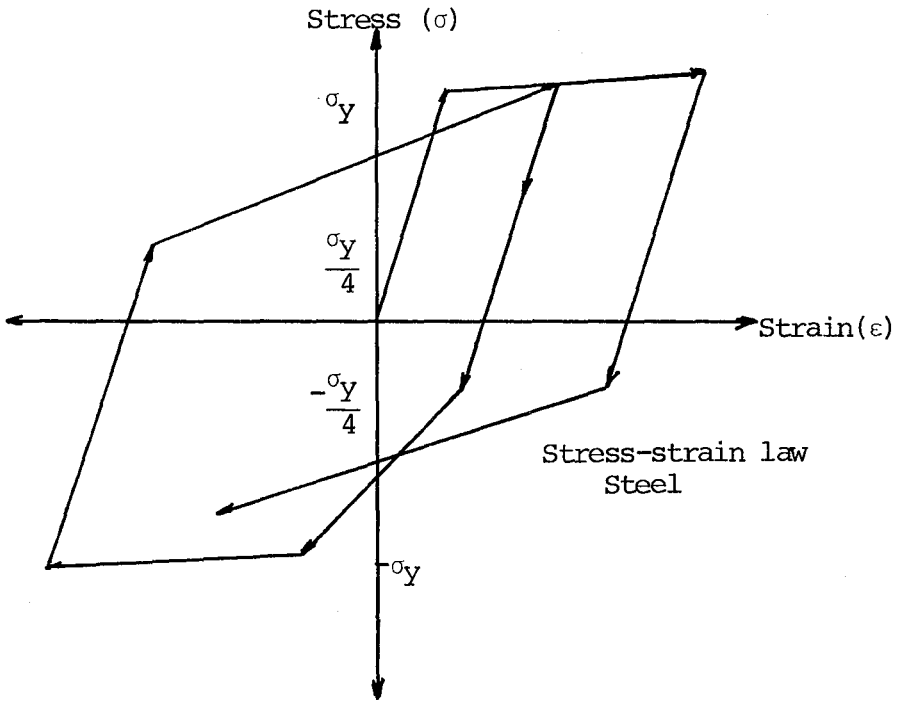

Fig. 4.3 Stress-strain Laws Used in the Numerical Model

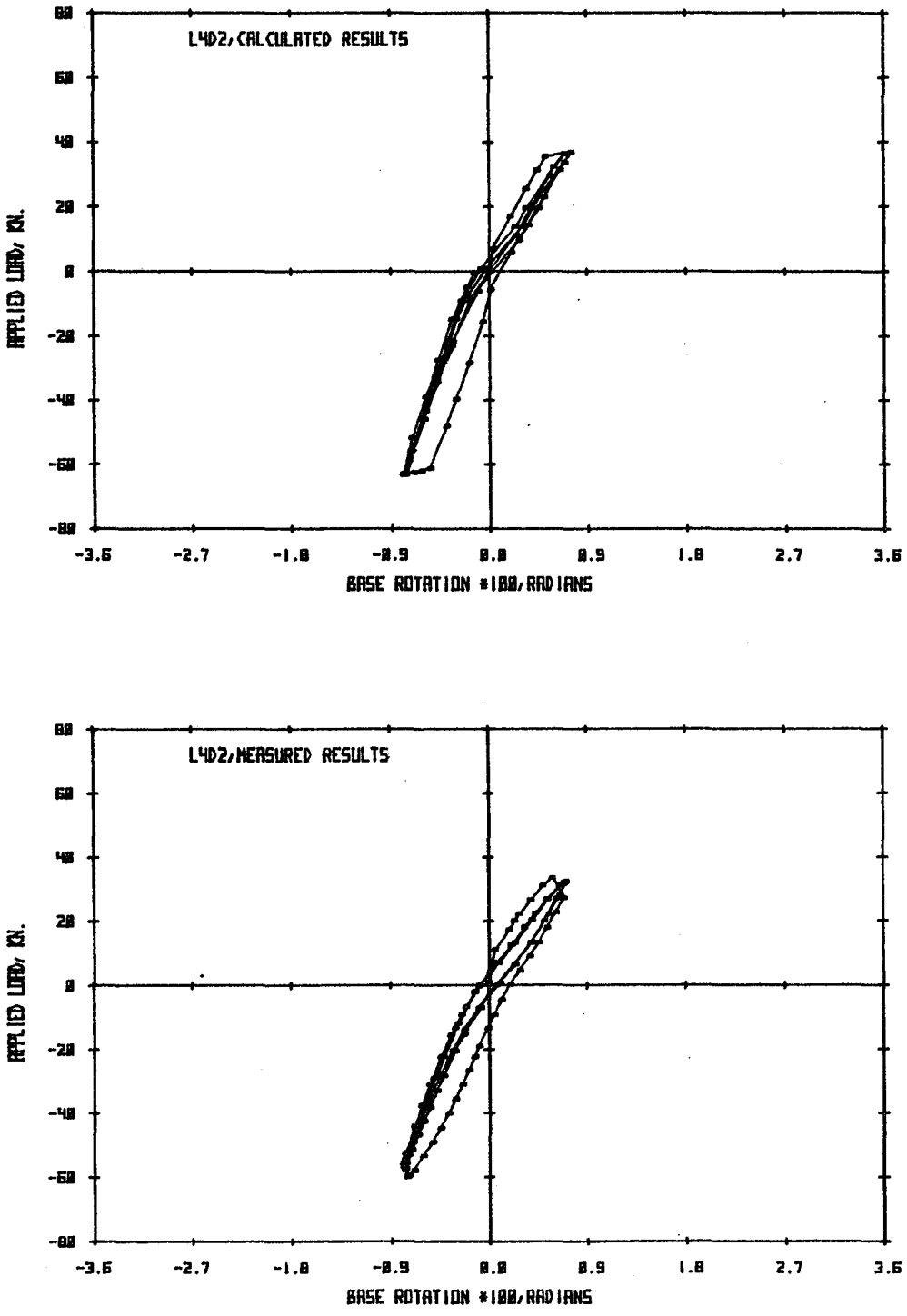

Fig. 4.4 Comparison of Measured and Calculated Response, Specimen L4D2

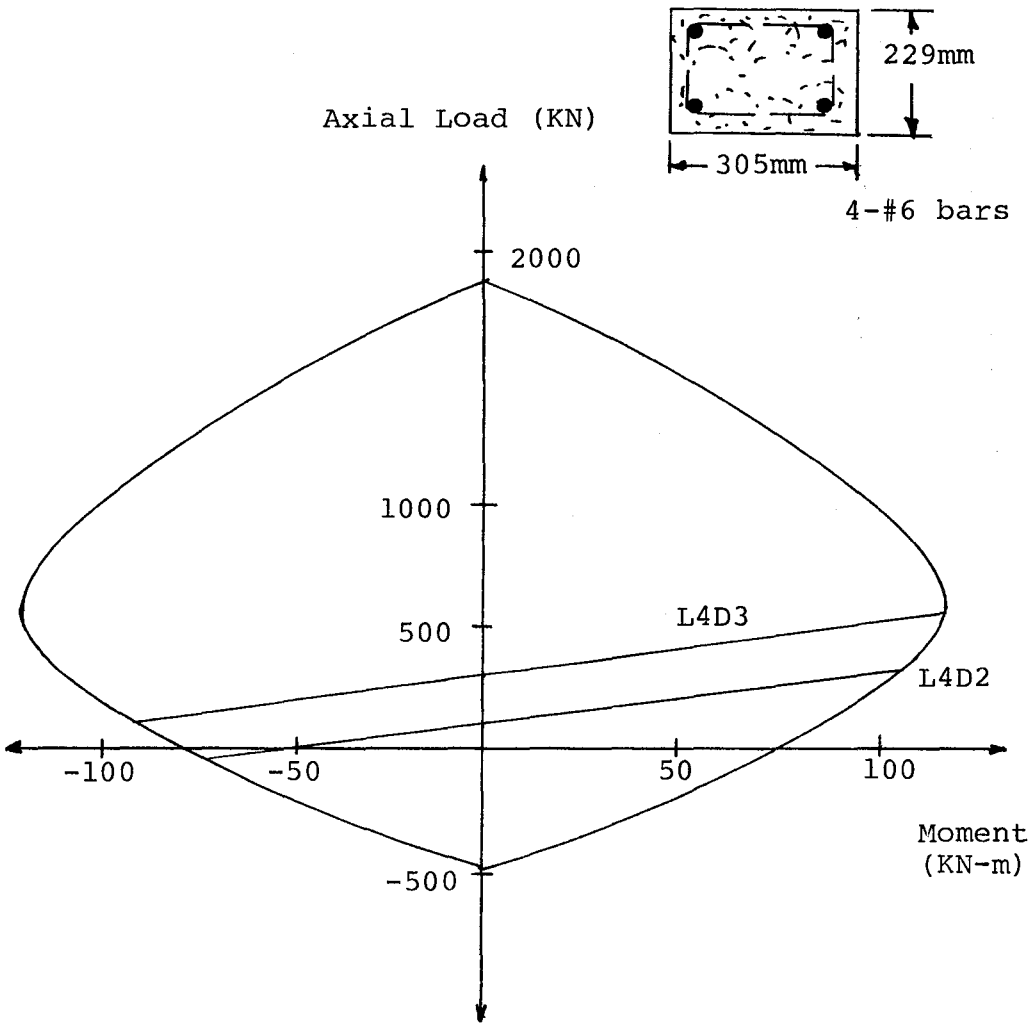

Fig. 4.5 Load-Moment Interaction Diagram
Specimens L4D2 and L4D3

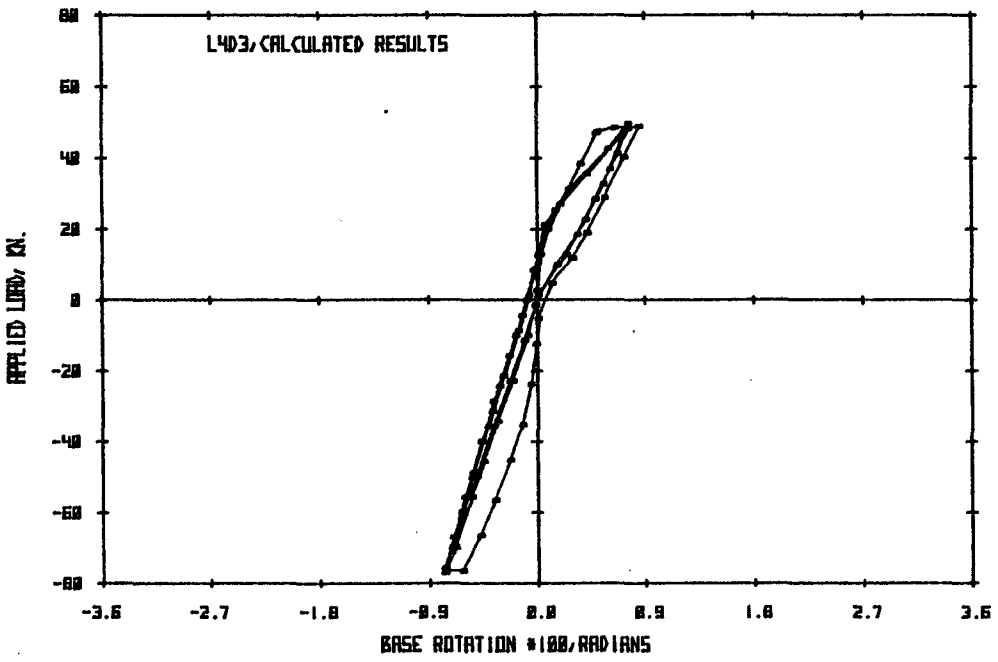

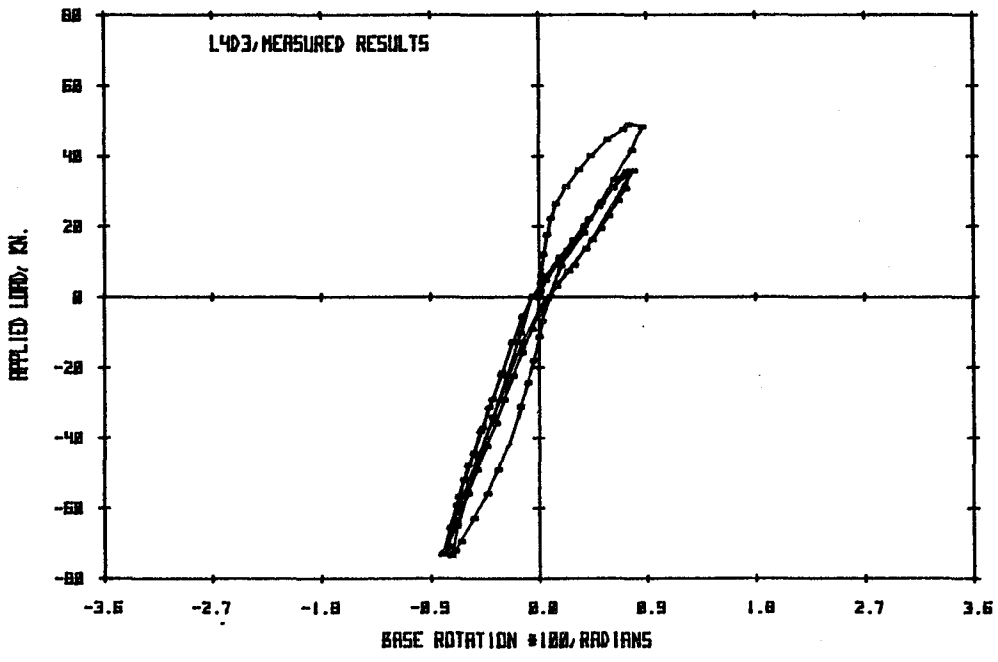

Fig. 4.6 Comparison of Measured and Calculated Response, Specimen L4D3

CHAPTER V

INVESTIGATION OF SCALING

5.1 Introduction

Scaling differences between small-scale models and large-scale reinforced concrete columns are examined in this chapter. More specifically there are two questions that need to be addressed: do the section properties scale; and does the response vary significantly because of possible inconsistent scaling of the gravity load?

Past research has been done concerning the relationship between small-scale microconcrete models and large-scale reinforced concrete prototypes. Evans and Clarke (Ref. 7) suggested that moment-curvature can be reasonably modeled in beams for monotonically increasing loads (Fig. 5.1). Stewart and Abrams (Ref. 20) also showed a good correlation between large- and small-scale reinforced concrete beam-column assemblages for slowly applied load reversals (Fig. 5.2). A large-scale column (Specimen L4D2) tested in this study with a varying ratio of horizontal to vertical load is compared with a small-scale model tested by Gilbertson and Moehle (Ref. 9) in

this chapter. Each specimen was loaded with the same gravity load stress and subjected to several slowly applied load reversals.

The differences in response due to inconsistent gravity load scaling are also addressed in this chapter. Measured results relating load and deflection are presented for the two large-scale specimens tested. These specimens were loaded with either a light (Specimen L4D2) or a heavy (Specimen L4D3) simulated gravity load. To assist in the identification of the response differences, the numerical model was used to simulate the change in stiffness of a column subjected to a strong earthquake motion. The hysteretic behavior is presented in terms of the load-deflection relationship and associated time deformation characteristics.

5.2 Comparison of Behavior for Small and Large Specimens With Equal Gravity Load Stress

Large- and small-scale specimens with the same gravity load stress were subjected to a series of slowly applied loading reversals. To compare large- and small-scale load-deflection and load-rotation relationships, the measured results of the small-scale test were adjusted by the length scale factor (x=6). The small-scale displacement was increased by the scale factor while the load was multiplied by the square of the scale factor according to the following criteria.

Deflection at the top of the column can be calculated using fundamental moment area techniques. Assuming that plane sections remain plane, a curvature diagram can be constructed that should vary as the length scale factor. The area under the curvature diagram would produce a value for the rotation that is scale free. The moment of this area results in a value for deflection that should vary as the length scale factor.

The specimen resists applied axial loads and moments through a combination of compressive force in the concrete and tensile force in the steel.

$$C = b\int_0^c f_c \, dy$$

$$T = A_s f_s$$

where,

C = compressive force in concrete

f_c = compressive stress in concrete

b = width of section

c = distance from outermost compression fiber to the neutral axis

T = tensile force in steel

A_s = area of tensile reinforcement

f_s = stress in the steel

Each force varies as the square of the length scale factor. The sum of these forces (an imbalance could exist to account for any axial load present) multiplied by the distance between them produces the resisting moment that varies by the cube of the length scale factor. Hence, as the moment is divided by the height of the specimen, the applied horizontal load should vary as the square of the length scale factor. Since both large- and small-scale concrete and steel properties were similar, a good comparison should be possible. For a comparison of small- and large-scale material properties, see Fig. 5.3.

A comparison of the first three cycles (Phase I) of the large- and small-scale specimens is shown in Fig. 5.4. The same general trends of hysteretic response appeared to govern both large- and small-scale response. Maximum loads as well as loading paths appear to correspond quite well. As was the case with Specimen L4D2, the small-scale specimen was significantly stiffer below the axis of zero load. An analysis of the portion of the column above the base in terms of EI for large-scale Specimen L4D2 (Sec. 4.2) suggested a linear response. The same analysis for the small-scale specimen also suggested a linear response. A selection of points for the first three cycles is shown in Fig. 5.5. Although slightly stiffer than the large-scale specimen, the ratio of EI to the EI for the gross section remained constant with an average value of 0.40 in the

range of decreasing axial compression and 0.60 in the range of increasing axial compression.

Similar tendencies in energy-dissipation characteristics were observed for small- and large-scale specimens in Phase I. Subsequent cycles at equal displacements (cycles 2 and 3) enclosed a smaller area than for the initial cycle curve, for each specimen.

Cycles 4 through 5 for the small-scale specimen and cycles 4 through 6 for the large-scale specimen are shown in Fig. 5.6. The specimens were displaced approximately $\pm 2\%$ of the column height for each cycle. Even with a high degree of nonlinear behavior a good correlation can be seen between large and small specimens. Maximum loads associated with a very shallow slope on cycle 4 showed good correspondence between the two specimens. The characteristic pinching effect due to yielding of the compression reinforcement before the flexural cracks closed (Sec. 4.3) can also be seen in the small-scale response as the load path crosses the axis of zero displacement, approaching maximum negative displacement. Each specimen also displayed a gradual change in stiffness through unloading from maximum negative displacement to loading toward maximum positive displacement. Contrary to the pinching effect observed on the previous half cycle, the gradual change in stiffness was due to a failure to close the flexural cracks as proposed in Section 4.3.

Subsequent cycles were also similar in nature. Both large- and small-scale specimens were observed to have a significant decrease in stiffness after the fourth cycle due to damage that occurred during that cycle. Phase III, the remaining cycles in each test, are shown in Fig. 5.7. Each specimen displayed a loss of strength as well as a further degradation in stiffness in regions of increasing axial compression. No loss of strength was observed for either specimen in the region of decreasing axial compression.

Loading the small-scale specimen through regions of decreasing axial compression resulted in a substantial increase in displacement with little increase in load. Analogous loading of the large-scale specimen resulted in a slight resistance in this region. This difference may be attributable to different amounts of bond deterioration for the wire and the deformed bar.

5.3 Differences in Response Due to Inconsistent Gravity Load Scaling

Correct modeling of gravity loads can be an essential factor in predicting prototype response with small-scale models. For a model reduced in geometric proportions only, normal stress due to gravity loads should be the scale factor (less than one) times the stress in a full-scale structure (Appendix B). A one-tenth scale model, for instance, should have a gravity load stress one-tenth as large as the full-scale prototype stress.

To model the actual strength and behavior of the prototype structure, however, the full-scale gravity load stress should also be applied to the small-scale model. Therefore, a gravity load stress equal to that in a full-scale multistory building was applied to Specimen L4D3. With Specimen L4D2 (light gravity load stress) as a comparison, the differences in response due to inconsistent gravity load scaling can be examined.

A comparison of initial cycles for each specimen is shown in Fig. 5.8. For the first quarter cycle, the stiffness before the first crack was observed was 25% larger for Specimen L4D3. Once the specimen had cracked, Specimen L4D2 exhibited a nearly constant stiffness to the point of maximum positive displacement. Due to the higher compressive load, Specimen L4D3 was observed to have a gradual change in stiffness.

Neither specimen had a prominent change in stiffness as the load path crossed the axis of zero load towards maximum negative displacement. The cracked stiffness in this region was about 30% larger for Specimen L4D3. Once the first cycle was completed, each specimen exhibited the same energy dissipation characteristics for subsequent cycles of equal displacement. A tabular comparison of loads and stiffness for the two specimens is provided in Table 5.2.

In general, the greater gravity load stress of Specimen L4D3 resulted in greater loads and larger stiffnesses in regions of both increasing and decreasing axial compression. These differences in response were observed for slowly applied load reversals or essentially a static load condition. Therefore, a dynamic model was developed to illustrate further any variation in response of columns with different gravity load stresses.

The dynamic analysis consisted of a step-by-step integration method (Ref. 5). The procedure evaluated the response for short time increments and assumed that the properties of the system remained constant over the interval. Dynamic equilibrium was established at the beginning and end of each interval, and the properties of the system were also updated at this time. In this manner, the highly nonlinear behavior of the system could be approximated by a series of linear systems.

The nonlinear dynamic model consisted of a single-degree-of-freedom oscillator with a concentrated mass and a dashpot (Fig. 5.9). A nonlinear rotational spring was attached to the base of a linear column which was then excited by motion at the base.

The stiffness of the rotational spring was calculated using the numerical model (Sec. 4.2) which was modified for a small-scale structure. An incremental displacement from the

dynamic analysis was supplied to the numerical model which in turn updated the properties of the column and provided the current stiffness for the next time increment. A ratio of vertical to horizontal load of four to one was imposed to simulate the loading configuration on a base story column in a multistory building. The concentrated mass was estimated by approximating the overall stiffness of the system and dividing that quantity by the square of the angular velocity of the fundamental mode of small-scale structures tested at the University of Illinois (Ref. 1).

Excitation at the base consisted of recorded ground accelerations for the first ten seconds of the N-S component of the 1940 El Centro earthquake. The time scale was compressed by a factor of 2.5 resulting in a four second earthquake to be compatible with the small-scale multistory structure.

Response of a small-scale column with a light gravity load stress to motion at the base is shown in Fig. 5.10. The intensity of the earthquake was adjusted so that maximum response without failure (crushing of the concrete or fracture of the reinforcement) would result. Response of the lightly stressed model (Fig. 5.10) was characterized by extensive yielding of the tension reinforcement above the axis of zero load (displacement approximately +2% of the column height). Deformation below the axis of zero load was only 1.5% of the

column height but loads and stiffnesses were significantly greater.

The same dynamic model was subjected to a base motion of equal intensity but with a gravity load stress representing the full-scale gravity stress in a multistory building. This combination of gravity load and eccentricity intersects the failure-envelope of the load-moment interaction diagram near the balance point (Fig. 5.11). Response to the base excitation for this stress level is shown in Fig. 5.12.

Compared to the light gravity stress model, the response of the column with the heavy gravity stress was slightly stiffer and attained greater loads. These were essentially the same differences observed for the static case. However, for the same intensity earthquake, the greater compressive load reduced the ductility enough to cause a failure approximately halfway through the simulated base motions.

The dynamic response at these two stress levels corresponded well with observed behavior of Specimens L4D2 and L4D3. Specimen L4D2 (light gravity stress) was very ductile and exhibited only slight evidence of a compressive failure (Fig. 5.13). Specimen L4D3 (full-scale stress) displayed noticeable crushing of concrete (Fig. 5.13) and failed at approximately the same relative displacement as the dynamic model in Fig. 5.12.

To illustrate further the importance of consistent modeling of the gravity load an even larger gravity load was applied to the column. This gravity load produced an intersection with the failure envelope on the load-moment interaction diagram above the balance point (Fig. 5.11). Response to the same intensity earthquake as the previous two stress levels is shown in Fig. 5.14. Load-deflection and time-deformation characteristics are similar to the full-scale stress level response. The larger compressive load appeared to decrease the ductility further producing a compressive failure less than halfway through the earthquake.

The results from the dynamic analysis can be used to provide an upper bound on the response of a multistory structure subjected to a strong base motion. However, to infer behavior of the entire structure, the nonlinear model must be assumed to act in tandem with an identical model in which the applied axial load would have the opposite sense (Fig. 5.15). The applied shear loads would be in the same direction to resist the lateral loads.

As the structure displaces, a decreasing axial compression would be applied to one column while an increasing axial compression would be applied to the other column. The net affect on the structure would be an average response of the two columns. Unlike the response of the individual columns, the overall response would be symmetric about the axis of zero load.

In terms of the preceding discussion, results from the dynamic analysis for the light gravity stress and the full-scale gravity stress can be used to provide an upper bound on the differences in response of structure due to inconsistent scaling of gravity loads. The average response of the column with a full-scale gravity stress (Fig. 5.12) would have larger maximum shear load and a larger stiffness than the average response of the column with the light gravity stress (Fig. 5.10). The overall response of the structure would behave in the same manner. Further differences in the overall response of the structure would result from the lack of ductility of the structure with the full-scale gravity stress.

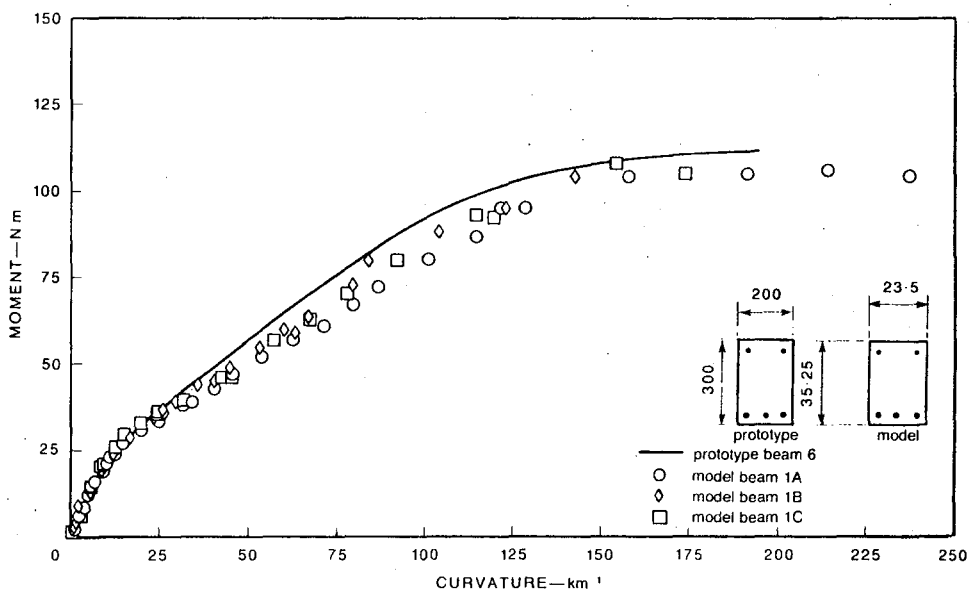

Fig. 5.1 Moment-Curvature Relations for Three Identical Model Beams, with Typical Prototype Relation for Comparison (Evans and Clarke)

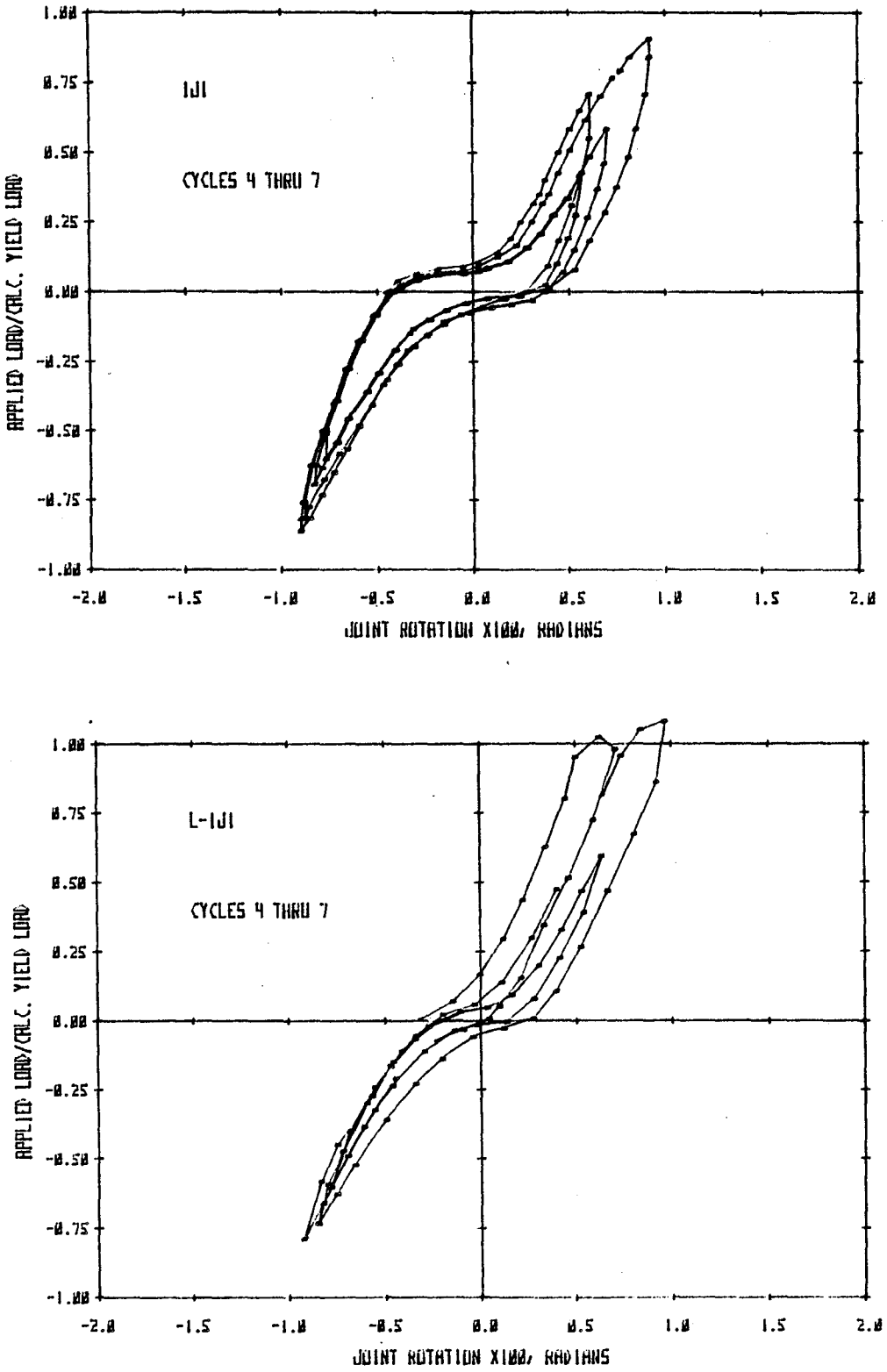

Fig. 5.2(a) Comparison of Large- and Small-Scale Interior Joints (Stewart and Abrams)

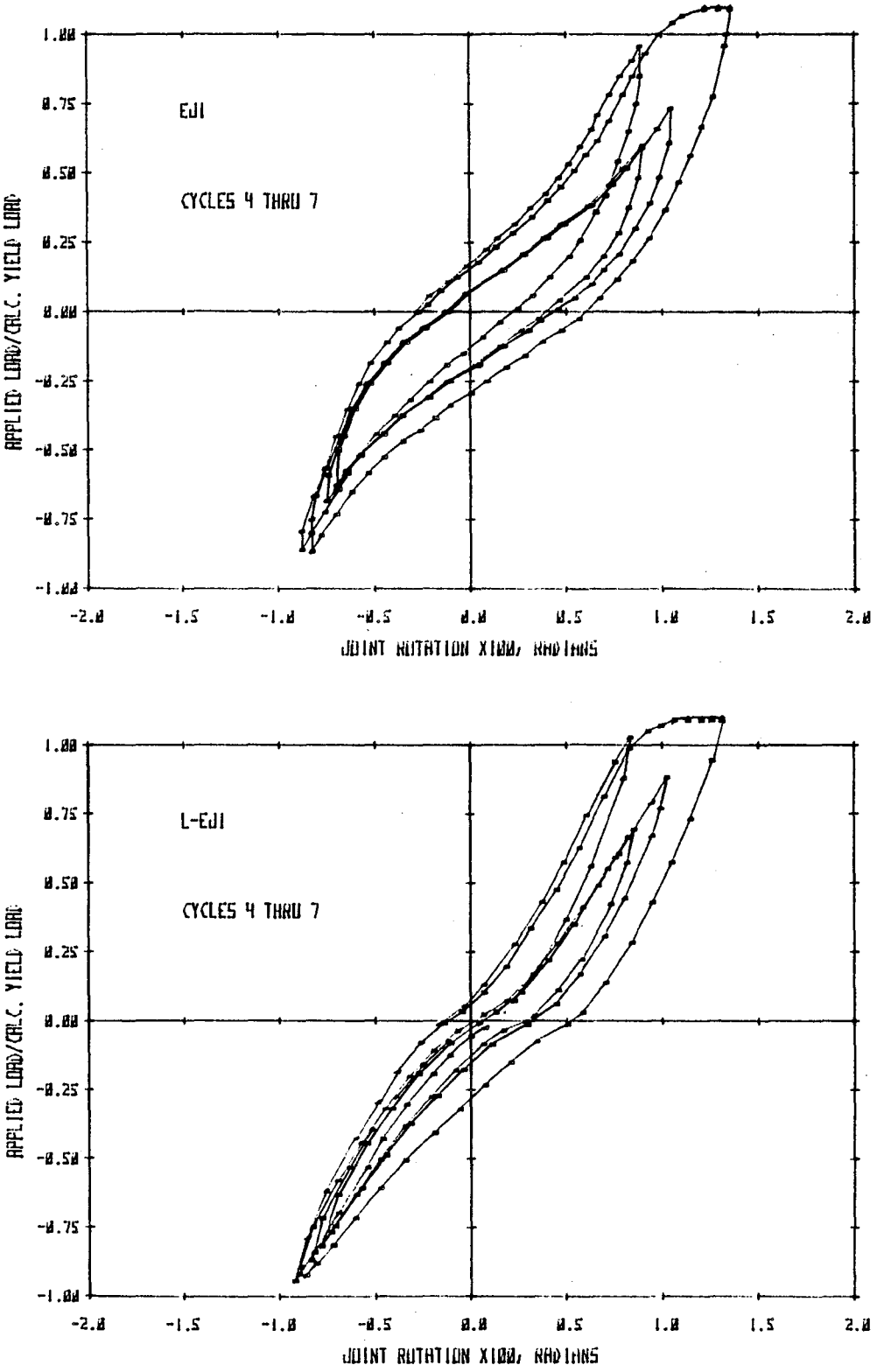

Fig. 5.2(b) Comparison of Large- and Small-Scale Exterior Joints (Stewart and Abrams)

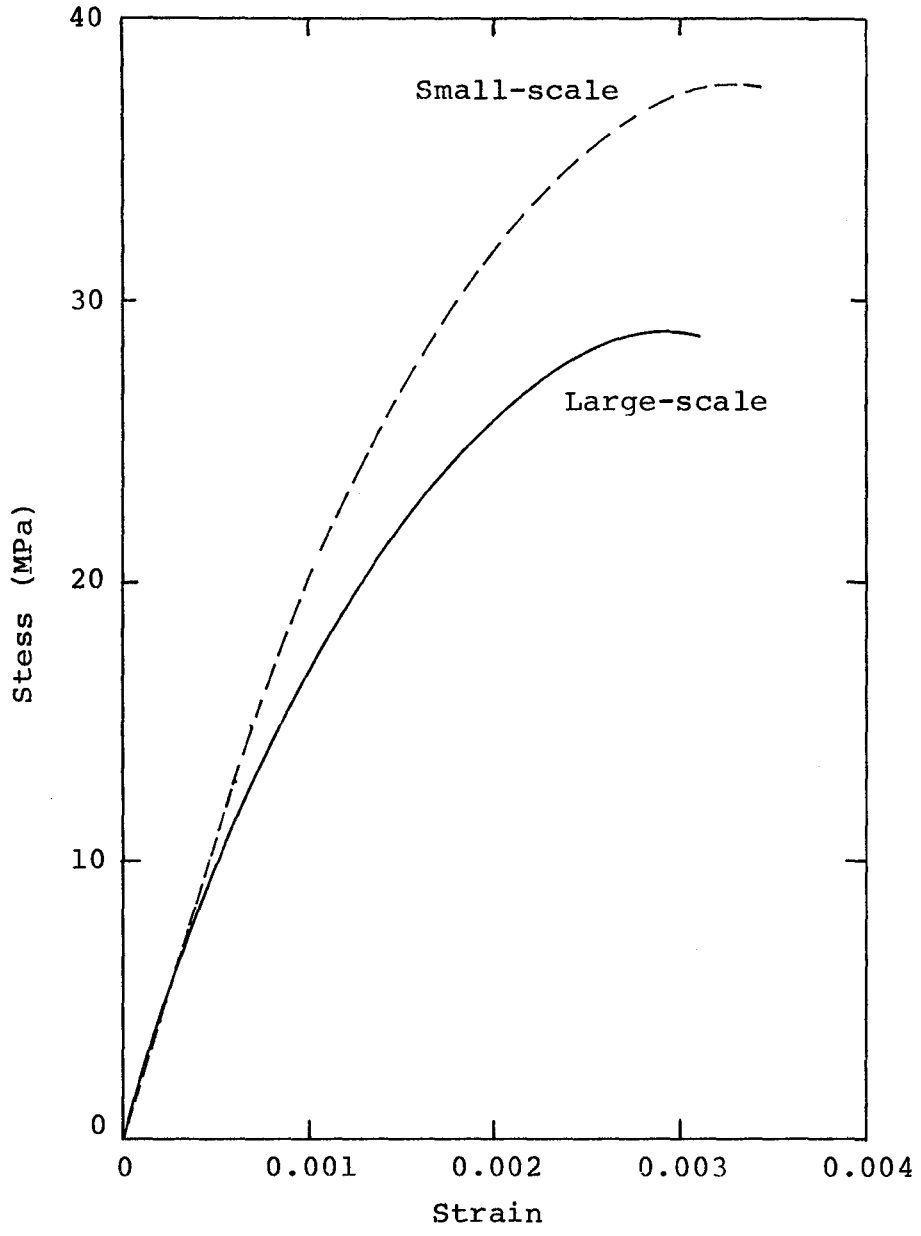

Fig. 5.3(a) Comparison of Concrete Properties for Large- and Small-Scale Specimens

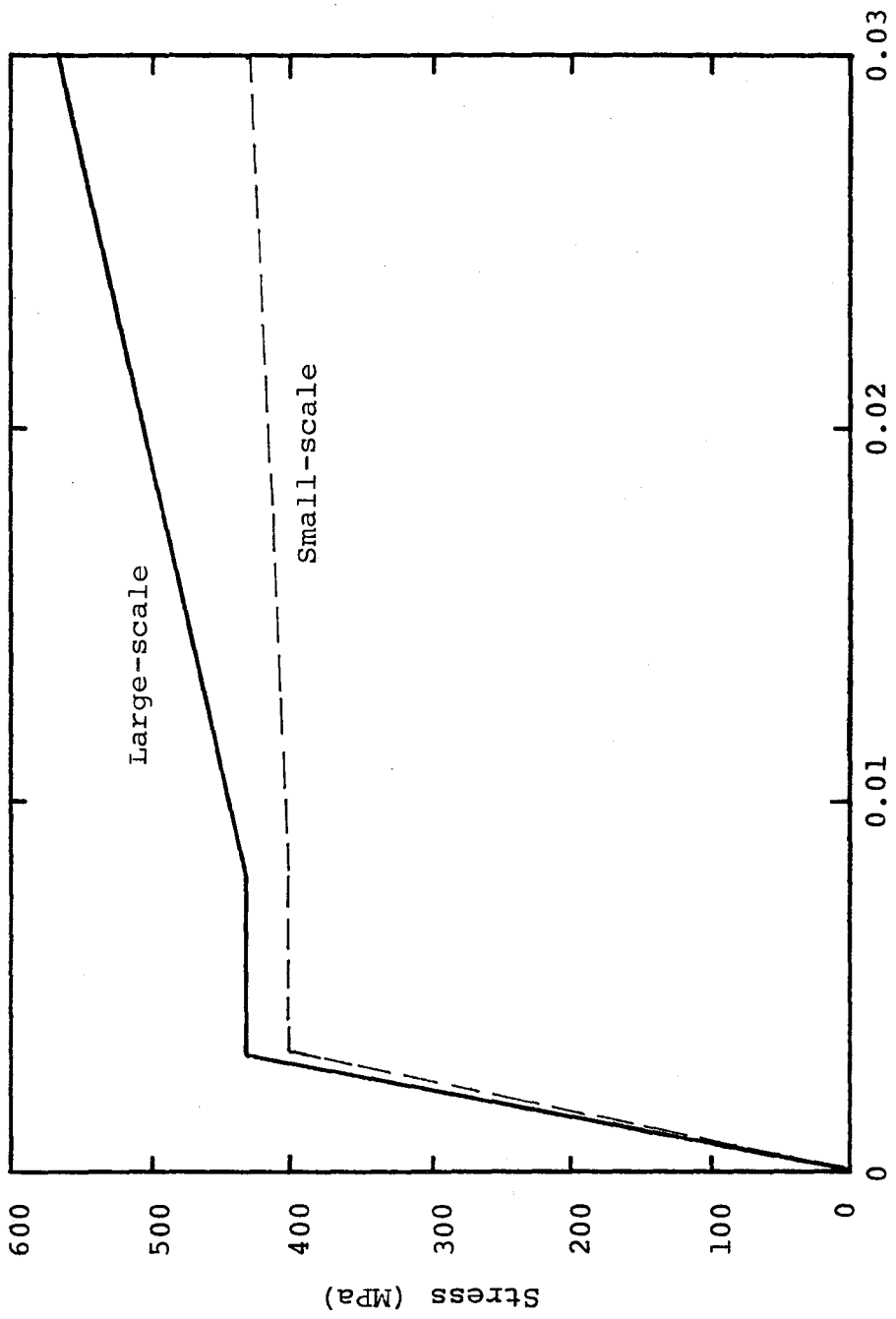

Fig. 5.3(b) Comparison of Steel Properties, Large- and Small-Scale

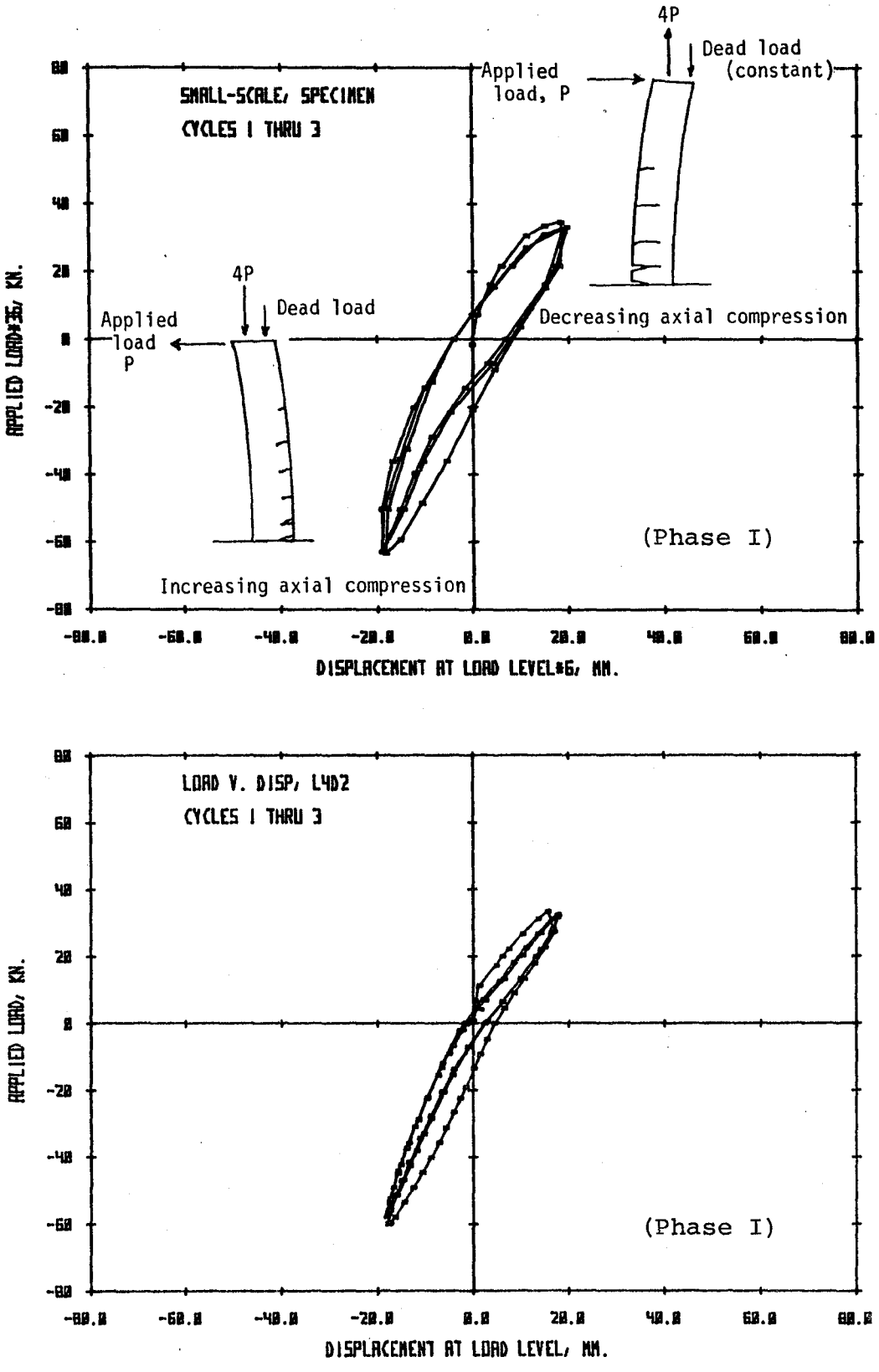

Fig. 5.4 Comparison of Large- and Small-Scale Results

Point	Cycle	Load (KN)	EI/EIg
1	1	0.84	0.46
2	1	0.40	0.41
3	1	-0.98	0.55
4	1	-0.98	0.49
5	2	0.67	0.38
6	2	0.36	0.40
7	2	-0.89	0.56
8	2	-1.20	0.60
9	3	0.71	0.39
10	3	-0.49	0.56
11	3	-1.69	0.58
12	3	-.93	0.61
13	3	0	0.37

Table 5.1 Comparison of EI/EI_g for Small-Scale

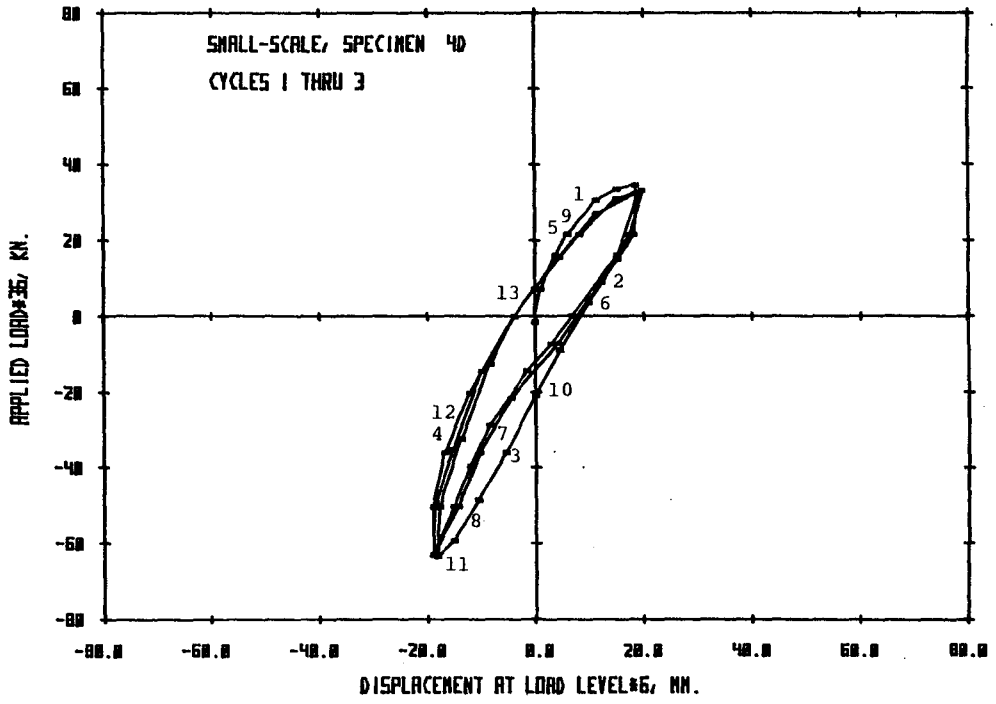

Fig. 5.5 Identification of Points for Table 5.1

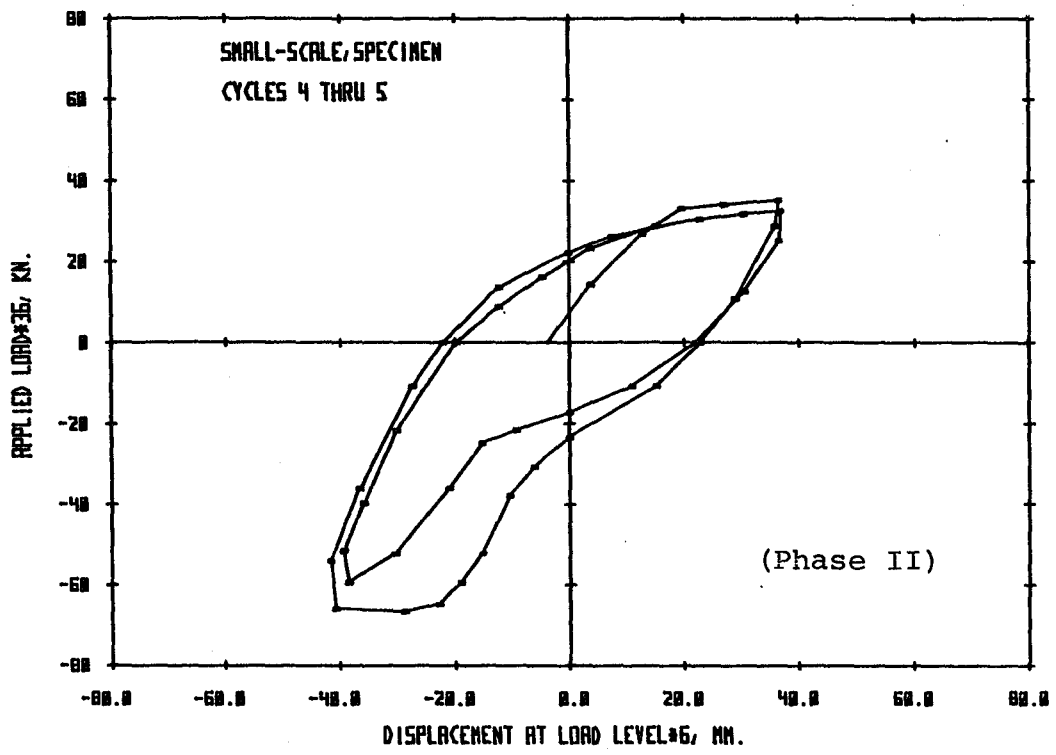

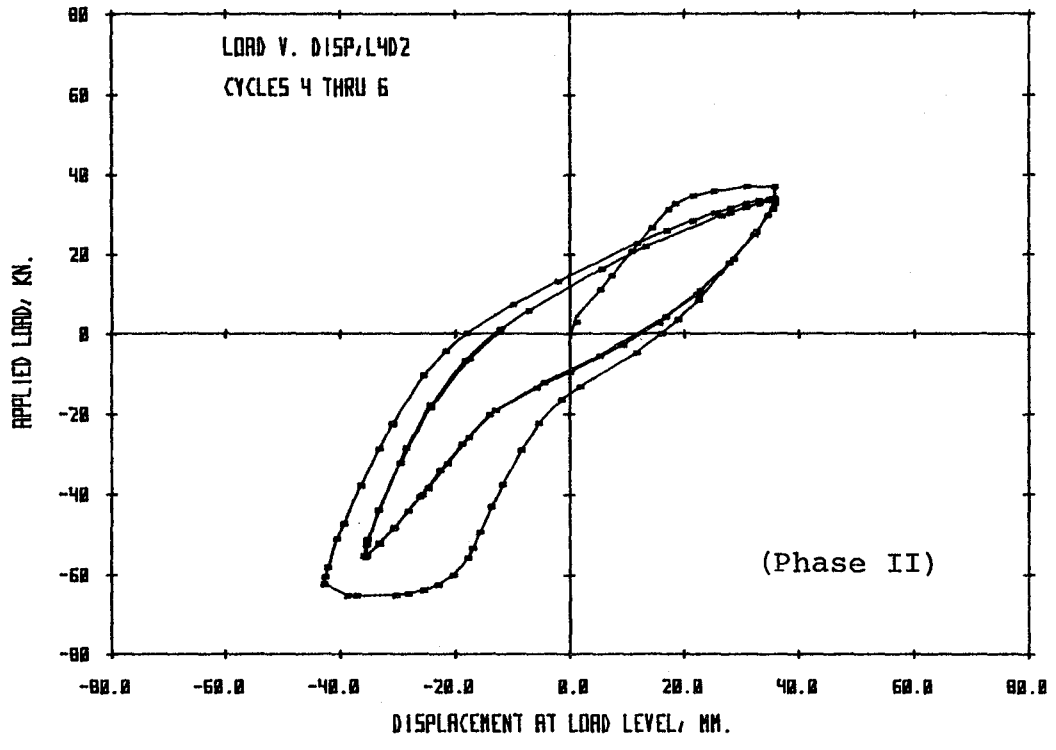

Fig. 5.6 Comparison of Large- and Small-Scale Specimens

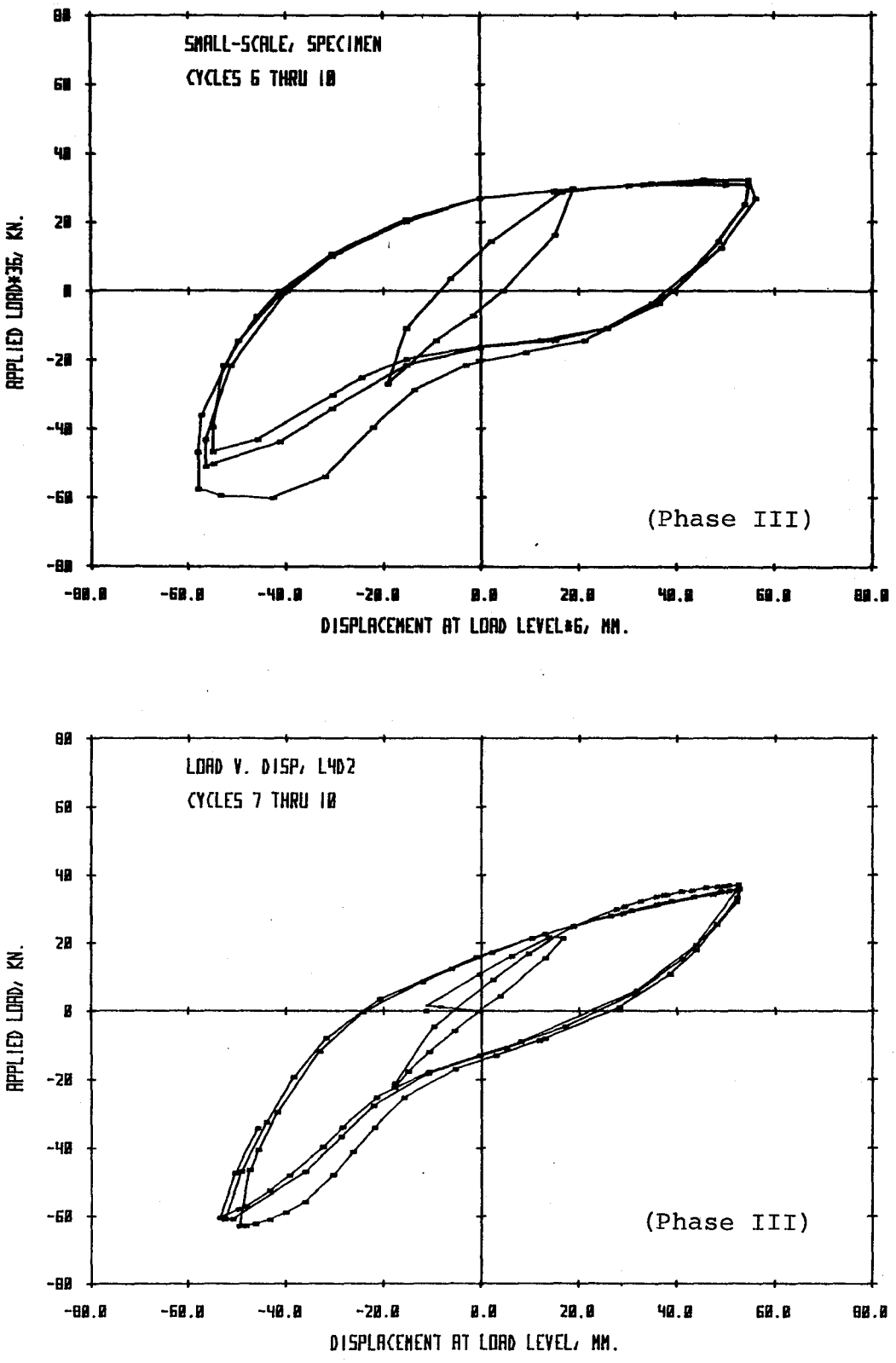

Fig. 5.7 Comparison of Small- and Large-Scale Specimens

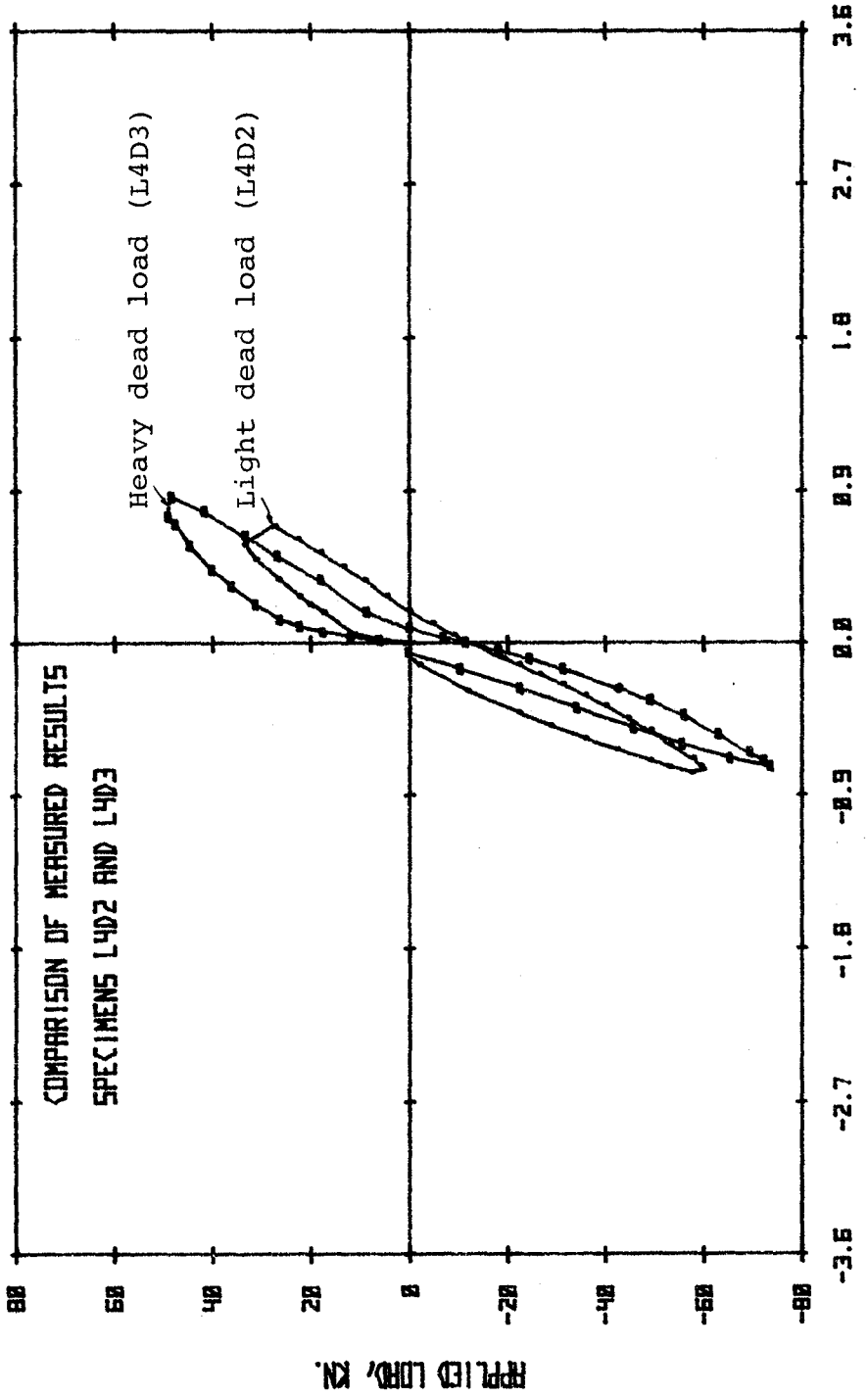

Fig. 5.8 Comparison of Initial Cycles of Large-Scale Specimens

	Property	L4D2	L4D3
Decreasing Axial Compression	Cracking load	11KN	22KN
	Cracking stiffness	8.2 $\frac{KN}{mm}$	1.8 $\frac{KN}{mm}$
	Yield load	35KN	48KN
	Stiffness to yield	1.6 $\frac{KN}{mm}$	1.8 $\frac{KN}{mm}$
Increasing Axial Compression	Cracking load	18KN	27KN
	Yield load	60KN	74KN
	Stiffness to yield	2.4 $\frac{KN}{mm}$	3.6 $\frac{KN}{mm}$

Table 5.2 Comparison of Measured Properties Specimens L4D2 and L4D3

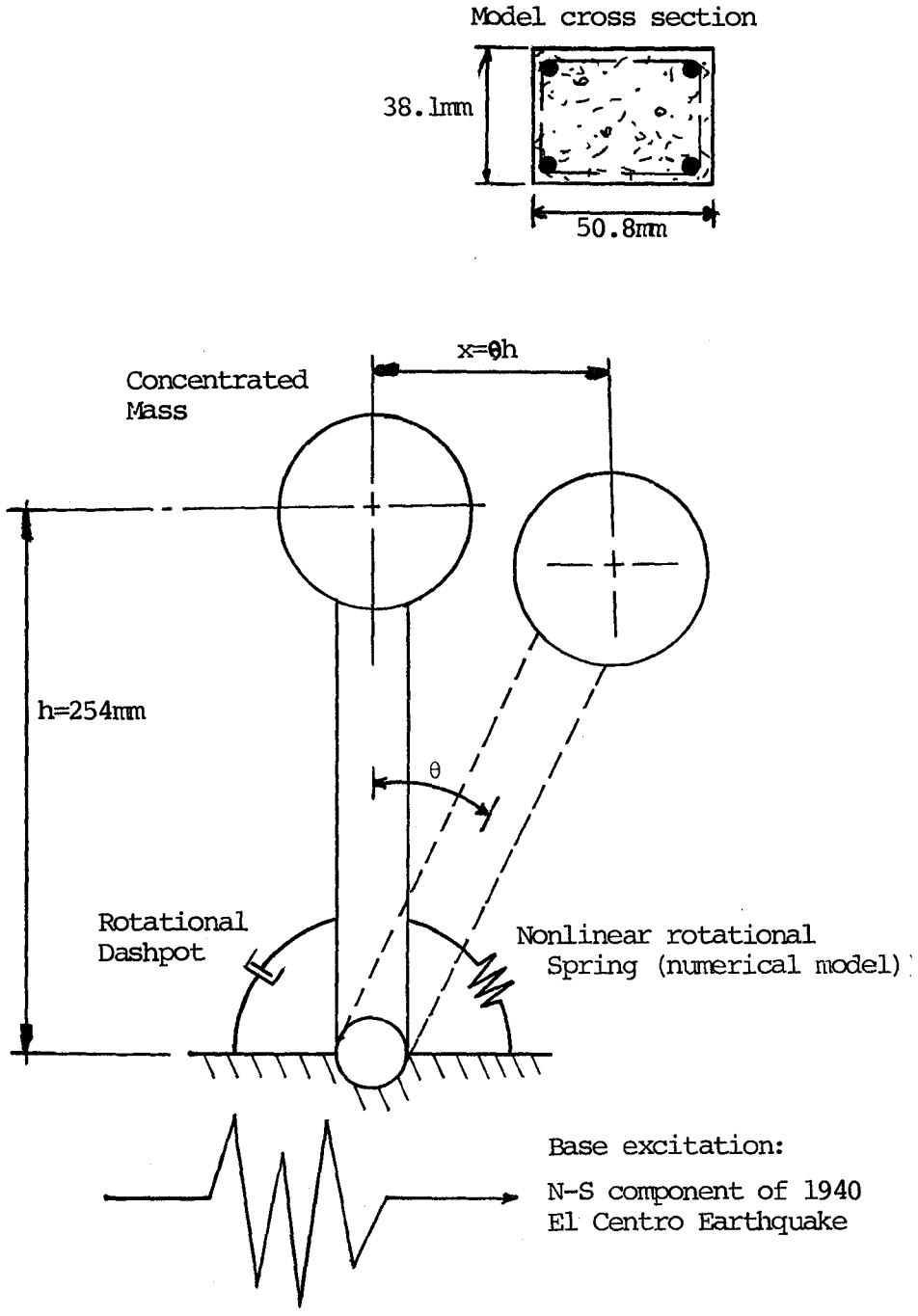

Fig. 5.9 Nonlinear Dynamic Model

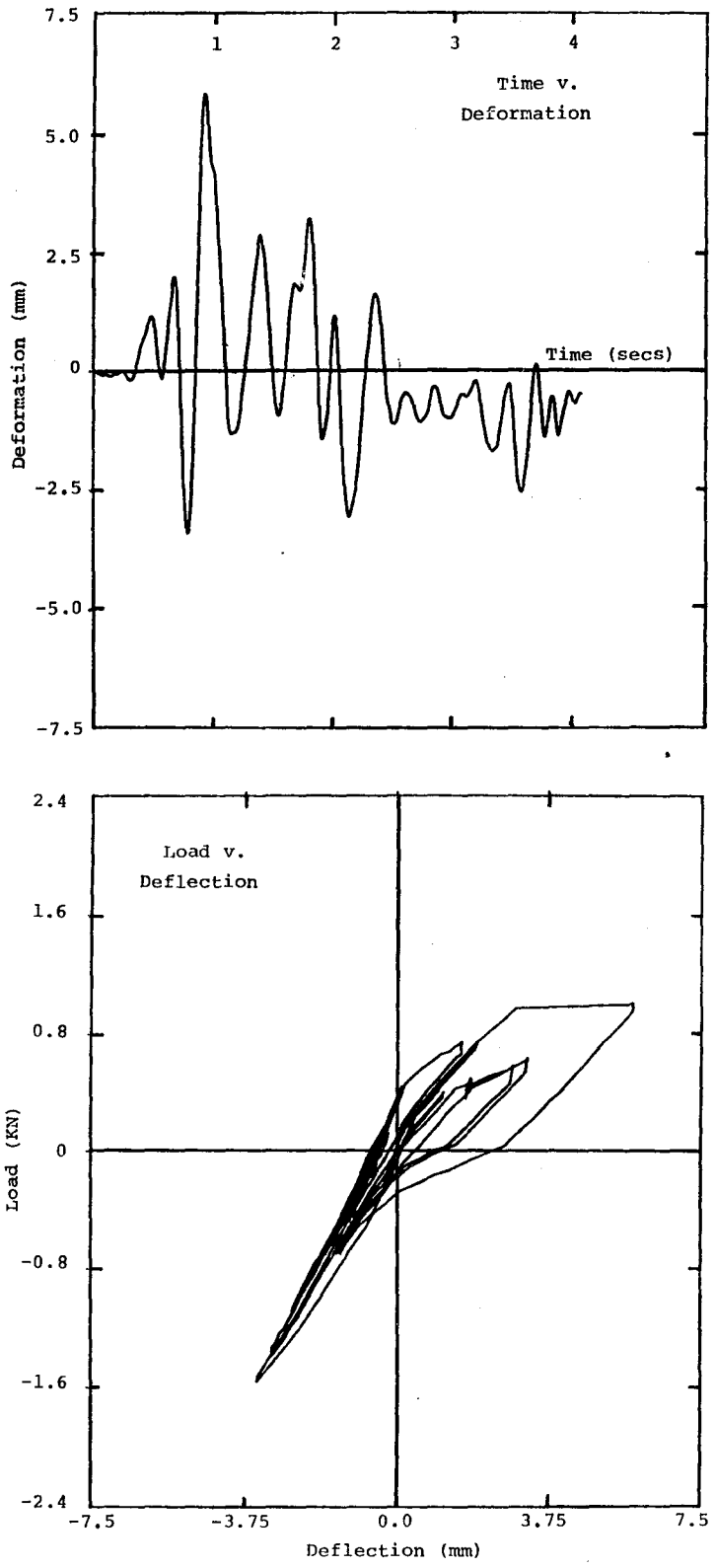

Fig. 5.10 Dynamic Response with Light Gravity Stress

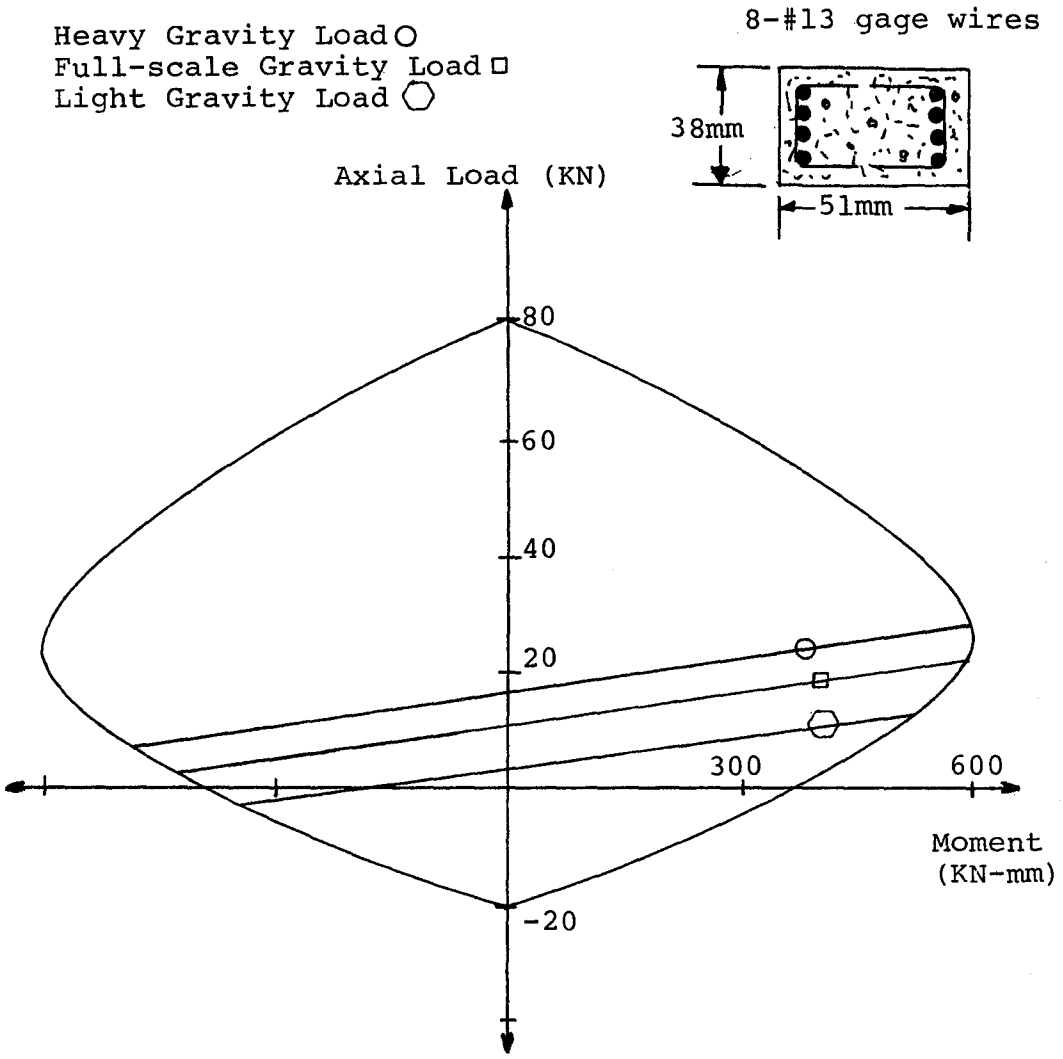

Fig. 5.11 Load-Moment Interaction Diagram for Small-Scale Model in the Dynamic Analysis

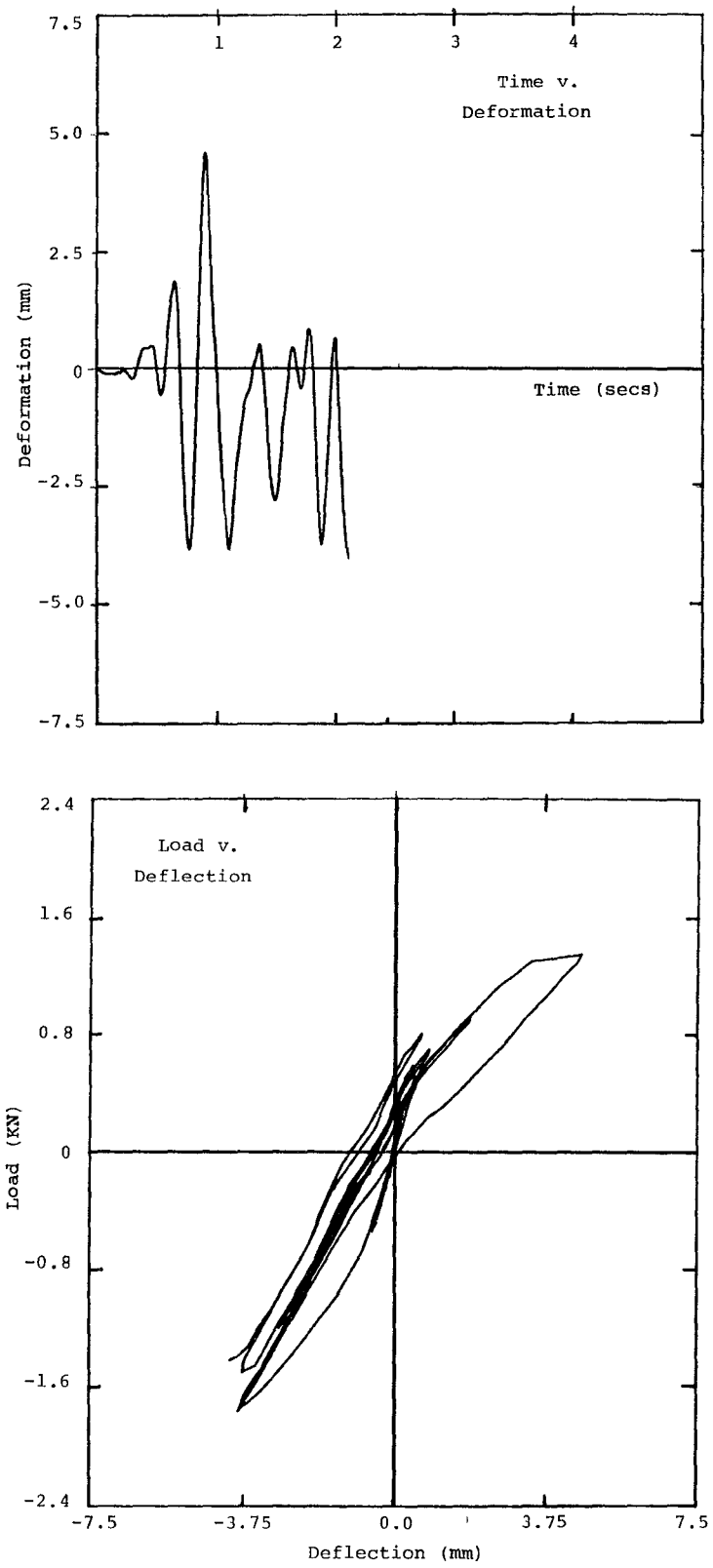

Fig. 5.12 Dynamic Response to Full-Scale Gravity Stress

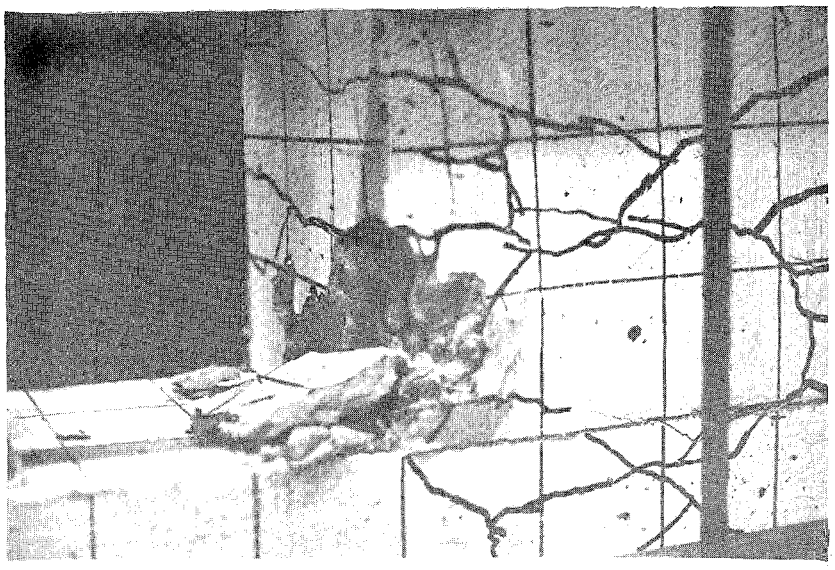

L4D2, Light Gravity Stress

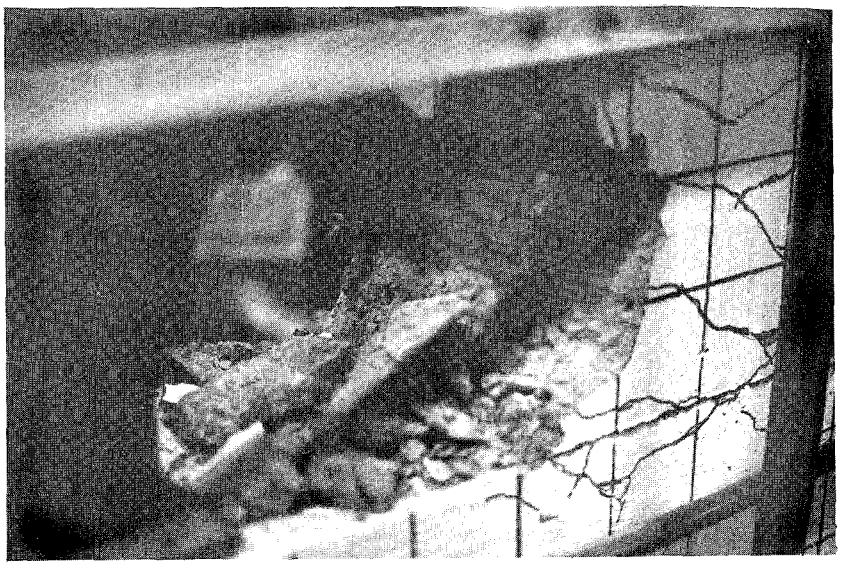

L4D3, Actual Full-Scale Gravity Stress

Fig. 5.13 Comparison of Failure Damage

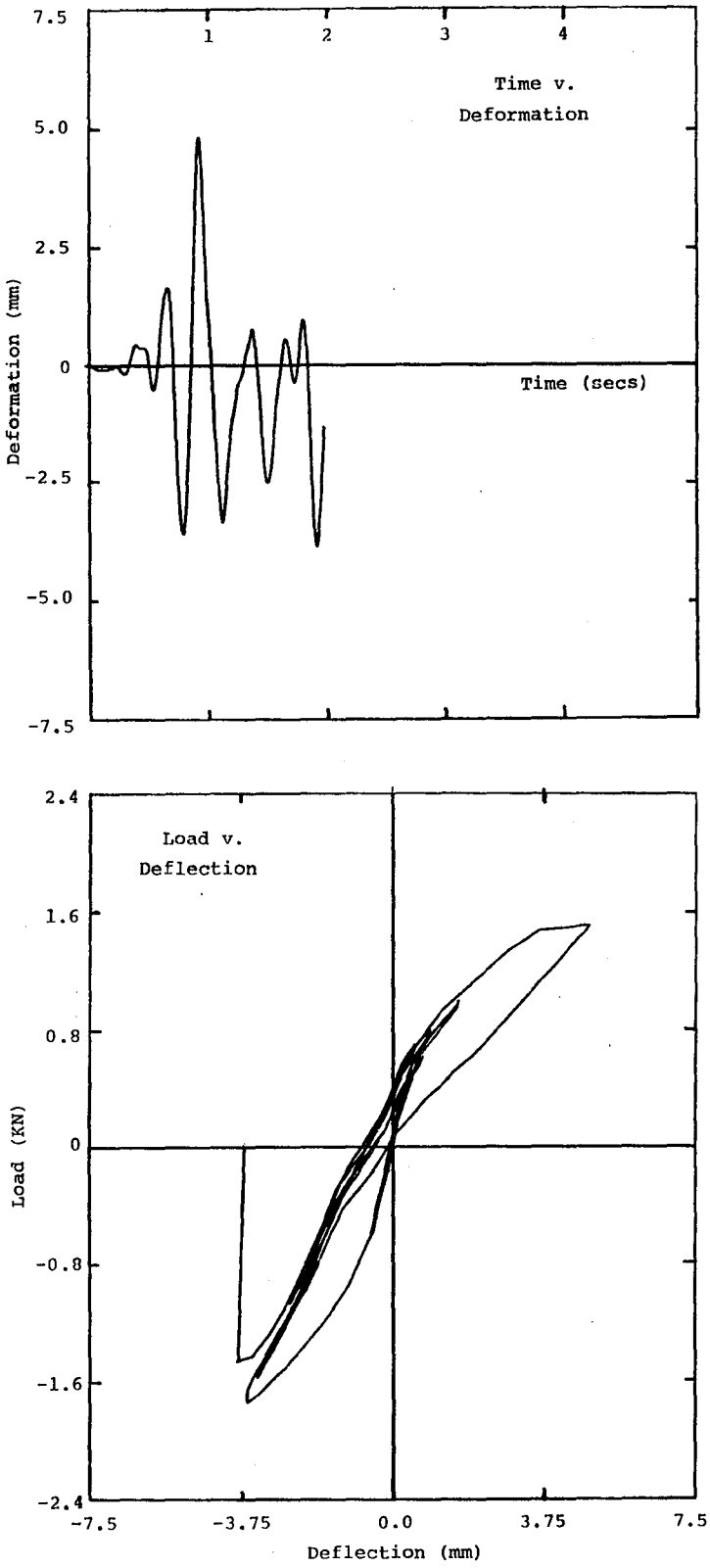

Fig. 5.14 Dynamic Response with Heavy Gravity Stress

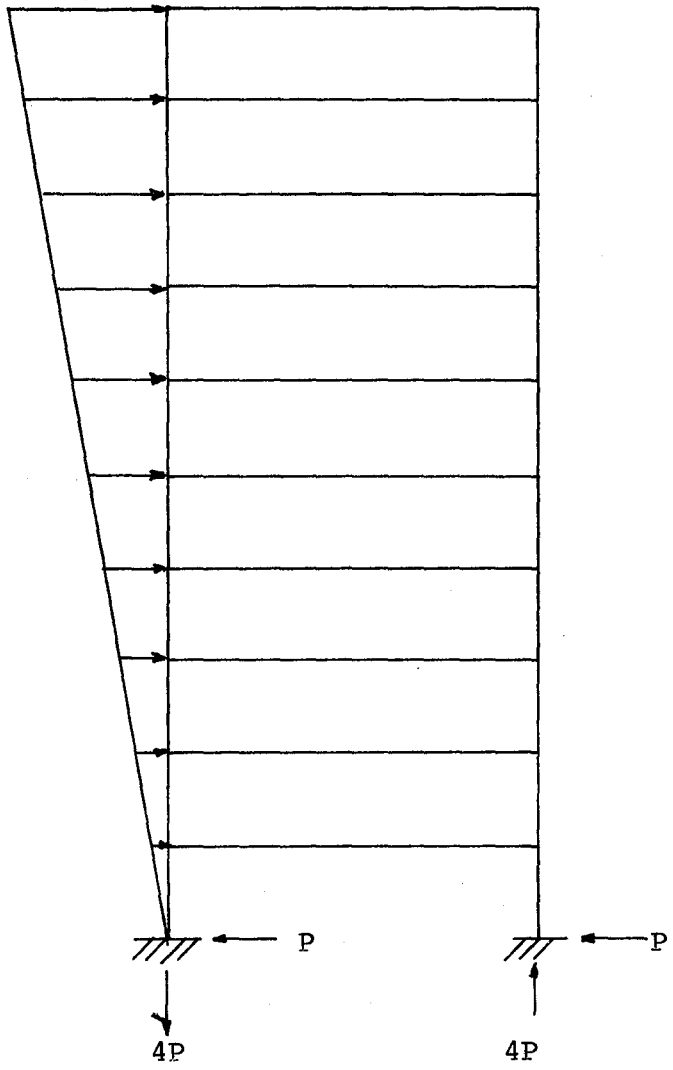

Fig. 5.15 Idealized Structural Model

CHAPTER VI

SUMMARY AND CONCLUSIONS

6.1 Summary

The objective of this experimental study was to examine the behavior of reinforced concrete columns subject to shear and axial force reversals and to compare the response with small-scale models. Two large-scale reinforced concrete columns were tested with a ratio of shear to axial force of one to four (1:4) to simulate the load configuration on an exterior base story column in a slender multistory structure. A loading apparatus was developed to apply the shear and axial load at this ratio. Response of the large-scale specimens was compared with measured response of small-scale (approximately one-twelfth scale) models which were tested as part of a previous investigation.

The test parameter for the large-scale testing was the amount of sustained load which represented gravity load in a multistory structure. A sustained load was applied to the first specimen to provide a normal stress equal to that in a small-scale model so that size effects could be examined. A

second specimen was loaded with a sustained load three times larger than the first specimen to produce a gravity stress similar to that in a full-scale multistory building. In this manner, differences in response due to inconsistent scaling of gravity loads could be investigated.

A numerical model was developed to compute hysteresis relationships using information on the section properties and the stress-strain characteristics of the steel and the concrete. The model was verified using test results. As a result, a better understanding of the load-resistance mechanisms governing the response of the specimens was gained.

The numerical model was used in a nonlinear dynamic analysis to investigate the sensitivities of the overall response of a multistory building to variations in load-deflection relations of base story columns.

6.2 Conclusions

For large- and small-scale specimens with the same normal sustained stress, hysteretic behavior was similar. Flexural strengths, stiffness and energy-dissipation characteristics of large-scale reinforced concrete columns could be approximated reasonably well with small-scale models. Correlation in behavior of the two columns was valid for the entire range of response. Stiffness of the uncracked as well as

cracked specimen corresponded well. Mechanisms comprising the ultimate strength of the section were independent of size. Unloading slopes were similar. The closing of major flexural cracks (in regions of large deformations) was modeled well by the small-scale specimen as the "pinching" effect was observed in the same range for both specimens. The absence of crack closure on opposite half cycles also modeled well as no pinching was observed for either specimen. Overall response of both large- and small-scale specimens was dependent on loading histories.

For large- and small-scale specimens with different sustained normal stresses, the behavior was dissimilar. The small-scale model which had a sustained-load stress lighter than the large-scale reinforced concrete column behaved in a ductile manner characteristic of a section below the balanced point on an axial load-moment interaction diagram. The large-scale specimen responded typically of a member controlled by axial compression, or above the balanced point. The load-deflection curve was rounded under monotonically increasing loads suggesting a dominance of the concrete behavior on the overall behavior of the member. The stiffness upon initial loading was significantly larger for the large-scale specimen which resulted in higher shears being attracted to the column during an excitation at the base. The relatively ductile behavior of the

small-scale specimen resulted in little strength deterioration with successive cycles of loading. This behavior was not representative of an actual column, however, where the concrete may crush at a maximum load resulting in a reduction of strength.

In conclusion, base-story columns of a reduced-scale model building may represent the hysteretic response of full-scale reinforced concrete construction reasonably well. The designer of such a test structure should be aware, however, of the sensitivities of the response due to inconsistent modeling of gravity loads, and in some way account for these differences.

6.3 Recommendations for Future Research

A larger body of experimental data needs to be developed concerning the behavior of reinforced concrete columns. A better understanding of the response of the base story could provide a safer and possibly a more economical seismic design. This may be accomplished by performing cyclic load tests with different ratios of shear to axial force so that bounds for various building configurations can be examined.

REFERENCES

1. Abrams, D.P. and M.A. Sozen, "Experimental Study of Frame-Wall Interaction in Reinforced Concrete Structures Subjected to Strong Earthquake Motions," Civil Engineering Studies, University of Illinois, Urbana, May 1979.

2. Abrams, D.P. and M.E. Kreger, "Measured Hysteresis Relationships for Small-Scale Beam-Column Joints," Civil Engineering Studies, Structural Research Series No. 453, University of Illinois, Urbana, August 1978.

3. Aktan, A.E., B.I. Karlsson and M.A. Sozen, "Stress-Strain Relationships of Reinforcing Bars Subjected to Large Strain Reversals," Civil Engineering Studies, Structural Research Series No. 397, University of Illinois, Urbana, June 1973.

4. Building Code Requirements for Reinforced Concrete, ACI Standard 318-77.

5. Clough, R.W. and J. Penzien, Dynamics of Structures, McGraw-Hill, 1975.

6. EERC News, Earthquake Engineering Research Center, Vol. 6, No. 3, University of California, Berkeley, September 1982.

7. Evans, D.J. and J.L. Clarke, "A Comparison Between the Flexural Behavior of Small-Scale Microconcrete Beams and that of Prototype Beams," Cement and Concrete Association, Technical Report No. 542, March 1981.

8. Garas, F.K. and G.S.T. Armer, "Reinforced and Prestressed Microconcrete Models," The Construction Press, 1980.

9. Gilbertson, N.D. and J.P. Moehle, "Experimental Study of Small-Scale R/C Columns Subjected to Axial and Shear Force Reversals," Civil Engineering Studies, Structural Research Series No. 481, University of Illinois, Urbana, July 1980.

10. Healey, T.J. and M.A. Sozen, "Experimental Study of the Dynamic Response of a Ten-Story Reinforced Concrete Frame with a Tall First Story," Civil Engineering Studies, Structural Research Series No. 450, University of Illinois, Urbana, August 1978.

11. Keyser, C.A., Materials of Engineering, Prentice-Hall, 1956.

12. Lybas, J.M. and M.A. Sozen, "Effect of Beam Strength and Stiffness on Dynamic Behavior of Reinforced Concrete Coupled Walls," Civil Engineering Studies, Structural Research Series No. 444, University of Illinois, Urbana, July 1977.

13. Moehle, J.P. and M.A. Sozen, "Experiments to Study Earthquake Response of Reinforced Concrete Structures with Stiffness Interruptions," Civil Engineering Studies, Structural Research Series No. 482, University of Illinois, Urbana, August 1980.

14. Park, R., M.J.N. Priestley and W.D. Gill, "Ductility of Square-Confined Concrete Columns," Journal of the Structural Division, Vol. 108, No. ST4, April 1982, pp. 929-952.

15. "Recommendations for a U.S.-Japan Cooperative Research Program Utilizing Large-Scale Testing Facilities," U.S.-Japan Planning Group Cooperative Research Program Utilizing Large-Scale Testing Facilities, Earthquake Engineering Research Center, University of California, Berkeley, Report No. 79-26, September 1979.

16. Sabnis, G.M., H.G. Harris, R.N. White and M.S. Mirza, Structural Modeling and Experimental Techniques, Prentice-Hall Civil Engineering and Mechanics Series, 1983.

17. Sargin, M., "Stress-Strain Relationships for Concrete and the Analysis for Structural Concrete Sections," Solid Mechanics Division, SM Study No. 4, University of Waterloo, Canada, 1971, pp.23-46.

18. Sozen, M.A. and P.J. Wilson, "Dynamic Response of a One-Tenth Scale Model of the BRI Reinforced Concrete Test Structure," A Report to U.S.-Japan Cooperative Research Program Utilizing Large-Scale Testing Facilities, University of Illinois, Urbana, July 1982.

19. Staffier, S.R. and M.A. Sozen, "Effect of Strain Rate of Yield Stress of Model Reinforcement," Civil Engineering Studies, Structural Research Series No. 415, University of Illinois, Urbana, February 1975.

20. Stewart, J.H. and D.P. Abrams, "Comparison of Large- and Small-Scale Reinforced Concrete Behavior," Masters Thesis, University of Colorado, Boulder, July 1981.

21. Vallenas, J.M., V.V. Bertero and E.P. Popov, "Hysteretic Behavior of Reinforced Concrete Structural Walls," Earthquake Engineering Research Center, University of California, Berkeley, Report No. 79-20, August 1979.

22. Viwathanatepa, S., E.P. Popov and V.V. Bertero, "Seismic Behavior of Reinforced Concrete Interior Beam-Column Subassemblages," Earthquake Engineering Research Center, University of California, Berkeley, Report No. 79-14, June 1979.

23. Wilby, G.K., "Response of Concrete Structures to Seismic Motions," Ph.D. Thesis, Department of Civil Engineering, University of Canterbury, Christchurch, New Zealand, July 1975.

24. Zia, P., R.N. White and D.A. VanHorn, "Principles of Model Analysis," Models for Concrete Structures, Special Publication of American Concrete Institute No. 24, 1970.

INTENTIONALLY BLANK

APPENDIX A

Listing of Computer Program

to Calculate

Moment-Curvature Relations

The Numerical Model

The program was written in Fortran IV and compiled on the CDC 7600 computer at the University of Colorado. The most important calculation in the program was a value for the curvature of the scetion for a given axial load and moment. The curvature was defined by the following expression.

$$\phi = \frac{M}{EI}$$

The nonlinear characteristics of the section were accounted for by dividing the section into several elements.

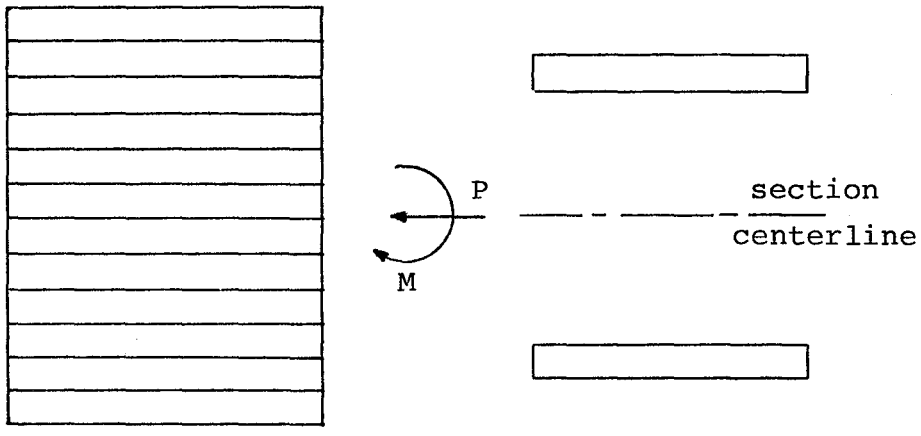

Each element had its own stress-strain characteristics according to the models in Fig. 4.3. The slope of the stress-strain relation was used to approximate the modulus E, for each load step. These values were updated at the end of each load step. Once the tangent modulus for each element was modified for the current load conditions, the axial load and moment were incremented and the procedure was repeated.

A flowchart and the listing of the program are presented on the following pages.

Flowchart
Program Section

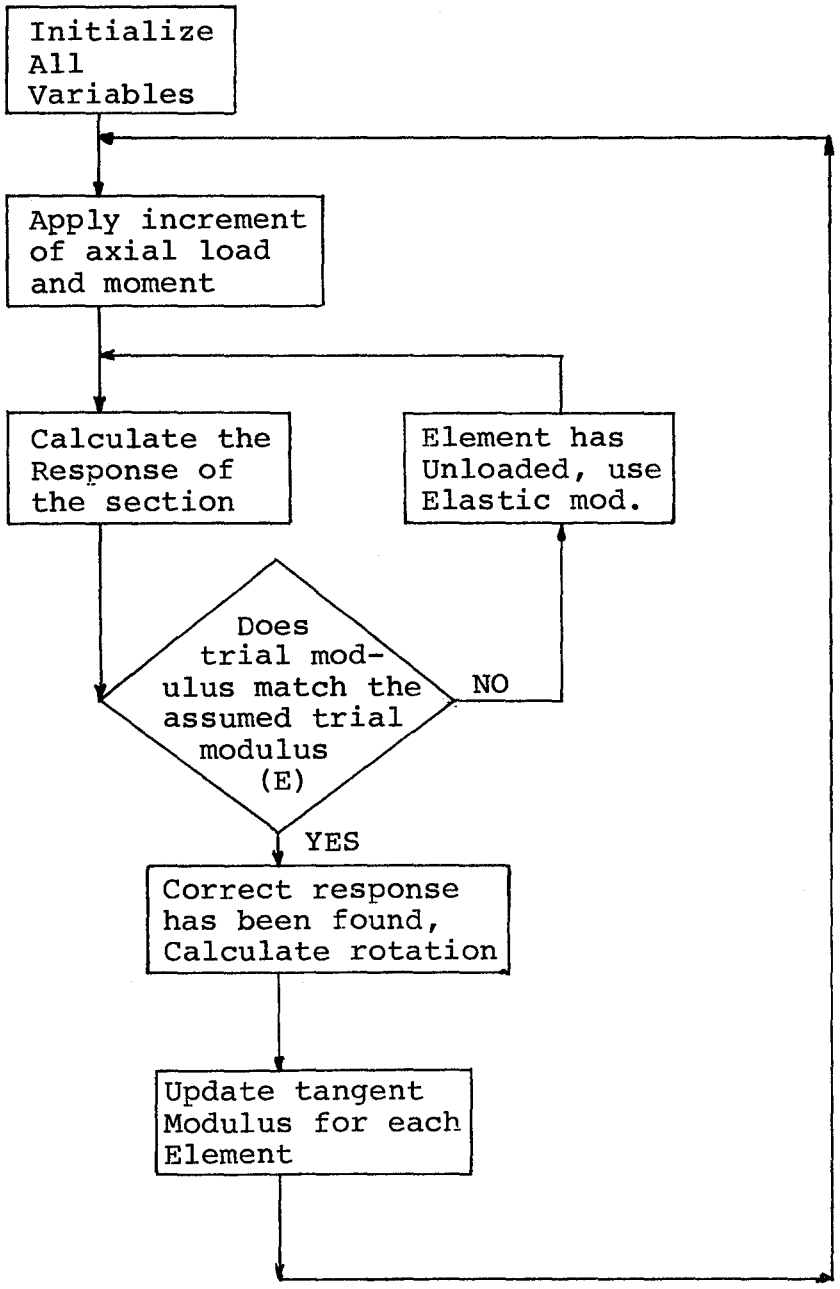

```
      PROGRAM SECTION(INPUT,OUTPUT,TAPE5=INPUT,TAPE6=OUTPUT)
      DIMENSION DSTRN(7),CSTRN(7),TSTRS(5),TRIMOD(7),TENSMOD(7),
     1          COMPMOD(7),ETAN(7),LDIR(7),GSIG(7),GSTRN(7),
     2           SIG(7),IFLG(5),F(7),CSIG(7),TSTRN(7)
      COMMON H,DO,NE,H1
C
C*****H IS THE LENGTH OF THE SECTION
C*****DO IS THE WIDTH OF ONE ELEMENT
C*****NE IS THE NUMBER OF ELEMENTS
C*****H1 IS THE DIST FROM CENTERLINE OF SECT TO CENTROID OF THE
C     FIRST ELEMENT
C*****DELTA IS THE HORIZONTAL DISPLACEMENT AT LOAD LEVEL
C*****THETA IS THE ROTATION NEAR THE BASE
      XPHI=0.
C
C     INITALIZE ALL VARIABLES
C
      N=0
      L=0
      A=1.
      M=1
      DELTAS=0.
      TLOAD=0.
      YBAR=0.
      YYBAR=0.
      THETAS=0.
      ROT=0.
      LPO=0
      DELTA=0.
      THETA=0.
      H=12.
      TDISP=.0068
      CDISP=.0077
      XSTRN=0.
      PHI=0.
      DO=2.4
      H1=H/2.-DO/2.
      NE=5
      NET=NE+2
      DO 10 I=1,NET
      DSTRN(I)=0.
      TRIMOD(I)=0.
      TENSMOD(I)=0.
      COMPMOD(I)=0.
      LDIR(I)=0
      SIG(I)=0.
      TSTRN(I)=0.
      GSTRN(I)=0.
      CSTRN(I)=0.
   10 CONTINUE
      GSIG(NE+1)=62.
      GSIG(NE+2)=62.
      CSIG(NE+1)=-62.
      CSIG(NE+2)=-62.
      DO 11 J=1,NE
```

```
      TSTRS(J)=0.
      GSIG(J)=0.
      IFLG(J)=0
      ETAN(J)=3000.
   11 CONTINUE
      ETAN(NE+1)=29000.
      ETAN(NE+2)=29000.
C
C*****SET INITIAL HORIZONTAL LOAD INCREMENT
C
C
C*****CALCULATE THE CURVATURE(XPHI) AT THE BASE FOR EACH
C     LOAD INCREMENT
C
   50 IF(L .LT. 6)GO TO 71
      A=A+1.
      TDISP=.007*A
      L=0
C
C     THE FOLLOWING STATEMENTS DEFINE A VARIABLE LOADING
C     TO ACCOUNT FOR NONLINEAR EFFECTS
C
   71 CONTINUE
      IF(ABS(SIG(NE+1)) .GE. 60.)GO TO 60
      IF(ABS(SIG(NE+2)) .GE. 60.)GO TO 60
      XM=0.
      XP=-5.2
      IF(N .LE. 4)GO TO 51
   61 IF((SIG(1) .GT. -1.) .AND. (SIG(NE+1) .LE. -60.))GO TO 72
      XM=19.2*M
      XP=1.28*M
   51 CONTINUE
      GO TO 70
   60 IF((TLOAD .GT. 0.) .AND. (LDIR(NE+1) .EQ.-1))GO TO 61
      IF((TLOAD .LT. 0.) .AND. (LDIR(NE+2) .EQ.-1))GO TO 61
      IF(((SIG(NE+1)) .LE. -60.) .AND. ((SIG(NE+2))
     1     .LE. 60.))GO TO 61
      XM=.96*M
      XP=.064*M
      GO TO 70
   72 XM=.48*M
      XP=.032*M
   70 CONTINUE
C
C*****INITIALIZE THE MODULI FOR EACH ELEMEMT
C
      CALL INIT(NE,NET,TENSMOD,COMPMOD,TRIMOD,ETAN,LDIR)
C
C     ITERATE TO DETERMINE THE NUETRAL AXIS
C
      NATRY=0
   15 NATRY=NATRY+1
      CALL RESPONS(NET,YBAR,XM,XP,TRIMOD,XSTRN,DSTRN,XPHI)
      CALL CHKNA(K2,DSTRN,TRIMOD,TENSMOD,COMPMOD,NET)
      IF(K2 .EQ. 0)GO TO 30
      IF(NATRY .GT. 10) GO TO 20
      GO TO 15
   20 WRITE(6,100)
   30 CONTINUE
      DO 12 K=1,NET
```

```
      TSTRN(K)=TSTRN(K)+DSTRN(K)
   12 CONTINUE
      PHI=PHI+XPHI
C
C     CALCULATE PULLOUT OF REINFORCEMENT
C
      IF(ABS(PHI) .LT. .000002)GO TO 64
      YYBAR=-(TSTRN(3)/PHI)
      IF(PHI .GE. 0.)GO TO 62
      DELTAS=-TSTRN(NE+2)*3.
      THETAS=DELTAS/(4.25+ABS(YYBAR))
      GO TO 63
   62 DELTAS=TSTRN(NE+1)*6.
      THETAS=DELTAS/(4.25+ABS(YYBAR))
      GO TO 63
   64 CONTINUE
      THETAS=0.
   63 CONTINUE
C
C     DETERMINE ROTATIONS AND DEFLECTIONS FROM CURRENT CURVATURE
C
      THETA=PHI*30.+THETAS
      DELTA=THETA*40.
      ROT=PHI*10.+THETAS
C
C*****UPDATE ELEMENT MODULI
C
      CALL ELMNT2(CSTRN,DSTRN,TSTRN,LDIR,SIG,NE,GSTRN,ETAN,NET
     1           ,TSTRS,IFLG)
      CALL ELMNT1(TSTRN,DSTRN,LDIR,SIG,NET,NE,ETAN,GSIG,CSIG,GSTRN
     1           ,L,A,CSTRN)
      N=N+1
      IF(LPO .EQ. 0)GO TO 80
      WRITE(6,230)
      WRITE(6,225)SIG
      WRITE(6,225)TSTRN
      WRITE(6,225)ETAN
   80 CONTINUE
      IF((TLOAD .GT. 2.) .OR. (TLOAD .LT. -2.))GO TO 82
      IF((L.EQ.1).OR.(L.EQ.3).OR.(L.EQ.5))GO TO 81
      TDISP=.0069*A
      GO TO 82
   81 TDISP=CDISP*A
   82 CONTINUE
      IF(ABS(PHI) .GE. .0015)GO TO 75
      TLOAD=TLOAD+XM/60.
      WRITE(6,200)TLOAD,PHI,ROT,DELTA,YYBAR
      IF(N .GE. 900)GO TO 75
C
C
C     CHECK TO SEE IF MAXIMUM ROTATIONS HAVE BEEN REACHED
C
      IF(ABS(ROT) .GE. ABS(TDISP))GO TO 52
      GO TO 50
   52 M=-M
      TDISP=ROT
      L=L+1
      GO TO 50
  100 FORMAT(2X,'TRYS FOR NA HAVE BEEN EXCEEDED')
  225 FORMAT(2X,7E16.5)
```

```
  230 FORMAT(2X,'------------------')
  200 FORMAT(2X,F10.6,5X,F10.7,5X,F10.7,5X,F10.7,5X,F10.7)
   75 CONTINUE
      STOP
      END
C
C
C
C


      SUBROUTINE INIT (NE,NET,TENSMOD,COMPMOD,TRIMOD,ETAN,LDIR)
      DIMENSION TRIMOD(NET),TENSMOD(NET),COMPMOD(NET),ETAN(NET)
      DIMENSION LDIR(NET)
C
C     THIS SUBROUTINE INITIALIZES THE TANGENT MODULI FOR EACH
C     ELEMENT AND PROVIDES THE ELASTIC MODULI IN THE EVENT OF
C     A LOAD REVERSAL
C
      DO 200 I=1,NE
      TRIMOD(I)=ETAN(I)
      IF(LDIR(I) .EQ. -1)GO TO 100
      COMPMOD(I)=ETAN(I)
      TENSMOD(I)=ETAN(I)
      GO TO 200
  100 COMPMOD(I)=ETAN(I)
      TENSMOD(I)=3000.
  200 CONTINUE
      TRIMOD(NE+1)=ETAN(NE+1)
      TRIMOD(NE+2)=ETAN(NE+2)
      IF(LDIR(NE+1) .EQ. 1) GO TO 110
      TENSMOD(NE+1)=29000.
      COMPMOD(NE+1)=ETAN(NE+1)
      GO TO 220
  110 TENSMOD(NE+1)=ETAN(NE+1)
      COMPMOD(NE+1)=29000.
  220 IF(LDIR(NE+2) .EQ. 1) GO TO 115
      TENSMOD(NE+2)=29000.
      COMPMOD(NE+2)=ETAN(NE+2)
      GO TO 225
  115 TENSMOD(NE+2)=ETAN(NE+2)
      COMPMOD(NE+2)=29000.
  225 CONTINUE
      RETURN
      END
C
C
C


      SUBROUTINE CHKNA(K2,DSTRN,TRIMOD,TENSMOD,COMPMOD,NET)
      DIMENSION DSTRN(NET),TRIMOD(NET),TENSMOD(NET),COMPMOD(NET)
C
C     THIS SUBROUTINE CHECKS TO SEE IF THE MODULI ASSUMED FOR
C     EACH ELEMNT IS CORRECT
C
      K2=0
      DO 20 I=1,NET
      IF(DSTRN(I) .LT. 0.) GO TO 10
      IF(TRIMOD(I) .EQ. TENSMOD(I))GO TO 20
```

```
      TRIMOD(I)=TENSMOD(I)
      K2=K2+1
      GO TO 20
   10 IF(TRIMOD(I) .EQ. COMPMOD(I))GO TO 20
      TRIMOD(I)=COMPMOD(I)
      K2=K2+1
   20 CONTINUE
      RETURN
      END
C
C
C
C


      SUBROUTINE RESPONS(NET,YBAR,TXM,XP,TRIMOD,XSTRN,
     1                   DSTRN,XPHI)
      DIMENSION TRIMOD(NET),DSTRN(NET)
      COMMON H,DO,NE,H1
C
C     THIS SUBROUTINE CALCULATES THE CURVATURE FOR THE GIVEN
C     INCREMENT USING THE CURRENT VALUE OF THE TANGENT MODULUS
C     AND MOMENT OF INERTIA FOR EACH ELEMENT
C
C
      AE=0.
      AEC=0.
      QE=0.
      QEC=0.
      P=0.
      Q=0.
      EI=0.
      EICT=0.
      A1=DO*9.
      AES1=0.
      AES2=0.
      QES=0.
      EISELF=.75*DO**3.
      DO 10 I=1,NE
      DE=H1-(Q*DO)
      Q=Q+1.
      AE=A1*TRIMOD(I)
      AEC=AEC+AE
      QE=AE*DE
      QEC=QEC+QE
      EI=AE*DE**2.+EISELF*TRIMOD(I)
   10 EICT=EICT+EI
      AES1=.88*TRIMOD(NE+1)
      AES2=.88*TRIMOD(NE+2)
      QES=4.25*(AES1-AES2)
      EIS=.03106*(TRIMOD(NE+1)+TRIMOD(NE+2))+(AES1+AES2)*4.25**2.
      AET=AEC+AES1+AES2
      QET=QES+QEC
      EIT=EICT+EIS
      YBAR=QET/AET
      EITT=EIT-QET*YBAR
      XM=TXM-YBAR*XP
      XPHI=XM/EITT
      XSTRN=XP/AET
      DO 15 J=1,NE
```

```
      DC=H1-(P*DO)
      P=P+1.
   15 DSTRN(J)=XPHI*(DC-YBAR)+XSTRN
      DSTRN(NE+1)=XPHI*(4.25-YBAR)+XSTRN
      DSTRN(NE+2)=XPHI*(-4.25-YBAR)+XSTRN
      RETURN
      END
C
C
C
C
C
      SUBROUTINE ELMNT1(TSTRN,DSTRN,LDIR,SIG,NET,NE,ETAN,GSIG
     1                  ,CSIG,GSTRN,L,A,CSTRN)
      DIMENSION GSIG(NET),CSIG(NET),CSTRN(NET),GSTRN(NET)
      DIMENSION TSTRN(NET),DSTRN(NET),LDIR(NET),SIG(NET),ETAN(NET)
C
C     THIS SUBROUTINE UPDATES THE TANGENT MODULUS FOR EACH
C     STEEL ELEMENT ACCORDING TO THE PERSCRIBED STRESS-STRAIN
C     CHARACTERISTICS
C
      NE1=NE+1
      DO 16 J=NE1,NET
      IF(ABS(DSTRN(J)) .LE. .000001)GO TO 16
      LDIR(J)=ABS(DSTRN(J))/DSTRN(J)
      SIG(J)=SIG(J)+DSTRN(J)*ETAN(J)
      LDIR(J)=ABS(DSTRN(J))/DSTRN(J)
      IF((L .LT. 2) .AND. (A .EQ. 1.))GO TO 50
      IF((A .EQ. 2.) .AND. (L .EQ. 1))CSTRN(NE+1)=-.006
      IF(SIG(J) .LT. 0.)GO TO 24
      IF((LDIR(J) .EQ. -1) .AND. (SIG(J) .GE. 0.))GO TO 27
      IF(GSIG(NET) .LE. 62.)GSTRN(NET)=.00213
      IF(TSTRN(J) .GE. GSTRN(J))GO TO 32
      IF(SIG(J) .GE. 15.)GO TO 31
      ETAN(J)=29000.
      EPS=GSTRN(J)-TSTRN(J)
      GO TO 20
   27 ETAN(J)=29000.
      GO TO 20
   31 IF(SIG(J) .GE. GSIG(J))GO TO 32
      ETAN(J)=(GSIG(J)-15.)/EPS
      GO TO 20
   32 ETAN(J)=.29
      GSIG(J)=SIG(J)
      GSTRN(J)=TSTRN(J)
      GO TO 20
   24 IF((LDIR(J) .EQ. 1) .AND. (SIG(J) .LT. 0.))GO TO 25
      IF(J .EQ. NET)GO TO 28
      IF(TSTRN(J) .LE. CSTRN(J))GO TO 22
      IF(SIG(J) .LE. -15.)GO TO 21
      ETAN(J)=29000.
      CEPS=TSTRN(J)-CSTRN(J)
      GO TO 20
   25 ETAN(J)=29000.
      GO TO 20
   21 IF(SIG(J) .LE. CSIG(J))GO TO 22
      ETAN(J)=ABS((CSIG(J)+15.)/CEPS)
      GO TO 20
```

```
   28 IF(SIG(J) .GE. -15.)GO TO 29
      ETAN(J)=20000.
      GO TO 20
   29 ETAN(J)=29000.
      GO TO 20
   22 ETAN(J)=.29
      CSIG(J)=SIG(J)
      CSTRN(J)=TSTRN(J)
      GO TO 20
   50 CONTINUE
      IF(SIG(J) .LT. 0)GO TO 14
      IF(SIG(J) .GT. GSIG(J))GO TO 12
      ETAN(J)=29000.
      GO TO 20
   12 ETAN(J)=.29
      GSTRN(J)=TSTRN(J)
      GSIG(J)=SIG(J)
      GO TO 20
   14 IF(SIG(J) .LE. CSIG(J))GO TO 11
      ETAN(J)=29000.
      GO TO 20
   11 ETAN(J)=.29
      CSTRN(J)=TSTRN(J)
      CSIG(J)=SIG(J)
   20 CONTINUE
   16 CONTINUE
      RETURN
      END
C
C
C
C
C


      SUBROUTINE ELMNT2(CSTRN,DSTRN,TSTRN,LDIR,SIG,NE,GSTRN,ETAN,NET
     1                 ,TSTRS,IFLG)
      DIMENSION TSTRN(NET),DSTRN(NET),CSTRN(NET),LDIR(NET),SIG(NET)
      DIMENSION GSTRN(NET),IFLG(NE),TSTRS(NE),ETAN(NET)
C
C     THIS SUBROUTINE UPDATES THE TANGENT MODULUS FOR EACH
C     CONCRETE ELEMENT ACCORDING TO THE PERSCRIBED STRESS-STRAIN
C     CHARACTERISTICS
C
      ST=0.
      EC=3000.
      ITEST=2
      DO 16 J=1,NE
      IF(ABS(DSTRN(J)) .LE. .000001)GO TO 16
      LDIR(J)=ABS(DSTRN(J))/DSTRN(J)
C
C
C
      SIG(J)=SIG(J)+DSTRN(J)*ETAN(J)
      IF(SIG(J) .GE. 0.)GO TO 26
      IF(TSTRN(J) .LE. GSTRN(J))GO TO 15
      IF(TSTRN(J) .LE. 0.)GO TO 27
   26 IF(LDIR(J) .EQ. 1)GO TO 28
      IF(TSTRN(J) .LE. CSTRN(J))GO TO 27
   28 ETAN(J)=.0001*EC
```

```
      IF(IFLG(J) .EQ. 1)GO TO 45
      TSTRS(J)=SIG(J)
      CSTRN(J)=TSTRN(J)
      IFLG(J)=1
      GO TO 45
   27 ETAN(J)=EC
      IFLG(J)=0
      GO TO 45
C
C
C
   15 GSTRN(J)=TSTRN(J)
      IFLG(J)=0
      IF(ITEST .EQ. 3)GO TO 44
      SIG(J)=(3000.*TSTRN(J))/(1.-5.07*TSTRN(J)+212500.*TSTRN(J)
     1       **2.)
      ST=ABS(TSTRN(J))
      ETAN(J)=(3000.-637500000.*ST**2.)/(1.-(10.14*ST)+(425025.7
     1        *ST**2.)-(2154750.*ST**3.)+(45156250000.*ST**4.))
      GO TO 45
   44 CONTINUE
      SIG(J)=(3200.*TSTRN(J))/(1.+160000.*TSTRN(J)**2.)
      ST=ABS(TSTRN(J))
      ETAN(J)=(3200.-512000000.*ST**2.)/((25600000000.*ST**4.)+
     1         (320000.*ST**2.)+1.)
   45 CONTINUE
   16 CONTINUE
      RETURN
      END
```

APPENDIX B

Similitude of Gravity Load

To predict the response of the small-scale column, the same normal stress due to gravity loads should be applied to the large-scale specimen.

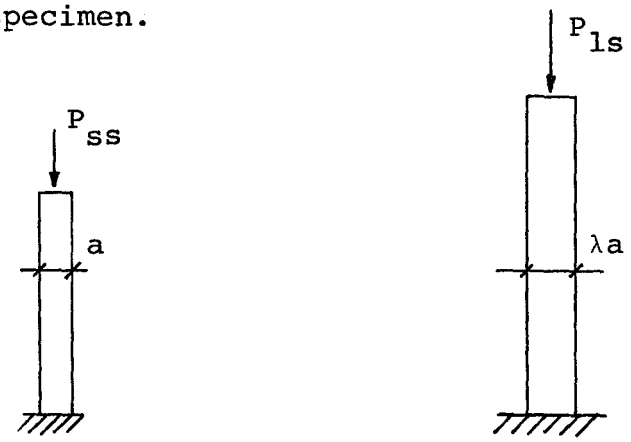

Equating stresses,

$$f_{ls}=f_{ss}$$

$$\frac{P_{ls}}{\lambda^2 a^2}=\frac{P_{ss}}{a^2}$$

$$\underline{\underline{P_{ls}=P_{ss}\lambda^2}}$$

where,

P_{ls} = Large-scale sustained load

f_{ls} = Large-scale normal stress

P_{ss} = Small-scale sustained load

f_{ss} = Small-scale normal stress

a = width of small-scale column

λ = scale factor

Considering only the weight of a structure, the gravity load should vary as the cube of the length scale factor as the weight is a function of the volume. Therefore, the stress should vary as the scale factor (volume/area). This is shown graphically below.

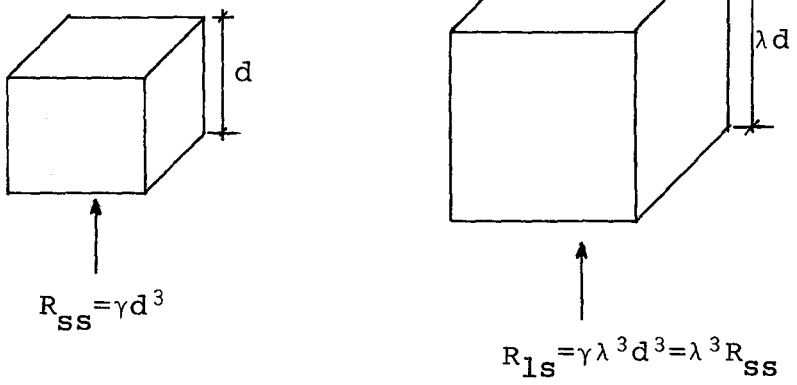

$$f_{ss}=\frac{R_{ss}}{d^2} \qquad f_{ls}=\frac{R_{ls}}{\lambda^2 d^2}=\frac{\lambda^3 R_{ss}}{\lambda^2 d^2}$$

$$\underline{\underline{\lambda f_{ss}=f_{ls}}}$$

where,

R_{ls}= Large-scale reaction

f_{ls}= Large-scale stress

R_{ss}= Small-scale reaction

f_{ss}= Small-scale stress

d = width of the cube

λ = scale factor

γ = weight density of the material